AN ABSTRACT OF THE THESIS OF

Lisa N. Freeman for the degree of Doctor of Philosophy in Mechanical Engineering, presented on May 9, 1996. Title: Stochastic Loads on Horizontal Axis Wind Turbine Blades.

Abstract approved: Redacted for Privacy

Robert E. Wilson

The objective of this work was to develop a method for determining stochastic loads on horizontal axis wind turbine blades. Stochastic loads caused by wind turbulence are a major consideration in designing for long life, cost effective wind turbines. The rotor blades are of particular concern because the blades are usually designed especially for a particular wind turbine. The FAST code has been developed to predict these loads, and has been validated with test data.

The FAST code simulates the structural response due to gravity and aerodynamic loads and is capable of modeling many geometries and up to 14 degrees of freedom. The wind applied to the turbine is made up of a deterministic portion and a stochastic portion. The mean wind is modified to include the effects of tower shadow, wind shear, and turbulence. Expressions for the accelerations and external forces are combined to form the equations of motion which are then solved numerically.

The model was validated by comparing its predictions to test data from two different machines. Both the ESI-80 and the AWT-P1, are two-bladed, teetered-rotor horizontal axis wind turbines. Rather than simply comparing the code and data time series point by point, each time series is first analyzed for its overall characteristics and these are compared. The

methods used to analyze the time series include a histogram, azimuth averaging, the power spectral density, and a rainflow cycle count.

The results show good agreement between data and code predictions over a range of wind speeds for two different machines. The code was successful at predicting the response frequencies of the structure, and the cyclic loads the blades will undergo.

Future work might include investigating other methods of representing turbulence, further validation of the code using other machines and a wider range of wind speeds, parametric studies to identify the model's sensitivity to certain parameters, and the design and design analysis of other machines.

# Stochastic Loads on Horizontal Axis Wind Turbine Blades

by

Lisa N. Freeman

A THESIS

submitted to

Oregon State University

in partial fulfillment of

the requirements for the

degree of

Doctor of Philosophy

Completed May 9, 1996

Commencement June 1996

Doctor of Philosophy thesis of Lisa N. Freeman presented on May 9, 1996

APPROVED:

*Redacted for Privacy*

Major Professor, representing Mechanical Engineering

*Redacted for Privacy*

Head of Department of Mechanical Engineering

*Redacted for Privacy*

Dean of Graduate School

I understand that my thesis will become part of the permanent collection of Oregon State University libraries. My signature below authorizes release of my thesis to any reader upon request.

*Redacted for Privacy*

Lisa N. Freeman, Author

# Table of Contents

Page

# Table of Contents (Continued)

Page

# Table of Contents (Continued)

Page

# Table of Contents (Continued)

# List of Figures

# List of Figures (Continued)

Figures Page

# List of Figures (Continued)

Figures Page

# List of Figures (Continued)

Figures Page

# List of Tables

# List of Appendices

Page

# List of Appendix Figures

# List of Appendix Tables

# Stochastic Loads on Horizontal Axis Wind Turbine Blades

## 1. Introduction

The objective of this work was to develop a method for determining stochastic loads on horizontal axis wind turbine (HAWT) blades. An important step in the design or analysis of a wind turbine is determining stochastic loads that occur on the structure. A structural dynamics model has been developed which simulates the behavior of the machine under cyclic loads, both deterministic and stochastic. By modeling two different machines and comparing the results to test data, the method can be validated. The model can then be used for further analysis to learn about the required complexity of the model. It can also be used for the design of new machines or the prediction of machine behavior under varying wind conditions.

### 1.1 Background

The cost of producing wind energy must be kept in a competitive range if it is to be a viable source of electricity. Machines are expensive to build, and this capital cost must be amortized over the life of the machine. Thus, annual costs will be reduced by longer machine life, which is primarily limited by fatigue damage. Current machines undergo $10^8$ to $10^9$ rotations of

the low speed shaft during a 20 year period of service, while the high speed shaft will undergo from 10 to 100 times as many rotations. Thus, the calculation of cyclic loads is fundamental in making wind energy economical.

The earliest documented work on wind turbine cyclic loads was done on the Smith-Putnam machine and the subsequent analyses of the War Production Board (Putnam, 1948). The cyclic loads investigated under the Smith-Putnam project were the deterministic loads caused by wind shear, yaw, gravity, and inertia.

During the resurgence of activity in wind energy in the early 1970's, cyclic load interest was focused on the above mentioned deterministic loads and cyclic loading due to tower shadow was added. The role of wind turbulence was treated, if at all, by consideration of a discrete gust.

Despite numerous wind turbine failures, the role of turbulence as a design driver was not recognized in the 1970's and the subject of stochastic loads for wind turbines remained unreported until the early 1980's. Discussion of turbulence-induced cyclic loads was held, and several papers dealing with turbulent loads were given at the Wind Turbine Dynamics Workshop in Cleveland in February 1981. Sundar and Sullivan (1981) of Purdue University reported on a turbulence simulation of the power output of various sizes of wind turbines, while Thresher, Holley, and Lin (1981) developed a simplified treatment of the turbulence. The so-called Holley model, together with linearized aerodynamics, was used by Holley, Thresher, and Jafarey (1981) to determine the wind response characteristics of horizontal-axis wind turbines. At the conclusion of the 1981 Wind Dynamics Workshop, a discussion group concerned with the state of the art in structural dynamics made the following statement: "... there was wide disagreement concerning the need for, and the value of, stochastic studies."

Analytical description of the turbulence experienced by the wind turbine started with Rosenbrock (1955) who used a simple argument to show that a rotating blade would experience higher frequency turbulence than a

non-rotating blade. Rotational turbulence models were developed by Kristensen and Frandsen (1982), Anderson (1982), and Connell (1981, 1982). Full field turbulence models were developed by Veers (1984, 1988). A disadvantage of the Veers model is that it can be computationally expensive, both in computer time and computer memory. Winkelaar (1991) suggested a faster method for the decomposition of the spectral matrix. Studies using turbulence simulation for wind turbine load analysis codes have been done by Powles and Anderson (1984), Holley (1985), Garrad and Hassan (1986), Madsen (1986), Malcolm (1987), Homicz (1987, 1988), and Wright and Butterfield (1992).

## 1.2 History of Loads Analysis

Stochastic loads caused by wind turbulence are presently universally accepted as a major consideration in designing for long life, cost effective wind turbines. The rotor blades are of particular concern not only because the blades are subject to the turbulence, but also because the blades are one of the unique items on the wind turbine which are usually designed especially for a particular wind turbine rather than being a catalog or modified off-the-shelf component. Extreme loads as evidenced by the work of Kelley (1993) and of Sutherland (1993) are also believed to be of stochastic origin.

Since cyclic loads are the key to long machine life, an estimate of the stochastic loads is an integral part of the design process. Along with several U. S. teetered rotors currently under development are a similar number of structural dynamics codes which are intended for the design, design-analysis, and analysis of teetered rotors. Additionally, there are a number of codes, both U. S. and European, which have already been developed, including the works of Thresher and Hershberg (1985), Wright and Butterfield

(1992), and Lindenburg (1993). The 1986 work of Garrad and Hassan outlined procedures for the determination of fatigue loads and in 1993 they continued to play a significant role in the determination and analysis of stochastic loads. The key ingredients for determination of stochastic loads are a structural dynamics model, a model for aerodynamic loads which are coupled to the structure motion, and turbulence input. Both frequency domain and time domain approaches have been used by Garrad, while recent U. S. efforts have focused on the time domain approach.

Another recent approach has been the use of a specialized finite element package, ADAMS, to model the behavior of wind turbines under stochastic loads (see Malcolm and Wright, 1994). Although this method has seen limited success, it requires many degrees of freedom and a significant amount of time to model even the simplest cases.

## 1.3 Scope of This Research

A current topic of considerable interest relates to the improvement of the accuracy and the reduction of time and effort needed to determine stochastic loads is, "how simple or complex must the structural dynamics model be?" This study compares calculated loads to measured loads for two contemporary lightweight teetered wind turbines using a structural model that has been incorporated into a computer code, FAST (Fatigue, Aerodynamic, Structural, Turbulence).

Before the accuracy associated with different levels of structural modeling can be ascertained, any model or code must first be validated. The FAST code results will be compared to test data from two different horizontal axis wind turbines.

The ESI-80 test results (Musial, 1985) represent a valuable data set based on the current existence of both the data tapes and the original test machine. Additionally, personnel associated with the tests are still active in the wind energy field. The original machine was at the University of Massachusetts during much of 1992 and 1993 where measurements were made on the rotor to determine the actual parameters of the test machine (Bywaters, 1992). By using the ESI-80 test data, the study relates most closely with ESI-80-like machines. The ESI-80 has a significant amount of excitation in the range from 6 per revolution to 8 per revolution. Most of the examples presented by European investigators do not exhibit large excitation energy at higher frequencies.

The AWT 26-P1 machine, also used to validate the model, is a prototype version of a more recently developed wind turbine. The available data for this machine includes blade edgewise bending moment, which allows a verification of this load prediction.

# 2. Theory

A model of the dynamic structural response of a horizontal axis wind turbine has been developed and incorporated into a computer code, FAST. The code simulates the structural response due to gravity and aerodynamic loads and is capable of modeling many geometries and degrees of freedom. The blades and tower are modeled as flexible beams which can bend in two directions, while the drive shaft can be modeled as flexible in torsion. The turbine nacelle is allowed to yaw about a vertical axis, and the rotor is allowed to teeter. The rotor rotation rate can be constant or variable. The turbine can have a tilted shaft, the teetered rotor can have a delta-3 angle, and the blades can be coned and/or pitched. Although the blades can have some structural pretwist, they are not considered flexible in torsion.

## 2.1 Identification of Structure

The dynamic response of a two bladed horizontal axis wind turbine has been modeled using five rigid bodies and three flexible bodies. There are up to 14 degrees of freedom in the system, the code allowing for operation with selected degrees of freedom turned on or off.

The first six degrees of freedom are associated with the bending motion of each blade. The blade has flexibility in two directions with the deflection modeled by two flatwise modes and one edgewise mode for each blade. The structural twisting of the blades principal axes is included in the model. Torsional motion of the blades was not included in this study. The

blade-to-blade variations can be modeled in the distribution of mass, stiffness, and blade geometry over each blade.

The seventh degree of freedom accounts for teeter motion of the rotor about a pin. A coned rotor is usually underslung so that the center of gravity of the rotor is located at the teeter pin. The FAST code includes provision for underslung rotors, as well as delta-3 and nonlinear teeter springs and/or dampers and Coulomb friction in the teeter bearing.

The eighth degree of freedom in the FAST code allows for variations in rotor speed. Thus, one can model an induction generator, start-up or shut-down operation. The ninth degree of freedom models the drive train flexibility using a linear lumped parameter model of the drive shift between the generator (or brake) and the rotor.

Yaw motion of the nacelle and rotor is the tenth degree of freedom. The yaw motion can be restrained by means of a torsional yaw spring. Either upwind or downwind rotors may be modeled in the FAST code and the main drive shaft may be set at fixed tilt angle.

The last four degrees of freedom are associated with tower motion. Two tower modes are available in the cross wind direction and two tower modes are available in the windwise direction. The tower also figures in two of the wind inputs. Wind shear is accounted for in the FAST code through a power law variation of the mean wind with distance above the ground. For downwind rotors, a tower shadow is included. The wake of the tower has a velocity deficit that is determined from the drag force on the tower.

By far the most significant loads on the rotor are the blade loads which are aerodynamic in origin. Modified strip theory along with the Glauert momentum equation is used to determine the induced velocity. The blade aerodynamics are driven by a wind model that consists of a deterministic portion made up of mean wind, shear, and tower interference, and a stochastic portion consisting of an atmospheric turbulence including time-varying wind direction. The aerodynamic loads are calculated in the blade

deformed position. The resulting nonlinear equations are solved in the time domain using a predictor corrector method with a fixed time step.

## 2.2 Equations of Motion

The equations of motion that are numerically integrated were derived using Kane's method. As with Lagrange's equations, Kane's equations are based on Newton's second law. Unlike the procedure of Lagrange, Kane's method is to reduce the vector equations of motion to special scalar equations which are fairly compact. For relatively complex systems, this procedure is far simpler, and hence less error prone, than that of Lagrange.

The following sections cover the steps that lead to the equations of motion. First, the various rigid bodies in the system are defined, as well as the coordinate systems used to define their configuration. Next, expressions for velocity and acceleration are formulated, and the aerodynamic, elastic, and drive train loads are then described along with the wind model. Finally, the method used to solve the equations of motion is outlined.

## 2.3 Mechanical Elements

FAST models a horizontal axis wind turbine with five rigid and three flexible bodies as shown in Figure 2.3-1. A flexible tower which can bend in two directions is rigidly attached to the earth. The top of the tower is fixed to a base plate, which supports a yaw bearing and nacelle. The yaw bearing allows everything atop the tower to rotate as the wind direction changes. The nacelle houses the generator and gearbox, and the entire assembly can be

tilted to account for tower clearance. The low speed shaft connects the gearbox to the rotor. The rotor consists of a hub, blades, and tip brakes. A teeter hinge may be included between the rotor and the low speed shaft, and can be offset by a delta-3 angle. The hub supports the blades, each of which can be coned and can have aerodynamic pitch and twist. The blades are flexible and have properties that can vary along their length. Each blade can be structurally pretwisted, but no torsional vibration is allowed. Bending can occur about the stiffer principal axis of the blade section (defined by one vibration mode per blade), or about the more flexible principle axis of the blade section (defined by two modes of vibration per blade).

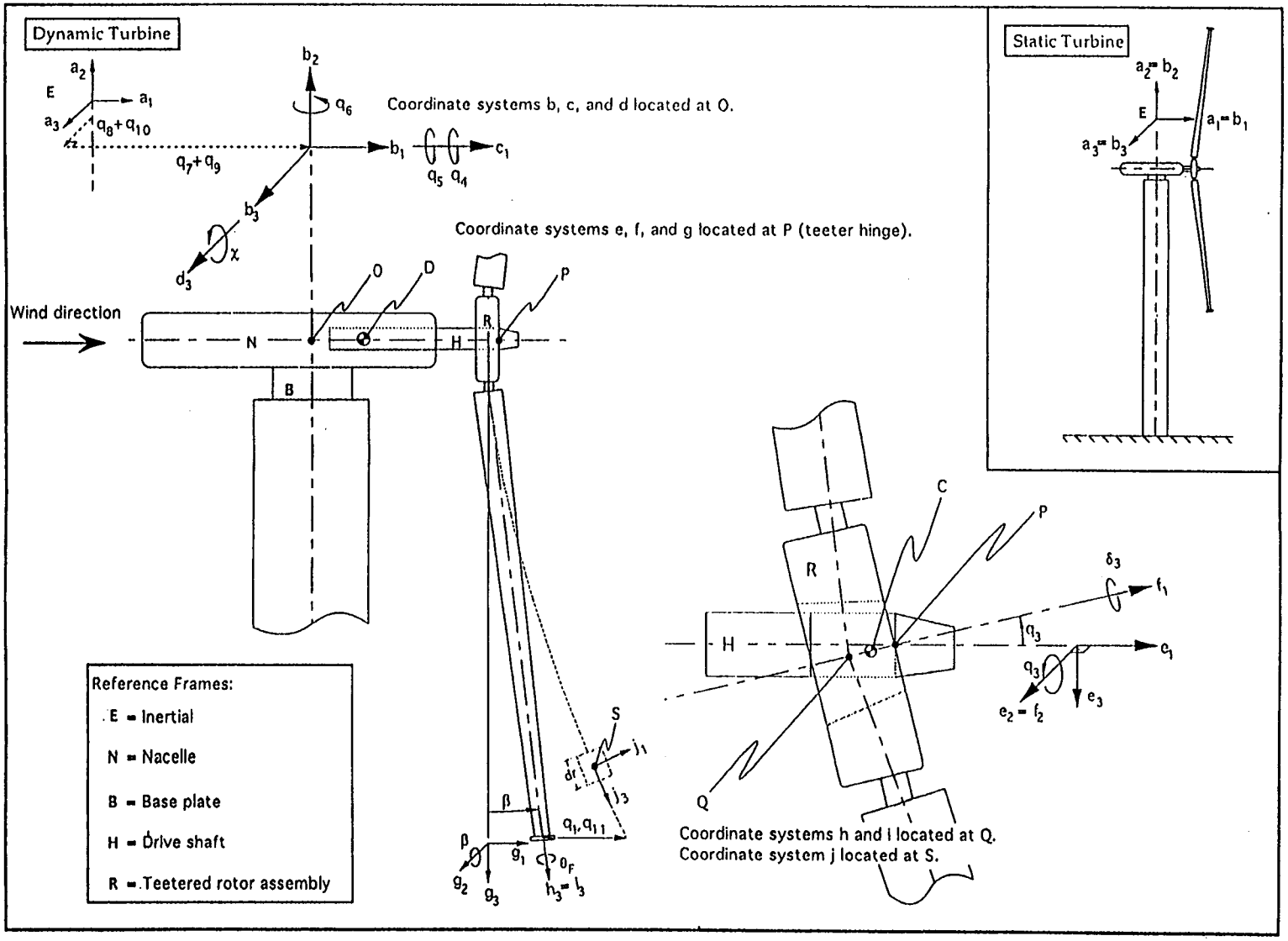


**Figure 2.3-1** Definition of Bodies, Points, and Coordinate Systems for a HAWT

## 2.4 Geometry and Coordinate Systems

To manage the analysis of orientations of the various bodies, sets of orthonormal unit vectors are defined as indicated in Table 2-1. The direction cosines that connect pairs of sets are summarized in the following relationships. Many of the orientation angles appearing in these relationships are themselves dynamic coordinates (see Table 2-2), while others are functions of dynamic coordinates or are angles inherent to the structure of the machine (see Table 2-3). The relationships are used to express the many products among vectors that constitute the terms used in the equations.

**Table 2-1** Coordinate System Locations

| Unit Vector Set | Fixed in Body | Description of Coordinate System |
|---|---|---|
| **a** | E | Inertial coordinates, fixed to earth |
| **b** | B | Tower top coordinates, fixed to base plate |
| **d** | N | Yaw coordinates, fixed to nacelle |
| **c** | N | Tilt coordinates, fixed to nacelle |
| **e** | H | Azimuth coordinates, fixed to low speed shaft |
| **g** | R | Delta-3 coordinates, fixed to rotor assembly |
| **f** | R | Teeter coordinates, fixed to rotor assembly |
| **i** | R | Coning coordinates, fixed to rotor assembly |
| **j** | S | Local blade coordinates, fixed to local blade element |

From Inertial to Tower Top:

$$\begin{vmatrix} \mathbf{a}_1 \\ \mathbf{a}_2 \\ \mathbf{a}_3 \end{vmatrix} = \begin{vmatrix} c\theta_7 & -s\theta_7 & 0 \\ s\theta_7 c\theta_8 & c\theta_7 c\theta_8 & -s\theta_8 \\ s\theta_7 s\theta_8 & c\theta_7 s\theta_8 & c\theta_8 \end{vmatrix} \begin{vmatrix} \mathbf{b}_1 \\ \mathbf{b}_2 \\ \mathbf{b}_3 \end{vmatrix}$$

where:

c = cosine of angle
s = sine of angle
$\theta_7$ = longitudinal angle of tower top slope
$\theta_8$ = lateral angle of tower top slope

From Nacelle to Yaw:

$$\begin{vmatrix} \mathbf{b}_1 \\ \mathbf{b}_2 \\ \mathbf{b}_3 \end{vmatrix} = \begin{vmatrix} cq_6 & 0 & sq_6 \\ 0 & 1 & 0 \\ -sq_6 & 0 & cq_6 \end{vmatrix} \begin{vmatrix} \mathbf{d}_1 \\ \mathbf{d}_2 \\ \mathbf{d}_3 \end{vmatrix}$$

where $q_6$ = yaw angle

From Yaw to Tilt:

$$\begin{vmatrix} \mathbf{d}_1 \\ \mathbf{d}_2 \\ \mathbf{d}_3 \end{vmatrix} = \begin{vmatrix} c\chi & -s\chi & 0 \\ s\chi & c\chi & 0 \\ 0 & 0 & 1 \end{vmatrix} \begin{vmatrix} \mathbf{c}_1 \\ \mathbf{c}_2 \\ \mathbf{c}_3 \end{vmatrix}$$

where $\chi$ = shaft tilt angle

From Tilt to Azimuth:

$$\begin{vmatrix} \mathbf{c}_1 \\ \mathbf{c}_2 \\ \mathbf{c}_3 \end{vmatrix} = \begin{vmatrix} 1 & 0 & 0 \\ 0 & cq_4 & -sq_4 \\ 0 & sq_4 & cq_4 \end{vmatrix} \begin{vmatrix} \mathbf{e}_1 \\ \mathbf{e}_2 \\ \mathbf{e}_3 \end{vmatrix}$$

where $q_4$ = azimuth angle

From Azimuth to Delta-3:

$$\begin{vmatrix} \mathbf{e}_1 \\ \mathbf{e}_2 \\ \mathbf{e}_3 \end{vmatrix} = \begin{vmatrix} 1 & 0 & 0 \\ 0 & c\delta_3 & -s\delta_3 \\ 0 & s\delta_3 & c\delta_3 \end{vmatrix} \begin{vmatrix} \mathbf{g}_1 \\ \mathbf{g}_2 \\ \mathbf{g}_3 \end{vmatrix}$$

where $\delta_3$ = delta-3 angle

From Delta-3 to Teeter angle:

$$\begin{vmatrix} g_1 \\ g_2 \\ g_3 \end{vmatrix} = \begin{vmatrix} cq_3 & 0 & sq_3 \\ 0 & 1 & 0 \\ -sq_3 & 0 & cq_3 \end{vmatrix} \begin{vmatrix} f_1 \\ f_2 \\ f_3 \end{vmatrix}$$

where $q_3$ = teeter

From Delta-3 to Coning angle:

$$\begin{vmatrix} f_1 \\ f_2 \\ f_3 \end{vmatrix} = \begin{vmatrix} c\beta & 0 & s\beta \\ 0 & 1 & 0 \\ -s\beta & 0 & c\beta \end{vmatrix} \begin{vmatrix} i_1 \\ i_2 \\ i_3 \end{vmatrix}$$

where $\beta$ = coning

From Elastic to Local:

$$\begin{vmatrix} i_1 \\ i_2 \\ i_3 \end{vmatrix} = \begin{vmatrix} c\xi & 0 & s\xi \\ 0 & 1 & 0 \\ -s\xi & 0 & c\xi \end{vmatrix} \begin{vmatrix} 1 & 0 & 0 \\ 0 & c\eta & s\eta \\ 0 & -s\eta & c\eta \end{vmatrix} \begin{vmatrix} j_1 \\ j_2 \\ j_3 \end{vmatrix}$$

where $\xi$ = local out-of-plane blade bending angle

and $\eta$ = local in-plane bending angle

There are 14 coordinates which are used in formulating the equations of motion for the two bladed machine. Table 2-2 lists and describes each. These variables are used to describe all of the motion that the wind turbine model exhibits.

Blade 1 is at an azimuth angle of $q_4$ and teeter angle of $q_3$. Since blade 2 is on the opposite side of the rotor, an azimuth angle of $q_4 + \pi$ is used. However, rotating the azimuth angle also rotates the teeter axis, so in order to keep the same teeter orientation, the opposite sign is used for the teeter angle, rate, and acceleration.

**Table 2-2** Time Varying Angles and Displacements

| Variable | Description |
|---|---|
| $q_1$ | Blade 1 flapwise tip displacement for mode 1 |
| $q_2$ | Blade 2 flapwise tip displacement for mode 1 |
| $q_3$ | Teeter angle |
| $q_4$ | Azimuth angle, rotor side |
| $q_5$ | Azimuth angle, generator side |
| $q_6$ | Yaw angle |
| $q_7$ | Longitudinal tower top displacement for mode 1 |
| $q_8$ | Latitudinal tower top displacement for mode 1 |
| $q_9$ | Longitudinal tower top displacement for mode 2 |
| $q_{10}$ | Latitudinal tower top displacement for mode 2 |
| $q_{11}$ | Blade 1 flapwise tip displacement for mode 2 |
| $q_{12}$ | Blade 2 flapwise tip displacement for mode 2 |
| $q_{13}$ | Blade 1 edgewise tip displacement for mode 1 |
| $q_{14}$ | Blade 2 edgewise tip displacement for mode 1 |

Other important angles used in the above transformations are listed in Table 2-3. Tower-top rotations are time varying since they are related to the tower degrees of freedom through the shape of the deflected tower, as shown in figure 2.4-1. Shaft tilt is represented by a tilt angle which does not change the axis of yaw. The delta-3 angle, shown in Figure 2.4-2, orients the teeter hinge so that teeter is no longer perpendicular to the unconed blade axis. Blades can be angled downwind slightly by the coning angle, $\beta$. Blade structural pretwist is represented by $\theta_s$ and orients the local axes of flapwise and edgewise bending. These angles used to define the geometry of the wind turbine are constant. The local blade element can have both out-of-

plane and in-plane rotation. The previous three angles vary along the blade so that each blade segment has a different orientation. These are shown in figure 2.4-3 through 2.4-6.

**Table 2-3** Other Angles Used in Model

| Angle | Description |
|---|---|
| $\theta_7$ | Longitudinal tower top rotation angle |
| $\theta_8$ | Latitudinal tower top rotation angle |
| $\chi$ | Shaft tilt angle |
| $\delta_3$ | Delta-3 angle (teeter hinge orientation) |
| $\beta$ | Coning angle |
| $\theta s$ | Structural pre-twist angle |
| $\xi$ | Local blade out-of-plane rotation |
| $\eta$ | Local blade in-plane rotation |

Note that the coordinate systems are defined to be right handed and all angular rotations are positive.

Some position vectors are used to define the wind turbine model. The magnitudes and directions of these vectors are listed in Table 2-4. These distances will be used in the kinematics expressions.

Finally, several points on the system are important in writing the equations of motion. These are listed in Table 2-5 and defined in Figure 2.3-1. Each of these points is attached to one or two rigid bodies or reference

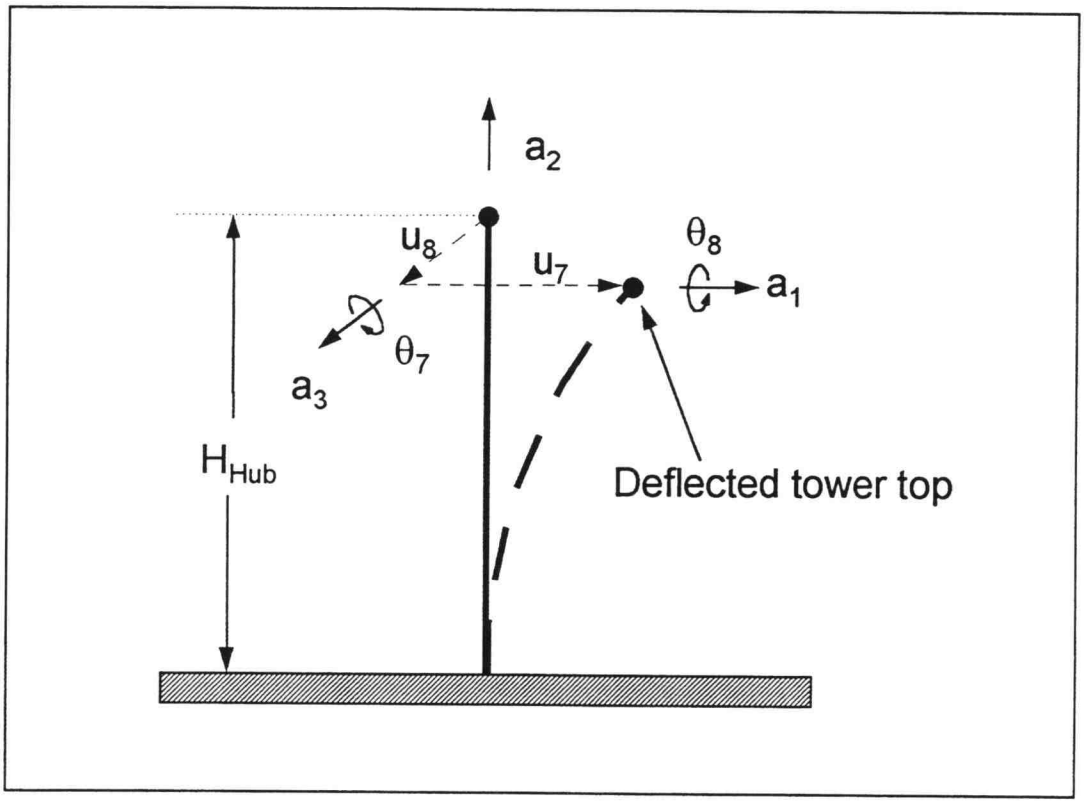


**Figure 2.4-1** Tower Bending and Location of Tower Top

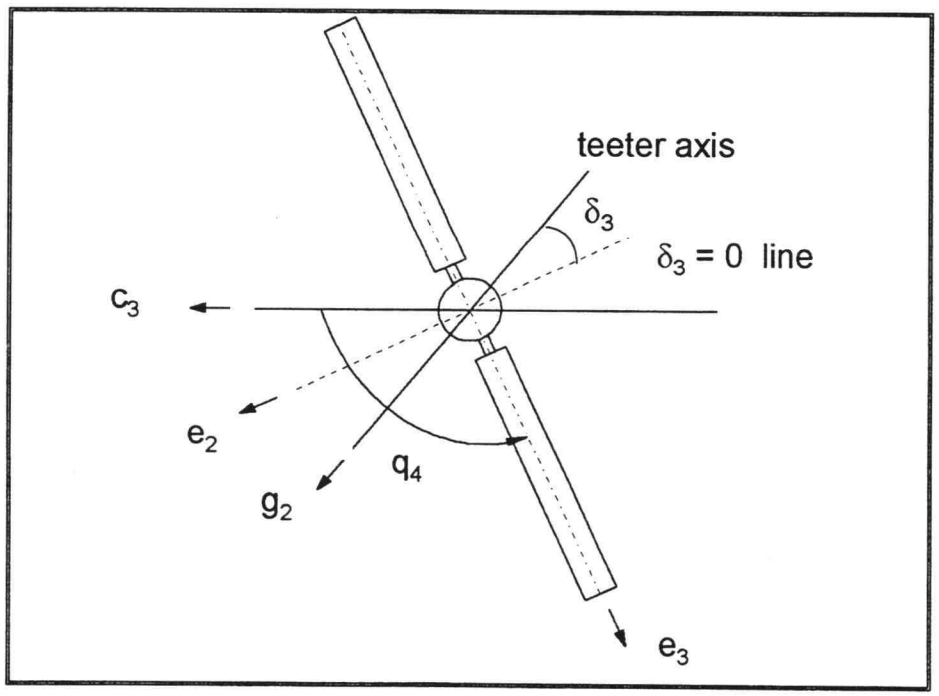


**Figure 2.4-2** Orientation of Delta-3 Angle

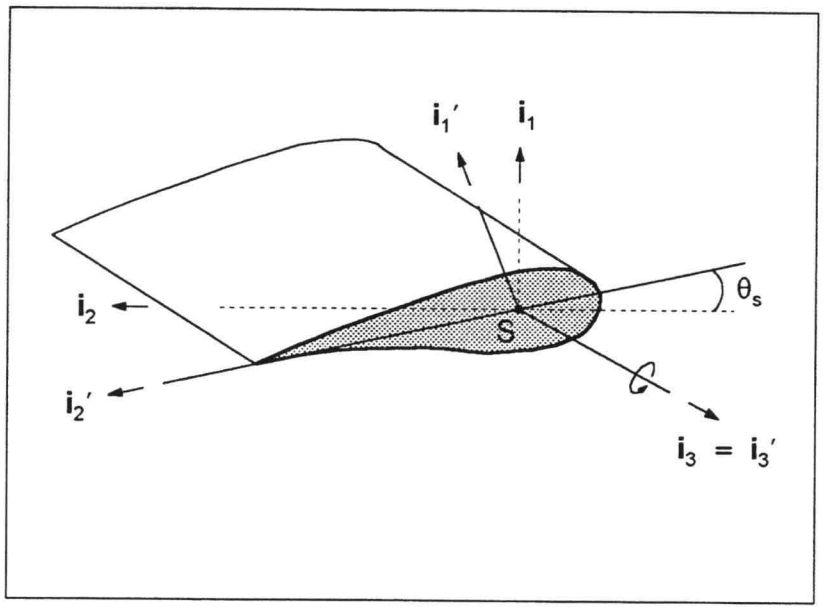


**Figure 2.4-3** Orientation of Local Blade Structural Twist Angle

**Table 2-4** Position Vectors Used in Model

| Variable | Direction | Description |
|---|---|---|
| $H_s$ | $\mathbf{a}_2$ | Height of rigid base of tower |
| $H_H$ | $\mathbf{a}_2$ | Height of flexible portion of tower |
| $D_N$ | $\mathbf{c}_1$ | Distance from tower top to teeter axis |
| $D_{NM}$ | $\mathbf{c}_1$ | Distance from tower top to nacelle center of mass |
| $R_U$ | $-\mathbf{g}_1$ | Distance from teeter pin to blade axis intersection |
| $R_{UM}$ | $-\mathbf{g}_1$ | Distance from teeter pin to hub center of mass |
| R | $\mathbf{i}_3$ | Distance from blade axis intersection to local blade element |

frames. For example, point O is the origin for both the tower top coordinates and the yaw coordinates.

**Table 2-5** Points on the System

| Point | Description |
|---|---|
| O | Tower top |
| P | Teeter hinge |
| Q | Intersection of blade inertia axes |
| S | Location of local blade segment |
| D | Mass center of nacelle |
| C | Mass center of hub |

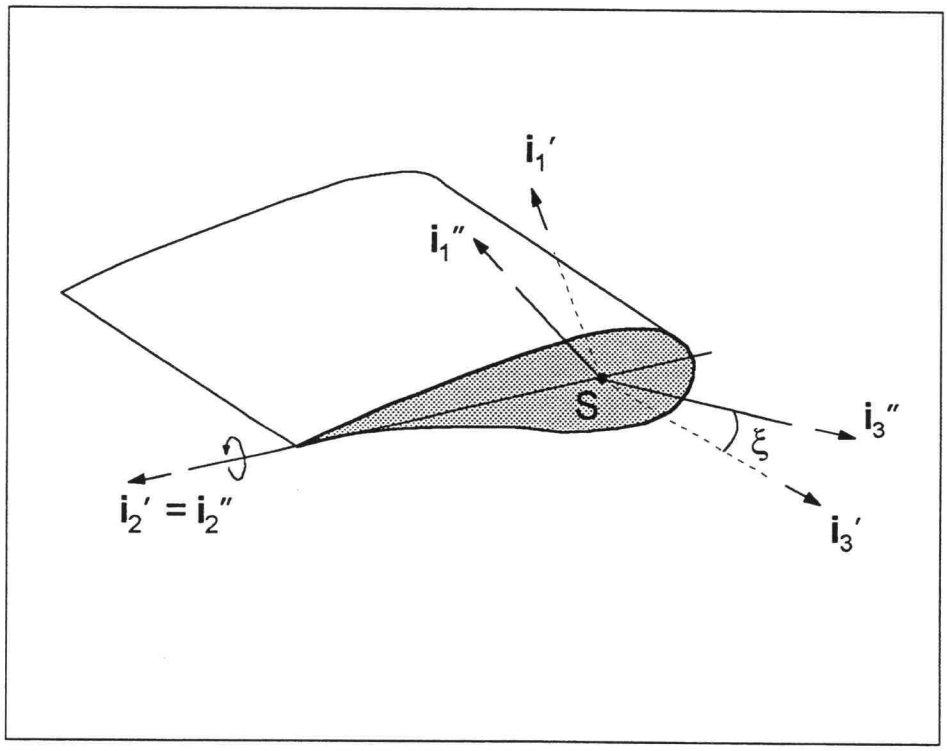


**Figure 2.4-4** Blade Flapwise Bending Angle

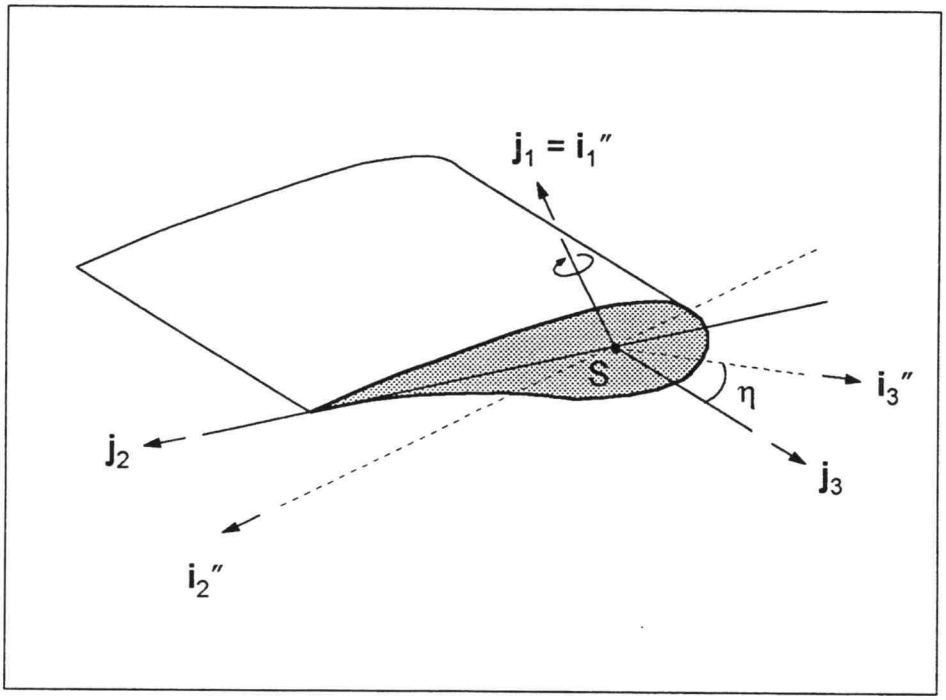


**Figure 2.4-5** Blade Edgewise Bending Angle

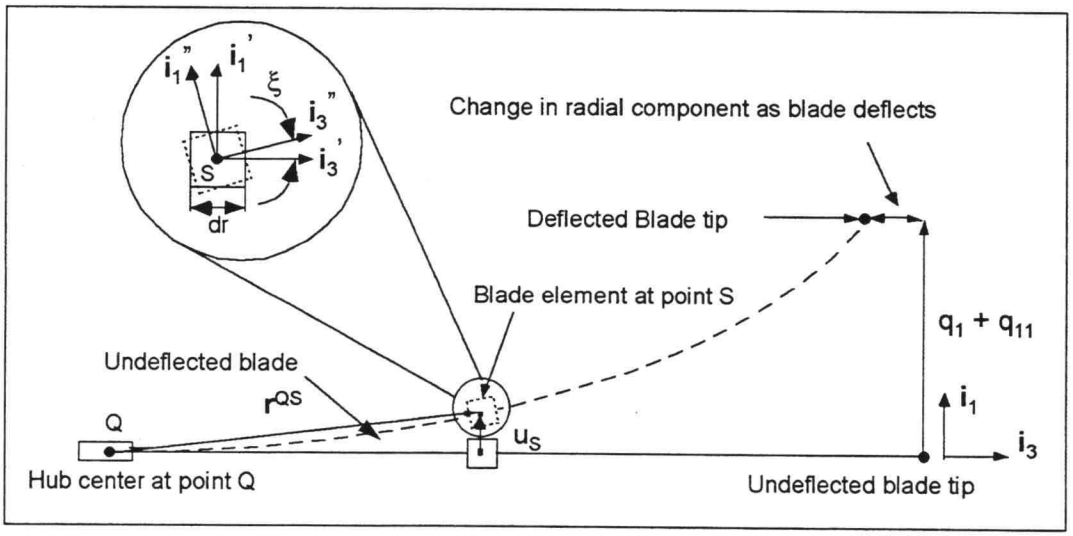


**Figure 2.4-6** Blade Bending in Flapwise Direction

## 2.5 Blade and Tower Deflections

Our treatment of flexible bodies uses an approximation so that the general deflection can be represented by only a few degrees of freedom. Both blades and tower can be treated as cantilever beams, fixed at one end and free at the other. Both have point masses attached at the free end, either the tip mass or the nacelle. The deflection of a cantilever beam can be represented as a linear combination of the known shapes of the first two vibration modes. For a flexible beam represented by only one vibration mode, the displacement anywhere on the flexible body is given as a product of the end displacement and a function which represents the normalized shape of the mode. This method is used to represent bending in two directions, and uses more than one mode in each direction to give greater accuracy. Specifically, the tower deflection in both longitudinal and lateral directions is modeled by two modes, which requires two degrees of freedom in each direction to scale the shape functions. The blade curvature in the flapwise direction is also modeled with two vibration modes, requiring two degrees of freedom for each blade. The edgewise curvature of the blade is modeled with only one mode since the flexibility in the in-plane direction is much lower. This requires a total of three degrees of freedom (and three mode shapes) for each blade.

The blades are treated as flexible beams fixed at the hub and free at the tip. Because the blade can have some structural pretwist, defining the deflection in two directions which change along the blade can be complicated. A better method is to define the total blade curvature as the combination of curvature in each direction, oriented by the structural pretwist. This curvature is resolved into in-plane and out-of-plane components which are then integrated twice to get the deflection shape. Let $f_1$ and $f_2$ be the flapwise mode shapes for the non-pretwisted blade, and g be the edgewise

mode shape for the non-pretwisted blade. For this discussion let $q_1$ represent the first flapwise tip deflection, $q_2$ the second flapwise tip deflection, and $q_3$ the edgewise tip deflection. Note that for blade 1, $q_1$, $q_2$ and $q_3$ are designated $q_1$, $q_{11}$, and $q_{13}$ in the code; and for blade 2 they are designated $q_2$, $q_{12}$, and $q_{14}$ in the code. The local curvature in the flapwise direction is

$$q_1(t)\, f_1''(z) + q_2(t)\, f_2''(z)$$

while the local edgewise curvature is

$$q_3(t)\, g''(z)$$

where z is a coordinate along the blade. If the local pre-twist angle is $\theta_o(z)$, then the local coordinate system can be transformed back to the system fixed at the blade root. The out-of-plane curvature is

$$u'' = \cos\theta_o \{q_1(t)\, f_1''(z) + q_2(t)\, f_2''(z)\} - \sin\theta_o \{q_3(t)\, g''(z)\}$$

while the in-plane curvature is

$$v'' = \sin\theta_o \{q_1(t)\, f_1''(z) + q_2(t)\, f_2''(z)\} + \cos\theta_o \{q_3(t)\, g''(z)\}$$

These can be represented by twisted shape functions, as follows:

$$u'' = q_1\, \phi_1'' + q_2\, \phi_2'' + q_3\, \phi_3''$$

$$v'' = q_1\, \psi_1'' + q_2\, \psi_2'' + q_3\, \psi_3''$$

where

$$\phi_1'' = \cos\theta_o\, q_1(t)\, f_1''(z)$$

$$\phi_2'' = \cos\theta_o\, q_2(t)\, f_2''(z)$$

$$\phi_3'' = -\sin\theta_o\, q_3(t)\, g''(z)$$

$$\psi_1'' = \sin\theta_o\, q_1(t)\, f_1''(z)$$

$$\psi_2'' = \sin\theta_o\, q_2(t)\, f_2''(z)$$

$$\psi_3'' = \cos\theta_o\, q_3(t)\, g''(z)$$

These functions can be integrated twice with respect to z, the coordinate along the blade, to get the overall mode shapes for in-plane and out-of-plane bending. The deflection of the blade in each direction can then be written as

$$u(z,t) = \Sigma_i\, q_i(t)\, \phi_i(z)$$

$$v(z,t) = \Sigma_i \, q_i(t) \, \psi_i(z) , \qquad i = 1..3$$

Because the bending blade stays the same length, the distance from the root to the local segment along the blade changes. This shortening can be expressed as

$$w(z,t) = - 1/2 \int_0^z (u'^2 + v'^2) \, d\zeta$$

or, in terms of the above functions,

$$w = - 1/2 \, \Sigma_i \, \Sigma_j \, s_{ij} \, q_i \, q_j$$

$$s_{ij} = \int_0^z ( \phi_i' \phi_j' + \psi_i' \psi_j' ) \, dz \qquad i = 1..3 \qquad j = 1..3$$

The current position of the local blade segment as it is vibrating can now be expressed in root-fixed coordinates as

$$\mathbf{u}(z,t) = u(z,t) \, \mathbf{i}_1 + v(z,t) \, \mathbf{i}_2 + \{r(z) + w(z,t)\} \, \mathbf{i}_3$$

where $\mathbf{i}_3$ is along the blade, $\mathbf{i}_1$ is in the out-of plane direction, $\mathbf{i}_2$ is in the in-plane direction, and r(z) is the distance along the undeformed blade to the current blade segment.

Components of the longitudinal and lateral displacement of the tower top are shown in Figure 2.4-1. These displacements include contributions from the first and second mode shapes in both the longitudinal, $\mathbf{a}_1$, and lateral, $\mathbf{a}_3$, directions. They are related to the tower degrees of freedom as follows:

$$u_7 = q_7 + q_9$$

$$u_8 = q_8 + q_{10}$$

where $u_7$ is the total tower top displacement in longitudinal direction and $u_7$ is the total tower top displacement in the lateral direction. The corresponding tower top rotation angles are given by:

$$\theta_7 = - (\alpha_7 \, q_7 + \alpha_9 \, q_9)$$

$$\theta_8 = \alpha_8 \, q_8 + \alpha_{10} \, q_{10}$$

where $\theta_7$ is a rotation about $\mathbf{a}_3$, $\theta_8$ is a rotation about $\mathbf{a}_1$, and the $\alpha$'s are the first derivatives of the mode shapes evaluated at the top of the tower:

$$\alpha_7 = \partial\phi_{1T} / \partial h \qquad \alpha_9 = \partial\phi_{2T} / \partial h$$

$\alpha_8 = \partial\phi_{1T} / \partial h$ $\alpha_{10} = \partial\phi_{2T} / \partial h$

where $\phi_{1T}$ and $\phi_{2T}$ represent the first and second tower bending mode shapes, which are shown in Appendix E.

## 2.6 Kinematics

Once the dynamic system is defined as a series of rigid body reference frames related by several orientation angles, the kinematics of the system can be expressed. Vectors from any of the above coordinate systems can be used, since they are easily transformed to a common coordinate system. The accelerations of points in the system can be expressed using velocities and angular velocities, which must first be computed.

The relative angular velocities between neighboring reference frames can be written and then summed. Note that the angular velocities are vectors that relate the reference frame represented by the left superscript to the reference frame represented by the right superscript. The angular velocity of the base plate in the inertial reference frame is given by

$${}^{E}\omega^{B} = \dot{\theta}_8 \mathbf{a}_1 - \dot{\theta}_7 \mathbf{a}_3$$

The angular velocity of the nacelle relative to the base plate depends on the yaw rate

$${}^{B}\omega^{N} = \dot{q}_6 \mathbf{d}_2$$

The rotor speed relates the nacelle to the shaft reference frame:

$${}^{N}\omega^{H} = \dot{q}_4 \mathbf{e}_1$$

The rotor is related to the shaft reference frame by the teeter rate.

$${}^{H}\omega^{R} = \dot{q}_3 \mathbf{f}_2$$

Once the individual angular velocities are written, they can be combined to get the angular motion of each reference frame of interest in relation to the inertial frame.

$$^{E}\omega^{N} = {}^{E}\omega^{B} + {}^{B}\omega^{N}$$

$$^{E}\omega^{H} = {}^{E}\omega^{N} + {}^{N}\omega^{H}$$

$$^{E}\omega^{R} = {}^{E}\omega^{H} + {}^{H}\omega^{R}$$

The angular velocity of the rotor in the inertial frame can be expressed by substituting the above expressions into the last one:

$$^{E}\omega^{R} = \dot{\theta}_8 \mathbf{a}_1 - \dot{\theta}_7 \mathbf{a}_3 + \dot{q}_6 \mathbf{d}_2 + \dot{q}_4 \mathbf{e}_1 + \dot{q}_3 \mathbf{f}_2$$

These angular velocities can now be used with the geometry of the structure to express the velocity of various points of interest. Velocities are also vectors, but they describe the motion of a point, the right superscript, in a particular reference frame, the left superscript. The velocity of the tower top in the inertial frame is:

$$^{E}\mathbf{v}^{O} = (\dot{q}_7 + \dot{q}_9)\, \mathbf{a}_1 + (\dot{q}_8 + \dot{q}_{10})\, \mathbf{a}_3$$

The velocity of the teeter hinge can be related to the tower top velocity as follows:

$$^{E}\mathbf{v}^{P} = {}^{E}\mathbf{v}^{O} + {}^{E}\omega^{N} \times \mathbf{r}^{OP}$$

$$\mathbf{r}^{OP} = D_N\, \mathbf{c}_1$$

where the points O and P are fixed in reference frame N, $\mathbf{r}^{OP}$ is the vector that connects the points, and $D_N$ is the distance from tower top to teeter hinge.

The velocities of point Q can be expressed in a similar manner,

$$^{E}\mathbf{v}^{Q} = {}^{E}\mathbf{v}^{P} + {}^{E}\omega^{R} \times \mathbf{r}^{PQ}$$

$$\mathbf{r}^{PQ} = - R_U\, \mathbf{f}_1$$

where points Q and P are fixed in the rotor frame, separated by the distance $R_U$.

The velocity of an individual blade segment is related to the velocity of a point on the rotor as follows:

$$^{E}\mathbf{v}^{S} = {}^{E}\mathbf{v}^{Sr} + {}^{R}\mathbf{v}^{S}$$

where Sr is the location of point S if it were fixed to the rotor (as if the blade was not flapping). Effectively the motion of the segment away from its current position is added to the motion of the current position.

$$^{E}\mathbf{v}^{Sr} = {}^{E}\mathbf{v}^{Q} + {}^{E}\boldsymbol{\omega}^{R} \times \mathbf{r}^{QSr}$$

$$\mathbf{r}^{QSr} = \mathbf{u}$$

$$^{R}\mathbf{v}^{S} = \dot{\mathbf{u}}$$

where **u** describes the location of the deflected blade segment as discussed in the previous section.

These expressions can be combined to get the velocity of a blade segment in the inertial reference frame:

$$\begin{aligned} ^{E}\mathbf{v}^{S} = {} & (\dot{q}_7 + \dot{q}_9)\,\mathbf{a}_1 + (\dot{q}_8 + \dot{q}_{10})\,\mathbf{a}_3 + (\dot{\theta}_8\,\mathbf{a}_1 - \dot{\theta}_7\,\mathbf{a}_3 + \dot{q}_6\,\mathbf{d}_2) \times D_N\,\mathbf{c}_1 \\ & - (\dot{\theta}_8\,\mathbf{a}_1 - \dot{\theta}_7\,\mathbf{a}_3 + \dot{q}_6\,\mathbf{d}_2 + \dot{q}_4\,\mathbf{e}_1 + \dot{q}_3\,\mathbf{f}_2) \times R_U\,\mathbf{f}_1 \\ & + (\dot{\theta}_8\,\mathbf{a}_1 - \dot{\theta}_7\,\mathbf{a}_3 + \dot{q}_6\,\mathbf{d}_2 + \dot{q}_4\,\mathbf{e}_1 + \dot{q}_3\,\mathbf{f}_2) \times \mathbf{u} + \dot{\mathbf{u}} \end{aligned}$$

Many of the terms in this expression contain the first time derivative of a coordinate along with some vector. This can be more easily expressed in terms of coefficients multiplied by the degree of freedom rates and other terms not of this form.

$$^{E}\mathbf{v}^{S} = \Sigma\, {}^{E}\mathbf{v}_r^{S}\, \dot{q}_r + {}^{E}\mathbf{v}_t^{S} \qquad r = 1..14$$

where $^{E}\mathbf{v}_r^{S}$ is the coefficient of the time derivative of the $r^{th}$ coordinate, and $^{E}\mathbf{v}_t^{S}$ is all of the terms that are not of this form. Notice that these coefficients are vectors, and can contain the coordinate but not their time derivatives. In this case,

$$^{E}\mathbf{v}_3^{S} = \mathbf{f}_2 \times (-R_U\,\mathbf{f}_1 + \mathbf{u}), \text{ and}$$

$$^{E}\mathbf{v}_7^{S} = \mathbf{a}_1 - \alpha_7\,\mathbf{a}_3 \times (D_N\,\mathbf{c}_1 + R_U\,\mathbf{f}_1 + \mathbf{u})$$

The vector coefficients are called partial velocities. The dot product of these partial velocities with the equations of motion produces a greatly simplified system of equations, which is the main advantage of Kane's method.

The equation for the angular motion of the rotor frame can be put into a similar form:

$$^{E}\boldsymbol{\omega}^{R} = \Sigma\, {}^{E}\boldsymbol{\omega}_r^{R}\, \dot{q}_r + {}^{E}\boldsymbol{\omega}_t^{R} \qquad r = 1..14$$

where

$$^{E}\boldsymbol{\omega}_3^{R} = \mathbf{f}_2,$$

$^{E}\omega_6^{R} = \mathbf{d}_2$,

$^{E}\omega_7^{R} = -\alpha_7 \mathbf{a}_3$, and

$^{E}\omega_t^{R} = 0$

The velocities of points C and D can be expressed similarly to velocities of points Q and P respectively, only the distances are different.

$\mathbf{r}^{PC} = -R_{UM} \mathbf{f}_1$

$\mathbf{r}^{OD} = D_{NM} \mathbf{c}_1$

where $R_{UM}$ is the distance from teeter hinge to the mass center of the hub, and $D_{NM}$ is the distance along the shaft from the yaw axis to the mass center of the nacelle.

The acceleration is just the time derivative of the velocity, so starting with the simplified form of the velocity:

$$^{E}\mathbf{a}^{S} = \Sigma\, ^{E}\mathbf{v}_r^{S}\, \ddot{q}_r + \Sigma\, ^{d}/_{dt}\, ^{E}\mathbf{v}_r^{S}\, \dot{q}_r + ^{d}/_{dt}\, ^{E}\mathbf{v}_t^{S} \qquad r = 1..14$$

Notice that the second and third terms contain only first time derivatives of the coordinate, so this expression is already in the desired form if

$$^{E}\mathbf{a}_t^{S} = \Sigma\, ^{d}/_{dt}\, ^{E}\mathbf{v}_r^{S}\, \dot{q}_r + ^{d}/_{dt}\, ^{E}\mathbf{v}_t^{S} \qquad r = 1..14$$

Once the accelerations are expressed, we need to consider the forces acting on the system.

## 2.7 Kinetics

Once expressions for the accelerations and external forces are determined, these can be combined to form the equations of motion. These can be put into Newton's Second Law, $\mathbf{F} = m\mathbf{a}$, or $\mathbf{F} - m\mathbf{a} = 0$. Kane has simplified these vector equations by taking components in the direction of the partial velocities defined in the previous section. Each partial velocity produces a scalar equation related to a particular coordinate of the form

$$F_r + F_r^{*} = 0, \qquad r = 1, 2, ..14$$

where

$F_r = \Sigma\ {}^{E}\mathbf{v}_r^{S} \cdot F_i$ i = sum over all external forces

$F_r^* = \Sigma\ {}^{E}\mathbf{v}_r^{S} \cdot (-m_i\ \mathbf{a}_i)$ i = sum over all mass particles

These quantities are called generalized active forces and generalized inertia forces, respectively. The generalized active forces include all external forces acting on the body, such as aerodynamic forces, gravity, drive train forces, and forces due to the elastic bending of the blades and tower. These are detailed in the next section.

The generalized inertia forces include all effects of linearly and angularly accelerating mass. There will be some contribution from all bodies that have mass, including the tower, nacelle, hub, and blades. These can be summed to get the total generalized inertia force:

$$F_r^*|_{Total} = F_r^*|_{Tower} + F_r^*|_{Nacelle} + F_r^*|_{Hub} + F_r^*|_{Blades}$$

The hub contains all mass in the rotor assembly except that contained in the blades and tip brakes. The contribution to inertia forces from the hub mass, $m_{Hub}$, is given by:

$$F_r^*|_{Hub} = -\ {}^{E}\mathbf{v}_r^{C} \cdot m_{Hub}\ {}^{E}\mathbf{a}^{C} - {}^{E}\omega_r^{R} \cdot [\mathbf{I}_{Hub} \cdot {}^{E}\alpha^{R} + {}^{E}\omega^{R} \times \mathbf{I}_{Hub} \cdot {}^{E}\omega^{R}]$$

where ${}^{E}\mathbf{v}_r^{C}$ is the partial velocity of the hub mass center for the $r^{th}$ degree of freedom, ${}^{E}\mathbf{a}^{C}$ is the acceleration of the hub mass center, ${}^{E}\omega_r^{R}$ is the partial angular velocity of the rotor for the $r^{th}$ degree of freedom, and ${}^{E}\alpha^{R}$ is the angular acceleration of the rotor assembly, all in the inertial reference frame. The inertia matrix of the hub about its mass center, $\mathbf{I}_{Hub}$, is determined from the inertia of the hub about the teeter axis.

The nacelle mass includes everything on top of the tower that yaws except the rotor assembly. The mass of individual components is described in terms of the total mass, the location of the mass center, and the total inertia of the components about the yaw axis. The rotational inertia of the gears and other internal mechanisms is only used in the case when the rotor

speed can vary. The generalized inertia forces for the nacelle assembly is given by an equation similar to that for the hub:

$$F_r^*|_{Nacelle} = - {}^E\mathbf{v}_r^D \cdot m_{Nacelle}\, {}^E\mathbf{a}^D - {}^E\omega_r^N \cdot [\mathbf{I}_{Nacelle} \cdot {}^E\alpha^N + {}^E\omega^N \times \mathbf{I}_{Nacelle} \cdot {}^E\omega^N]$$

where ${}^E\mathbf{v}_r^D$ is the partial velocity of the nacelle mass center for the $r^{th}$ degree of freedom, ${}^E\mathbf{a}^D$ is the acceleration of the nacelle mass center, ${}^E\omega_r^N$ is the partial angular velocity of the nacelle for the $r^{th}$ degree of freedom, and ${}^E\alpha^N$ is the angular acceleration of the nacelle assembly, all in the inertial reference frame. The inertia matrix of the nacelle about its mass center, $\mathbf{I}_{Nacelle}$, is determined from the inertia of the nacelle about the yaw axis.

Contributions from the flexible tower to the generalized inertia forces depend on its distributed mass. The generalized inertia force for the entire tower is the integral of the inertia force for each tower segment. If $\mu_{Tower}$ is the mass per unit length of the local tower segment, the generalized inertia forces are given by

$$F_r^*|_{Tower} = - \int_0^H \mu_{Tower}\, {}^E\mathbf{v}_r^T \cdot {}^E\mathbf{a}^T\, dz$$

where T is the local tower element, ${}^E\mathbf{v}_r^T$ is the partial velocity of the local tower element for the $r^{th}$ degree of freedom, and ${}^E\mathbf{a}^T$ is the acceleration of the tower element. The velocity of the tower element is given by

$${}^E\mathbf{v}^T = (q_7\, \phi_{1T} + q_9\, \phi_{2T})\, \mathbf{a}_1 + (q_8\, \phi_{1T} + q_{10}\, \phi_{2T})\, \mathbf{a}_3$$

$${}^E\mathbf{v}^T = \Sigma\, {}^E\mathbf{v}_r^T\, q_r \qquad r = 1..14$$

so that the non-zero partial velocities are

$${}^E\mathbf{v}_7^T = \phi_{1T}\, \mathbf{a}_1 \qquad {}^E\mathbf{v}_8^T = \phi_{1T}\, \mathbf{a}_3$$

$${}^E\mathbf{v}_9^T = \phi_{2T}\, \mathbf{a}_1 \qquad {}^E\mathbf{v}_{10}^T = \phi_{2T}\, \mathbf{a}_3$$

where $\phi$'s are the tower shape functions which vary with z, the location of the current element, T. The acceleration of T is just the time derivative of the velocity,

$${}^E\mathbf{a}^T = {}^d/_{dt}\, {}^E\mathbf{v}^T = \Sigma\, {}^E\mathbf{v}_r^T\, \ddot{q}_r \qquad r = 7..10$$

Notice that the partial velocities are constant over time. This expression can be substituted into the expression for the generalized inertia force to give

$$F_r^* |_{Tower} = - \int_0^H \mu_{Tower} \, {}^E\mathbf{v}_r^T \cdot {}^E\mathbf{v}_r^T \ddot{q}_r \, dz$$

When the above expressions for the partial velocities are substituted into this equation, the terms involving $\mathbf{a}_1 \cdot \mathbf{a}_3$ go to zero. The others are of the form:

$$F_7^* |_{Tower} = - \int_0^H \mu_{Tower} \, \phi_{1T} \, \phi_{1T} \, dz \, \ddot{q}_7 - \int_0^H \mu_{Tower} \, \phi_{1T} \, \phi_{2T} \, dz \, \ddot{q}_9$$

Notice that because of orthogonality of the first two modes the second term will also go to zero.

The flexible blades contribute to the generalized inertia forces in a similar manner.

$$F_r^* |_{Blades} = - \int_0^{RT} \mu_{Blade} \, {}^E\mathbf{v}_r^{S1} \cdot {}^E\mathbf{a}^{S1} \, dr_1 - \int_0^{RT} \mu_{Blade} \, {}^E\mathbf{v}_r^{S2} \cdot {}^E\mathbf{a}^{S2} \, dr_2$$

where $S_1$ and $S_2$ are the local blade elements for blades 1 and 2, respectively, $R_T$ is the distance to the blade tip, and $\mu_{Blade}$ is the mass of the local blade element. This can be simplified in a manner similar to the tower equations, but the equations are still quite lengthy.

All of these expressions are combined to give a complete set of expressions for the generalized inertia forces. Once the generalized active forces are found, these can be combined to give the complete equations of motion, which can then be solved numerically.

## 2.8 Generalized Active Forces

The generalized active forces are composed of several different types of forces acting on the wind turbine. These include aerodynamic forces, gravity, drive train forces, and elastic restoring forces of the flexible bodies. The total contribution to the active forces is given by:

$$F_r|_{Total} = F_r|_{Aero} + F_r|_{Gravity} + F_r|_{Drive} + F_r|_{Elastic}$$

Each of these forces are described in the sections that follow.

### 2.8.1 Aerodynamic Loading

The major loading on the wind turbine blades is due to the aerodynamic forces of lift and drag. For unit span of the blade, the incremental lift and drag forces are

$$L = {}^1/_2 \rho W^2 c C_L$$

$$D = {}^1/_2 \rho W^2 c C_D$$

where $\rho$ is the ambient air density, c is the local blade chord length, $C_L$ and $C_D$ are the local sectional lift and drag coefficients, and W is the speed of the air relative to the blade. The local relative wind speed W contains contributions from the local wind, the rigid body motion of the blade due to rotation about the drive shaft, teeter and yaw axes, the flexible body motion of the blades and tower, and a contribution due to induction. The induced velocity is determined using strip theory wherein the local force on the blades due to lift is equated to the momentum flux. The blade force is based on the flow relative to the blade and contains the induced velocity explicitly in the velocity squared term and also contains the induced velocity implicitly in the lift coefficient and in the various trigonometric functions that are used to obtain the component of the blade force in the direction of the momentum flux.

The momentum flux through a segment of the rotor disk is obtained using Glauert's Momentum Equation. Whereas the blade force involves the flow relative to the blade, the momentum flux is determined in an inertial reference frame. The induced velocity appears both explicitly and implicitly in the momentum flux as well as in the blade force so that the induction must be solved for using iteration. A significant amount of computing time is used to determine the local induction at each time step.

The iteration process neglects the effects of the tangential component of the induced velocity, as well as the effects of turbulence. The effects of turbulence are ignored during the iteration because it is assumed that

turbulence does not have a fully developed wake and, therefore, does not contribute significantly to the induced velocity. Once the iteration process is completed, turbulence is used in determining the final aerodynamic coefficients.

When the induction is determined, the aerodynamic force per unit span transmitted to the blade is

$$\mathbf{f}_A = [L \cos \phi + D \sin \phi]\, \mathbf{i}_1 + [\, - L \sin \phi + D \cos \phi]\, \mathbf{i}_2$$

where $\phi$ is the relative inflow angle of the blades. Note that there is no $\mathbf{i}_3$ or spanwise component in the above equation.

The total aerodynamic generalized active force is then determined from the integral along the span

$$F_r|_{Aero} = \int_0^R {}^E\mathbf{v}_r^{S1} \cdot \mathbf{f}_A \, dr_1 + \int_0^R {}^E\mathbf{v}_r^{S2} \cdot \mathbf{f}_A \, dr_2$$

where subscripts 1 and 2 refer to the blade number. The aerodynamic forces on the tower and nacelle could be included in a similar manner, but not have been accounted for in this study.

The lift and drag coefficients are based on airfoil data in the form of either a curve fit or table which gives the variation with the local angle of attack and the thickness.

Dynamic stall can also be accounted for in the calculation of aerodynamic forces. Dynamic stall occurs when the airfoil section is near stall. A rapid change in angle of attack causes a vortex to be shed over the top surface of the airfoil, producing an extra lift followed by a rapid decrease in lift until the stall point is reached. In this case, the lift and drag are functions of not only the angle of attack but also its time rate of change.

### 2.8.2 Blade Internal Forces

The bending of flexible, elastic bodies produces forces which tend to restore the bodies to their undeflected position. There is also some internal structural damping which dissipates the elastic energy stored in the blade.

#### 2.8.2.1 Elastic Restoring Forces

The generalized active forces based on these restoring forces can be computed from the potential energy, V, of a bent beam:

$$F_r|_{Elastic} = \partial V / \partial q_r$$

For the tower, the potential energy of the bent tower is expressed as

$$V_{Tower} = {}^1/_2 (k_{7\,7}\, q_7^2 + k_{8\,8}\, q_8^2) + {}^1/_2 (k_{9\,9}\, q_9^2 + k_{10\,10}\, q_{10}^2)$$

where $k_{7\,7}$, $k_{8\,8}$, $k_{9\,9}$, and $k_{10\,10}$ are stiffness terms given by:

$$k_{7\,7} = k_{8\,8} = \int_0^H \sigma_{Tower} (\phi_{1T}'')^2\, dz - \int_0^H m_{Tower}\, g\, (\phi_{1T}')^2\, dz$$

$$k_{9\,9} = k_{10\,10} = \int_0^H \sigma_{Tower} (\phi_{2T}'')^2\, dz - \int_0^H m_{Tower}\, g\, (\phi_{2T}')^2\, dz$$

where $\sigma_{Tower}$ is the local tower flexural rigidity, g is the gravitational constant, and $m_{Tower}$ is the mass of everything above current tower element, including the nacelle, the rotor, and part of the tower. The first part of the expression comes from the strain energy of a bent beam, while the second term is the reduction in gravitational potential caused by axial compression.

For each blade, the potential energy expression is similar. Again, let the flapwise modes be represented by $q_1$ and $q_2$ and the edgewise mode be $q_3$.

$$V_{Blade\,1} = k_{1\,1}\, q_1^2 + 2\, k_{1\,2}\, q_1\, q_2 + k_{2\,2}\, q_2^2 + k_{3\,3}\, q_3^2$$

where

$$k_{ij} = {}^1/_2 \int_0^R EI_{Flap}\, f_i''\, f_j''\, dr \qquad i = 1, 2 \qquad j = 1, 2$$

$$k_{33} = {}^1/_2 \int_0^R EI_{Edge}\, (g'')^2\, dr$$

where $EI_{Flap}$ is the flapwise blade stiffness, $EI_{Edge}$ is the edgewise blade stiffness, the f's and g are the blade deflections defined previously in section 2.5. Note that for blade 1, $q_1$, $q_2$ and $q_3$ become $q_1$, $q_{11}$, and $q_{13}$; and for blade 2 they become $q_2$, $q_{12}$, and $q_{14}$.

#### 2.8.2.2 Internal Structural Damping

Part of the response is reduced because of structural damping. This is accounted for with a simple model known as *Rayleigh* or *proportional* damping (Cook et al). The structural damping is assumed to be linearly proportional to the blade stiffness calculated above. This method tends to damp out the higher frequencies faster than the lower ones. Although this method is commonly used, there is really no indication whether or not it is valid.

### 2.8.3 Drive Train Loading

There are four options available for modeling variations in shaft rotational speed. These include constant rotational speed, induction generator, start up, and shut down. Additionally, drive shaft flexibility may be included with all these options except the constant rotor speed case.

Significant drive train loads can occur during starting and stopping operations. During start up, the rotor starts as a result of the generator

acting as a motor. Here the drive shaft, particularly the low speed shaft, acts as a torsional spring and may cause large torsional oscillations.

For start up, the shaft speed and torque are modeled by three curve fits over the motor side of the curve shown in Figure 2.8-1. These curve fits are based on motor start up torque, $Q_0$, slope of linear region curve, $C_e$, and the synchronous speed, $\Omega_0$, all for the generator side of the shaft.

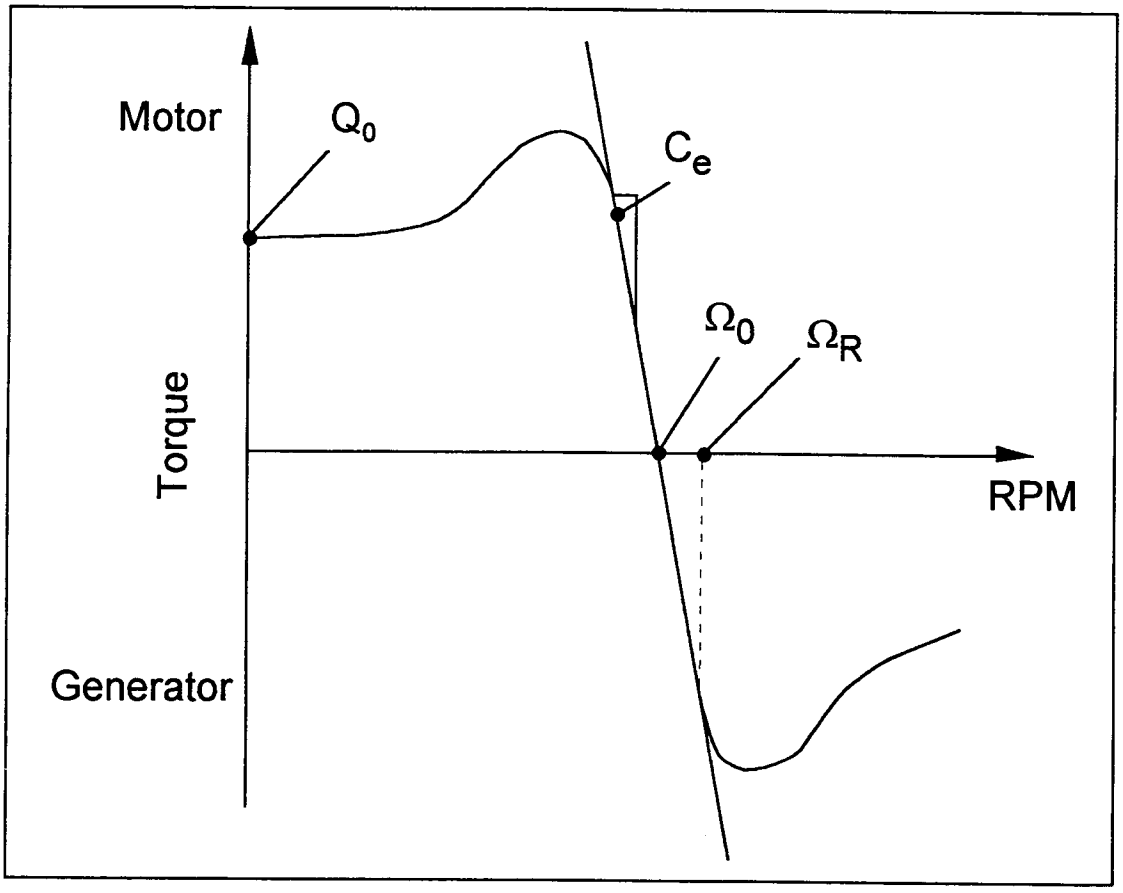


**Figure 2.8-1** Variation of Shaft Speed with Torque

For shut down or braking of the rotor, the drive train torque is modeled over the negative, linear region and is given by

$$T_{Brake} = - \text{sign}(\dot{q}_5) \left[1 - 0.2 \left(\dot{q}_5 / \Omega_0\right)^2\right] Q_B$$

where sign() gives the algebraic sign of the quantity in parenthesis, returning only +1 or -1, and $Q_B$ is the specified mechanical brake torque.

Induction generators are commonly used in wind turbines because of their ability to control the rotor during start up and shut down. For the induction generator option, the drive train torque is given by:

$$T_{Gen} + T_{Electrical} + T_{Losses}$$

where

$$T_{Electrical} = c_e n^2 (\dot{q}_5 - \Omega_0)$$

$$T_{Losses} = n [ T_{Fixed} (\dot{q}_5 / \Omega_0 ) + T_{Variable} \{ (\dot{q}_5 - \Omega_0 ) / (\Omega_R - \Omega_0) \}^2 ]$$

$$T_{Fixed} = f ( 1/ \eta_{Gen} - 1 ) P_{Rated} / ( n \Omega_R )$$

$$T_{Variable} = (1 - f) ( 1/ \eta_{Gen} - 1 ) P_{Rated} / ( n \Omega_R )$$

where f is the fixed loss fraction, $\eta_{Gen}$ is the maximum generator efficiency, and $P_{Rated}$ is the generator rated power output.

For cases involving a flexible drive shaft, the drive train between the rotor and generator is modeled as a single equivalent shaft characterized by a linear torsional spring, $k_D$, and a linear torsional damper, $c_D$. The equivalent drive shaft is massless and is modeled as an equivalent low speed shaft as shown in Figure 2.8-2. The drive train torque is then given by:

$$T_{Shaft} = k_D (q_4 - q_5) + c_D (\dot{q}_4 - \dot{q}_5)$$

where $k_D$ and $c_D$ are constants.

The generator armature, rotor brake, and other items with significant rotational inertias on the high speed shaft are lumped together to form one rotational generator inertia, $I_A$. The equation for the fifth degree of freedom acceleration is then given by:

$$\ddot{q}_5 = ( \eta_{GB} T_{Shaft} - T_{Gen} ) / ( n^2 I_A )$$

where $\eta_{GB}$ is the gearbox efficiency, n is the gearbox step-up ratio, and $T_{Gen}$ takes on values appropriate for motor start-up, induction generator, or shut-down.

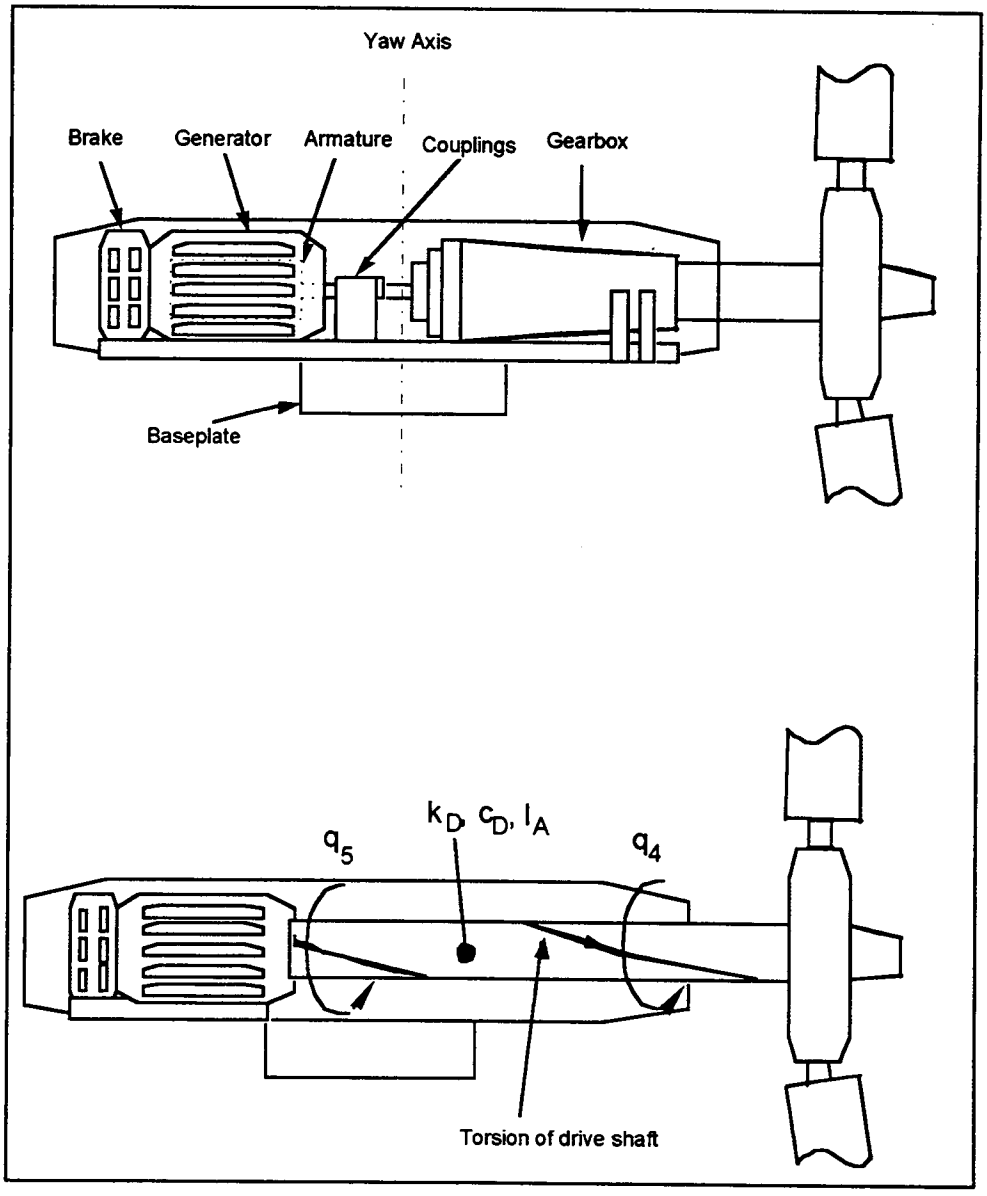


**Figure 2.8-2** Turbine Drive Train as Modeled in FAST

## 2.9 Wind Model

The wind applied to the turbine is made up of a deterministic portion and a stochastic portion. The mean wind is uniform and steady, coming from a prescribed direction which can vary over time. This steady wind input is then modified to include the effects of tower shadow, if the rotor is downwind from the tower, and wind shear, to account for the earth's boundary layer. Finally, if turbulence is considered, it is added to this steady wind. The final local wind vector is used to determine the relative velocity over a particular blade segment.

### 2.9.1 Tower Shadow

If the tower is upwind of the rotor, its wake affects the aerodynamic loads on the blades. The wind velocity seen by each blade is reduced as it pass through the wake once per revolution. This acts as a forcing function with a once per revolution frequency, which may excite any component of the system that has a natural frequency near this frequency. The tower shadow or wake is treated as a reduction in wind velocity of the form:

$$V = V_0 [\, 1 - \varepsilon \cos^2 (\pi\, y / L\,) \,]$$

where V is the lower velocity in the wake, $V_0$ is the local free stream velocity, $\varepsilon$ is the velocity deficit in the center of the wake, y is the horizontal distance from the center of the wake, and L is the width of the wake. The shape of the wake is shown in Figure 2.9-1. The parameters are determined by equating the drag force on the tower with the momentum loss between the uniform upwind stream and the deficit in the downstream wind. The center velocity deficit is based on the tower diameter, d, and the drag coefficient of the tower, $c_D$, as:

$$\varepsilon = {}^{2}/_{3} \{ 1 - \sqrt{[ 1 - (3 c_D d) / L ]} \}$$

This expression for the velocity deficit is only applied when the blade is in the wake region.

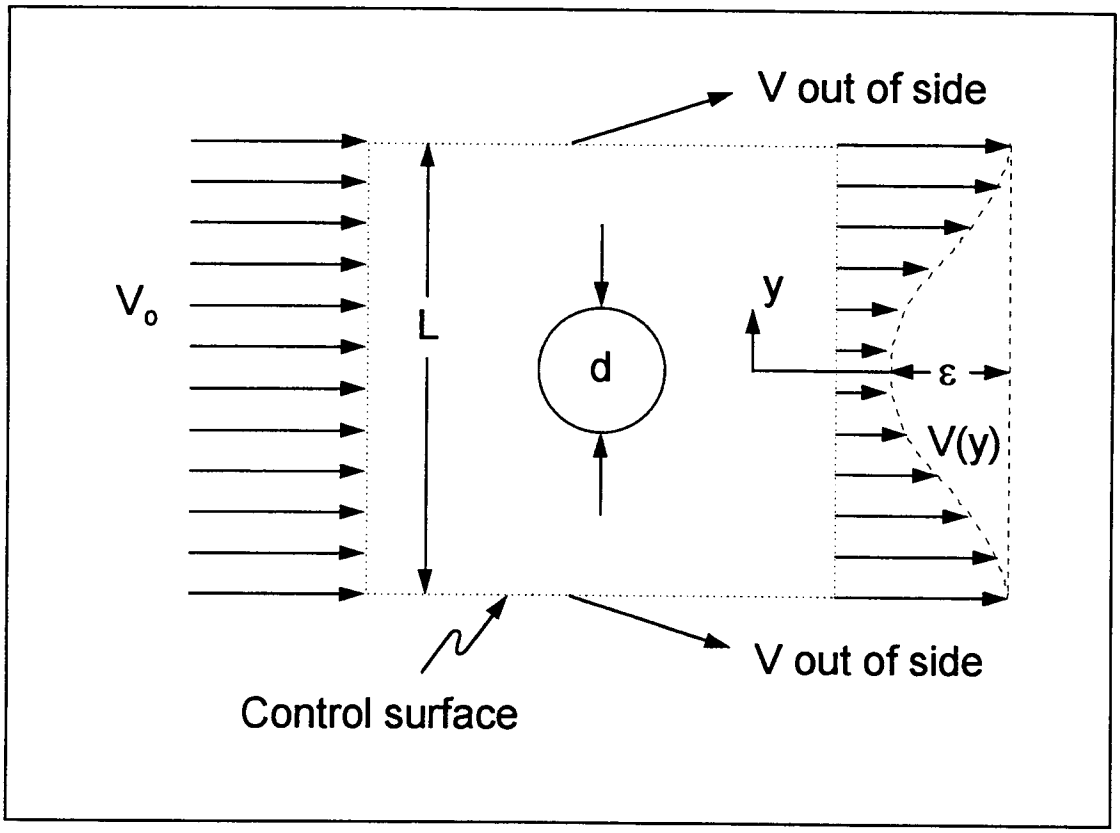


**Figure 2.9-1** Tower Shadow

### 2.9.2 Wind Shear

Wind shear occurs when the wind velocity decreases with height near the ground because of the earth's boundary layer. The velocity profile of the wind inside this boundary layer is assumed to have a shape given by a power

law expression, with the mean wind velocity at the hub height specified. The wind speed at the current location is given by

$$V = V_0 [1 + z/H ]^{\eta}$$

where $V_0$ is the mean wind velocity at the hub height, z is the vertical distance from the hub, H is the hub height, and $\eta$ is a power law exponent, usually between 0.1 and 0.2, with 0.2 indicating rougher terrain. The velocity profile of the wind is shown in Figure 2.9-2.

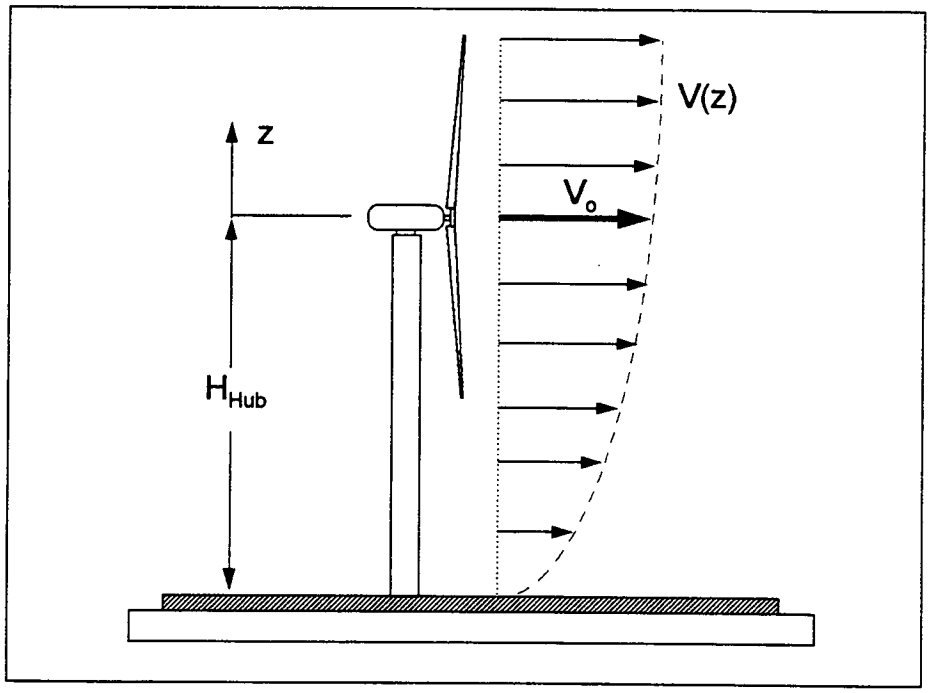


**Figure 2.9-2** Wind Shear

### 2.9.3 Turbulence

Turbulence in the wind can be accounted for by one of two different methods. The first turbulence model that can be used is the Sandia Three-Dimensional Wind Simulation (Veers, 1984). This gives a rotationally

sampled longitudinal turbulence component for each blade at one point on the blade. Each value represents the change in wind velocity due to turbulence. These values are superimposed on the steady component of the wind which already includes the effects of tower shadow and wind shear. In order to account for varying wind direction, a specified wind direction can be combined with the two dimensional turbulence simulation. This is shown in Figure 2.9-3. See Appendix B for more detail.

Another method of modeling wind turbulence is to generate a full three dimensional field of turbulent wind values and interpolate between them to get values at a particular location. In this case, the array of

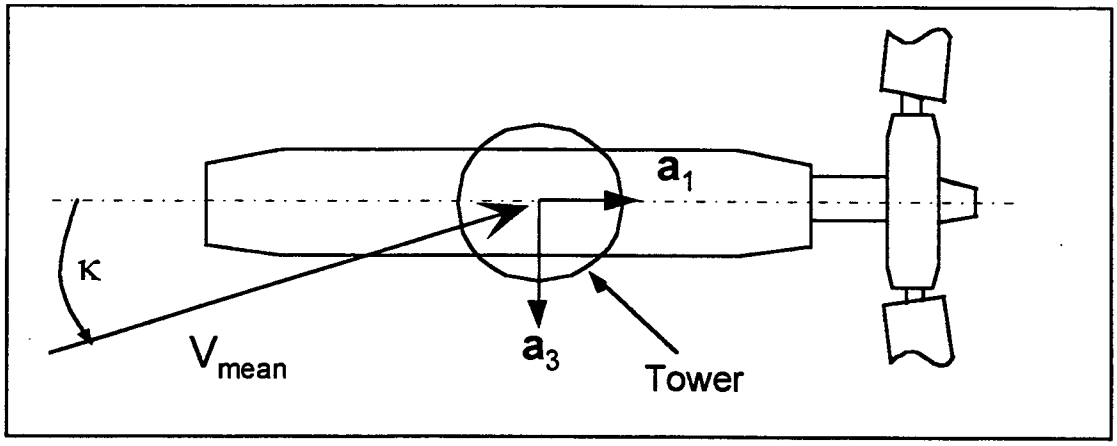


**Figure 2.9-3** Variable Wind Angle (Top View of Turbine)

turbulence values is read in initially and interpolated to give three components of wind once the current blade segment location is known. The turbulence field accounts for varying wind direction and can also include wind shear.

## 2.10 Numerical Solution Technique

The numerical solution to the equations of motion is computed at each time step. Once the equations of motion for the 14 degrees of freedom are formulated from $F_r + F_r^* = 0$, they can be put in the form

$$\Sigma\, C_{rs}\, \ddot{q}_s + f_r(\dot{q}, q) = 0 \qquad r = 1..14$$

where $C_{rs}$ are the known coefficients of the accelerations and $f_r$ are the functions containing lower order terms. This can also be expressed in matrix form:

$$\begin{vmatrix} C_{11} & C_{12} & \cdots & \cdots & \cdots & C_{1\,14} \\ C_{21} & & & \vdots & & \vdots \\ \vdots & & & \vdots & & \vdots \\ \vdots & & \cdots & C_{rs} & \cdots & \vdots \\ \vdots & & & \vdots & & \vdots \\ \vdots & & & \vdots & & \vdots \\ C_{14\,1} & \cdots & \cdots & \cdots & \cdots & C_{14\,14} \end{vmatrix} \begin{vmatrix} \ddot{q}_1 \\ \ddot{q}_2 \\ \vdots \\ \ddot{q}_s \\ \vdots \\ \ddot{q}_{13} \\ \ddot{q}_{14} \end{vmatrix} = \begin{vmatrix} -f_1(\dot{q}_1, q_1) \\ -f_2(\dot{q}_2, q_2) \\ \vdots \\ -f_r(\dot{q}_r, q_r) \\ \vdots \\ -f_{13}(\dot{q}_{13}, q_{13}) \\ -f_{14}(\dot{q}_{14}, q_{14}) \end{vmatrix}$$

with the accelerations and their known coefficients on one side, and functions containing lower order terms on the other. This matrix equation can be solved for the accelerations using a matrix inversion method, in this case Gauss elimination. The resulting differential equations can be solved with a fourth order Adams-Bashforth predictor and an Adams-Moulton corrector. Since this method is not self starting, a fourth order Runge-Kutta method is used for the first four time steps. The predictor method is used to estimate the lower order terms that make up the functions on the right side of the equations. These are used to form the above matrix equation which is solved for the accelerations. These are used to improve the estimate made by the predictor. After several iterations, the corrector is used to make a final

estimate, and a final determination of the acceleration is made. This gives the final solution for this time step.

The size of the time step is determined by a number of considerations. First, since the FFT (fast Fourier transform) is used to compute the rotationally sampled turbulence, the number of time steps for one revolution is taken as a multiple of two. Second, the highest natural frequency in the system, usually blade edgewise bending mode or second flatwise bending mode, requires a smaller time step so that the high frequency modes may be accurately modeled. Finally, the interaction between blade, teeter, and yaw is a strong function of the blade internal structural damping. When dealing with a teetering, yawing rotor with edgewise blade motion, the typical number of stations per revolution was 128 or 256, depending upon the blade structural damping.

## 2.11 Loads Produced on Structure

The loads of primary concern occur on the blade. The time series of flapwise and edgewise bending moments at the blade root gives a clear picture of the maximum cyclic loads the blades undergo. These blade loads will be the focus of this study. Other loads such as shaft bending moment, rotor thrust, and rotor torque are useful for determining the fatigue life of other wind turbine components.

## 2.12 Data Analysis Methods

The goal is not necessarily to exactly reproduce the time series seen in the data. Instead, the time series produced by the code should represent, as near as possible, another possible data sample in the same test. Instead of comparing the time series point by point, each time series is first analyzed for its overall characteristics and these are compared.

There are a number of methods of analyzing a time series to obtain information about its effect or to compare the general characteristics with another time series.

### 2.12.1 Probability Density Function

First, statistics such as mean and standard deviation can give an overall idea of the range of the values. Histograms of the time series can be plotted and compared to give more information about how the values are distributed.

### 2.12.2 Azimuth Averaging

If there is a corresponding record of the rotor rotation angle, the time series values can be binned according to their azimuthal position. This gives information about how the values relate to the fundamental rotor frequency.

### 2.12.3 Power Spectral Density

A power spectral density (PSD) can be computed of the time series, which indicates the frequency content of the original signal. This not only gives information about the response to the fundamental rotor frequency and its multiples, it also shows the distribution of power over the frequencies.

### 2.12.4 Rainflow Cycle Count

Finally, the cyclic nature of the time series can be evaluated using a Rainflow Cycle Count. This analysis method counts and bins the complete cycles made in the time series. The plot of number of cycles per bin size is similar to a fatigue S-N curve and gives information about the cyclic loads that would cause fatigue.

# 3. Results

The model was validated by comparing its predictions to test data. Two different machines were modeled in this study and the results were compared to test data. Both of these machines, the ESI-80 and the AWT-P1, are two-bladed, teetered-rotor horizontal axis wind turbines. Once the model is validated, further investigation can be performed for a particular machine to determine the number of degrees of freedom necessary to determine loads.

## 3.1 The ESI-80 Wind Turbine

The ESI-80 wind turbine was tested extensively (Musial et al., 1985) and has been selected to compare calculated results from the FAST code to field data. The wind turbine, which has two 40-foot (12.19 m) teetering blades, is a fixed pitch, free yaw, downwind machine with wood epoxy composite blades. The rotor blades employ the NASA LS(1) airfoil section. The specifications for the ESI-80 are summarized in Table 3-1.

**Table 3-1** ESI-80 Turbine Specifications

| Parameter | Specification |
|---|---|
| Rated power | 250 kW |
| Rated wind speed | 20.3 m/s (45 MPH) |
| Rotor diameter | 24.2 m (80 feet) |
| Rotor type | Teetered, underslung |
| Rotor orientation | Downwind |
| Blade construction | Wood-epoxy |
| Rotor airfoil | NASA LS(1) |
| Tip speed | 77.9 m/s (173 MPH) |
| Cut-in wind speed | 5.9 m/s (13 MPH) |
| Rotor RPM | 60 RPM |
| Generator type | 300 kW, induction |
| Gearbox | Planetary, 30:1 |
| Hub Height | 24.9 m (81.5 feet) |
| Tower | Open truss |
| Pitch | Fixed |
| Yaw | Passive |
| Overspeed control | Tip Vanes |
| Total system weight | 9750 kg (21,500 lb) |
| Coning angle | 7° |
| Natural Frequencies | |
| Teeter | 1 Hz |
| Tower | 1.31 Hz |
| First Flapwise | 2.03 Hz |
| Second Flapwise | 6.91 Hz |
| First Edgewise | ~ 7.7 Hz |

### 3.1.1 Field Measurements

The ESI-80 test turbine was located in the Altamont Pass near Tracy, California. A 120 ft (37 m) meteorological tower was located 160 ft (50 m) to the west of the wind turbine in the prevailing wind direction.

Table 3-2 lists the items that were measured during the test program and subsequently digitized at 50 Hz by the Solar Energy Research Institute (now NREL, National Renewable Energy Lab).

It may be noted that the blade edgewise bending moment was not measured in the ESI-80 tests. Thus, while the ESI-80 test results contain an abundance of comparisons, the accuracy of calculated edgewise moments must be examined on a different data set.

Turbulence induced loads on the ESI-80 were examined using 10 minute records of wind conditions and loads measurements as reported by Wright and Butterfield (1992). Two sets of data records were used, each with different wind conditions. The first case had a mean wind speed of 36.14 mph and turbulence intensity of 12.1%. The second case had a mean wind speed of 22.6 mph and a turbulence intensity of 9.7%.

**Table 3-2** Measured Parameters for the ESI-80 Test Turbine

| Channel | Description |
|---|---|
| 1 | Wind Speed @ 31.5 m (120 ft) |
| 2 | Wind Direction @ 31.5 m (120 ft) |
| 3 | Wind Speed @ 24.5 m (80 ft) |
| 4 | Wind Direction @ 24.5 m (80 ft) |
| 5 | Wind Speed @ 12.2 m (40 ft) |
| 6 | Wind Direction @ 12.2 m (40 ft) |
| 7 | Rotor Azimuth Position |
| 8 | Teeter Angle |
| 9 | Yaw Angle |
| 10 | Blade Root Flap Bending |
| 11 | Blade Flap Bending @ 60% R |
| 12 | Low-Speed Shaft Torque |

### 3.1.2 Wind Turbine Model

The degrees of freedom used for this model include teeter, yaw, tower motion in two directions, and six degrees of freedom for the blades, for a total of ten degrees of freedom. The generator was run at a constant rotational speed with a rigid shaft. Data on the configuration of the ESI-80 used for the tests was facilitated by measurements made at the University of Massachusetts (Bywaters, 1992). Of particular note is the presence of both teeter springs and teeter dampers which are discussed in Appendix F. The specific input values used to model the ESI-80 machine are included in the appendices.

For this particular machine, several degrees of freedom were found to have little effect on the results. Good agreement was achieved with the

generator operating at either constant or varying speed. The tower is stiff enough that accurate modeling is achieved with only one vibration mode. Although reasonable predictions could be made using only one blade flap mode, agreement was greatly improved when adding a second blade flap vibration mode and the blade edgewise degree of freedom.

### 3.1.3 Comparison of Mean Loads

For the ESI-80, the mean blade flap moment was measured at various wind speeds over the operating range. Figure 3.1-1 compares this data with results from the computer model. The code does a good job of predicting mean blade loads over the entire range of wind speeds. Not only are the values within the range of the data, but the shape of the curve also agrees with the data.

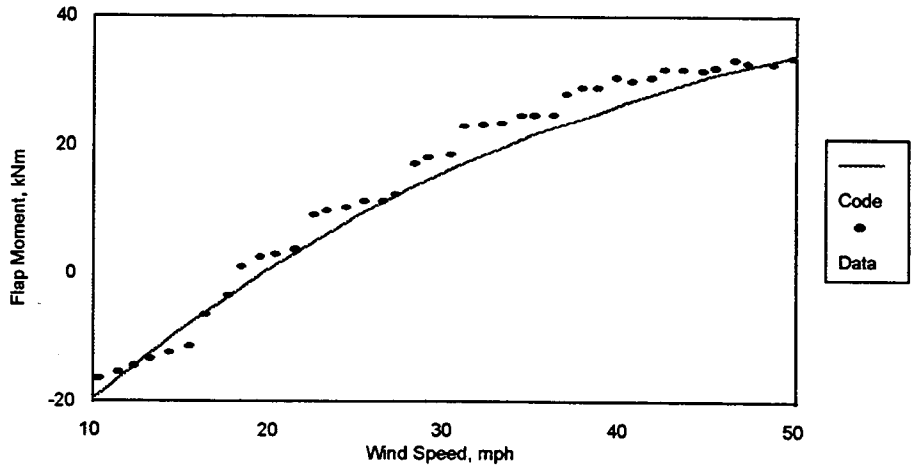


**Figure 3.1-1** Mean Blade Flap Moment over Several Mean Wind Speeds for the ESI-80 Machine

### 3.1.4 Comparisons at 36.1 mph Wind Speed

#### 3.1.4.1 Blade Flap Moment at Root

Figure 3.1-2, at the end of section 3.1, shows an azimuth averaged load plot as a form of comparison between test data and FAST calculations. Note that for the azimuth binned blade root flatwise bending moment at 36.1 mph the load scale covers the range from 10 to 40 kNm. Agreement between FAST calculations and data is good, since all fluctuations shown by the data are present in the calculations. The calculated loads are the difference between the aerodynamic and the centrifugal loads, both of which are much larger than their difference. The magnitude of the calculated moment between 90° and 135° (post tower shadow region) and between 270° and 315°, has a maximum difference of 9 kNm below the test data.

Histograms of test data and code calculations are the second method of comparison. Figure 3.1-3 shows a histogram for the 36.1 mph case for the blade root flatwise bending moment. Agreement between test data and code is good with a similar shape to both distributions. The test data mean was 26.34 kNm, while the FAST code mean was 3.6 kNm lower.

Power Spectral Density of the root flatwise bending moment is shown in Figure 3.1-4 for a wind speed of 36.1 mph. Agreement between code and test data is good including a broadening in the region of 2 Hertz. Without the addition of the edgewise degree of freedom, the code failed to predict the broad plateau between 2 and 3 Hertz that appears in the test data.

Rainflow cycle counting is shown in Figure 3.1-5 for the 36.1 mph case. Agreement between FAST calculations and test data is good over the entire range.

### 3.1.4.2 Blade Flap Moment at 60% Radial Station

The azimuth binning plots of the blade flapwise bending moment at a point 60% of the blade length from the root are shown in Figure 3.2-6. The cyclic nature of the blade oscillations is well represented here, and the magnitudes of the loads are within the range of experiment test error.

Figure 3.1-7 shows the flapwise bending moment histogram at a station 60% of the rotor radius. Here, the shape of the histogram shows excellent agreement between data and code. However, the mean for the data is 4.49 kNm while the mean for the code is 0.4 kNm lower than the data. Since the mean acceleration of the blade in the flatwise direction is zero, the difference between test data and code can be due to the mean aerodynamic loads, the mean centrifugal loads, or the data.

Figure 3.1-8 shows the PSD of the flap moment at the 60% radial station. There is good agreement between code and data, with a slight overprediction in the energy that occurs near 4 Hertz and an underprediction between 6 and 8 Hertz. The peaks that are multiples of the fundamental frequency are also of the correct magnitude.

The cycle count of the bending moment at the 60% station is compared in Figure 3.1-9. There is very good agreement between the FAST code and test data along the entire range of cycle amplitudes.

### 3.1.4.3 Teeter History

Figure 3.1-10 shows the teeter occurrence histogram at 36.1 mph. Several items may be mentioned concerning the data. First, the mean teeter angle from the test data is non-zero. Second, the effects of the teeter springs/dampers can be seen in the data: the plateau above +2° and a similar plateau at about -1°. While the FAST code results also exhibit "plateaus" in the region of ±2°, the code has a mean teeter angle of zero and the calculations are more or less symmetrical about the origin. Third, the "Gaussian" like distribution of teeter angle is thought to be a result of including the yaw degree-of-freedom. McCoy (1992) had modeled the ESI-80 using a code without a yaw degree-of-freedom and obtained a teeter occurrence histogram similar to the distribution that would be obtained from a harmonic oscillator.

### 3.1.4.4 Lift Coefficient Near Tip

Although there is no data for the lift coefficient of the blade airfoil section near the tip, the results of the model are of some interest. Figures 3.1-11 through 3.1-13 show the analysis of the tip lift coefficient for the ESI-80 at 36 mph wind speed.

The azimuth binning in Figure 3.1-11 clearly shows the location of the tower shadow in terms of azimuth coordinates. It also shows the effect of wind shear on the blade as it travels around the rotor plane.

Figure 3.1-12 shows the occurrence histogram for the lift coefficient. Note that the mean is near the highest occurring lift coefficient, suggesting the blade tip operates with a near maximum amount of lift much of the time.

The variation in lift coefficient is shown in Figure 3.1-13. This cycle count is not similar in shape to the shape of the blade flap moment cycle count, shown in Figure 3.1-4.

#### 3.1.4.5 Dynamic Stall Considerations

The calculations made for the 36.1 mph were made without consideration of dynamic stall. Since dynamic stall may occur when the static stall angle is exceeded, and the static stall angle was frequently exceeded during the 36.1 mph case, it is noted that no penalty in accuracy seems to have occurred from the static stall model.

### 3.1.5 Comparisons at 22.6 mph Wind Speed

#### 3.1.5.1 Blade Flap Moment at Root

The azimuth averaged flatwise blade bending moment shown in Figure 3.1-14 also shows good agreement between test data and calculation in magnitude, phase angle, and representation of major fluctuations.

A histogram of the blade root flatwise bending moment is shown in Figure 3.1-15. Agreement between FAST calculation is very good as the distributions are similar. The means are both about 5.7 kNm, but the code has a slightly higher standard deviation.

The power spectral density of the root flap moment is illustrated in Figure 3.1-16. While agreement between the test data and code is good,

there appears to be a scale shift in the frequency, the data peaks occurring at slightly lower than integer values of the rotor angular velocity while the code peaks occur at values slightly above integer values of the rotor angular velocity. With the rotor angular velocity of 1.005 Hertz, the differences are believed to be associated with the digitization of the data from the analog tape (Wright, 1991).

Rainflow cycle counting of the blade flap moment at 22.6 mph is shown in Figure 3.1-17. There is excellent agreement over the entire range of cycle amplitudes.

### 3.1.5.2 Blade Flap Moment at 60% Radial Station

Figures 3.1-18 through 3.1-21 show calculations at the 60% of rotor radius station. Good agreement between FAST calculations and test data is obtained at this station also. Test data and code have similar shapes in Figure 3.1-18, the azimuth binning plot. The histogram shown in Figure 3.1-19 also shows a similar shape, although the code shows a more symmetric, broader distribution. The PSD comparing the code with the data, shown in Figure 3.1.20, agrees as well as that for the blade root, with the code predicting both the peaks and the broadening near 2 and 8 Hertz. Figure 3.1.21 presents the rainflow cycle count, where the data and code have similar shapes, and excellent agreement over the entire range of cycle amplitudes.

### 3.1.5.3 Teeter History

The histogram of the teeter response is shown in Figure 3.1-22. The means are different, with the data being non-zero. They do however have similar standard deviations.

### 3.1.5.4 Lift Coefficient Near Tip

This data set does not contain information about the lift coefficient of the blade airfoil section near the tip either, but the results of the model are still of some interest. Figures 3.1-23 through 3.1-25 show the analysis of the tip lift coefficient for the ESI-80 at 23 mph wind speed. The azimuth binning of the lift coefficient in Figure 3.1-23 shows clearly the effect of tower shadow and wind shear on the lift near the tip of the blade. The lift coefficient histogram has a more symmetric shape than that for the higher wind speed case, suggesting that this station is operating within the linear portion of the lift curve. Finally, the rainflow cycle count shows a monotonically decreasing variation of lift coefficient, different from the variation for the higher wind speed case shown in Figure 3.1-13.

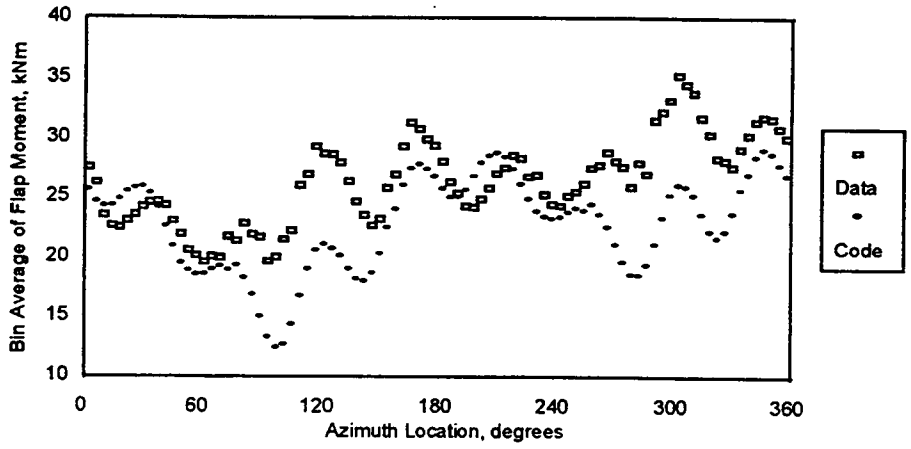


**Figure 3.1-2** Azimuth Binning of Blade Flap Moment at Root for ESI-80 Machine at 36 mph Wind Speed

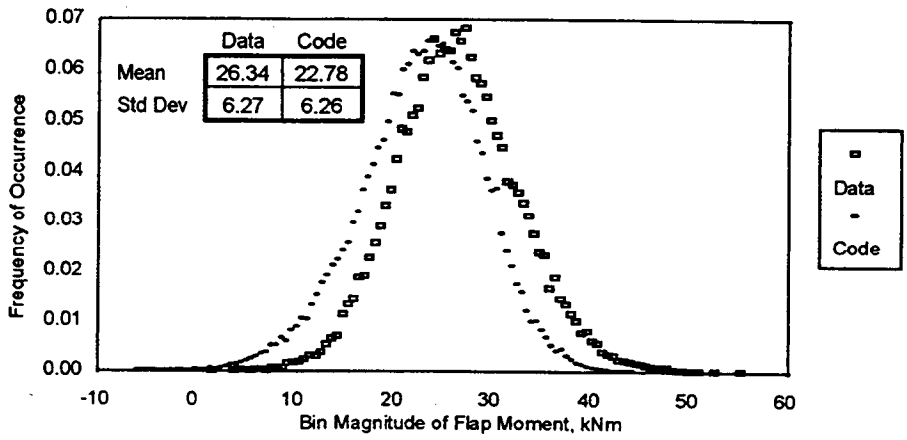


**Figure 3.1-3** Occurrence Histogram of Blade Flap Moment at Root for ESI-80 Machine at 36 mph Wind Speed

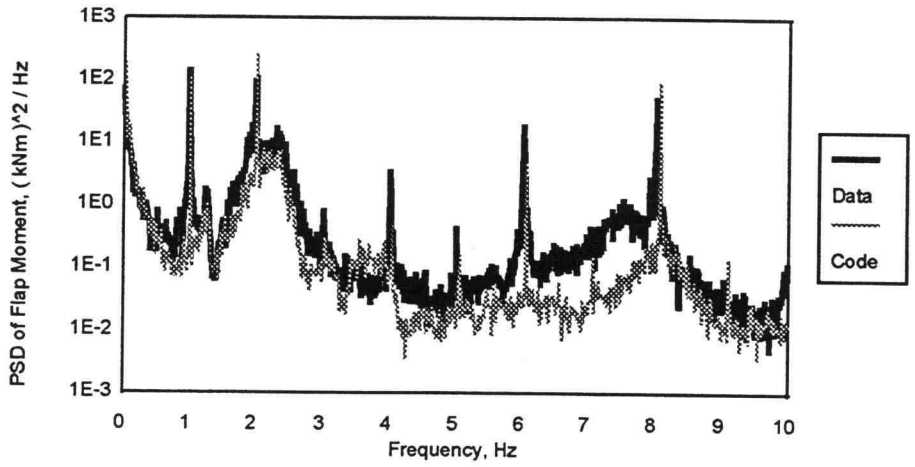


**Figure 3.1-4** Power Spectral Density of Blade Flap Moment at Root for ESI-80 Machine at 36 mph Wind Speed

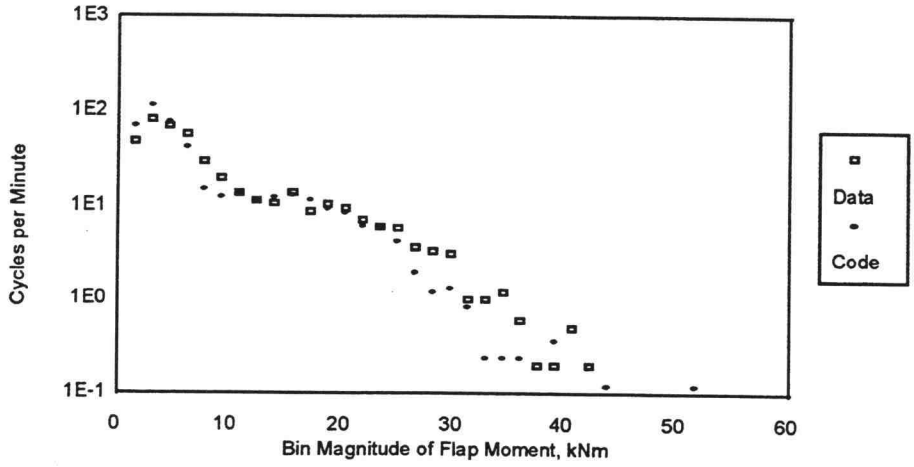


**Figure 3.1-5** Rainflow Cycle Count of Blade Flap Moment at Root for ESI-80 Machine at 36 mph Wind Speed

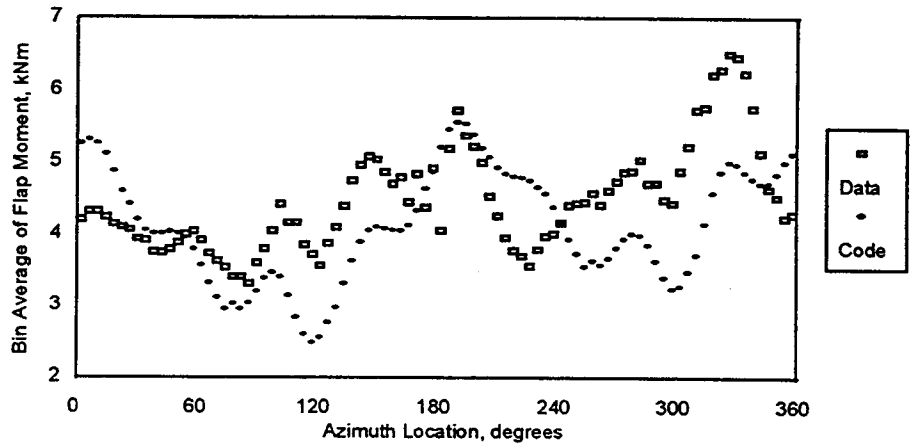


**Figure 3.1-6** Azimuth Binning of Blade Flap Moment at 60% Blade Station for ESI-80 Machine at 36 mph Wind Speed

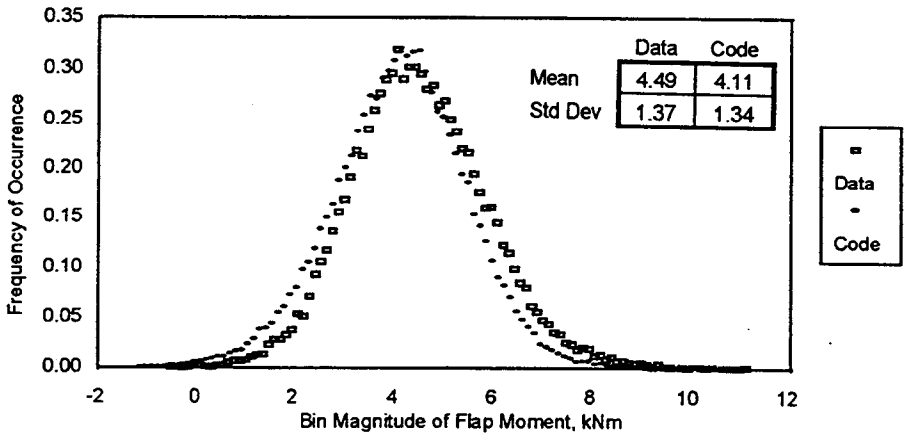


**Figure 3.1-7** Occurrence Histogram of Blade Flap Moment at 60% Blade Station for ESI-80 Machine at 36 mph Wind Speed

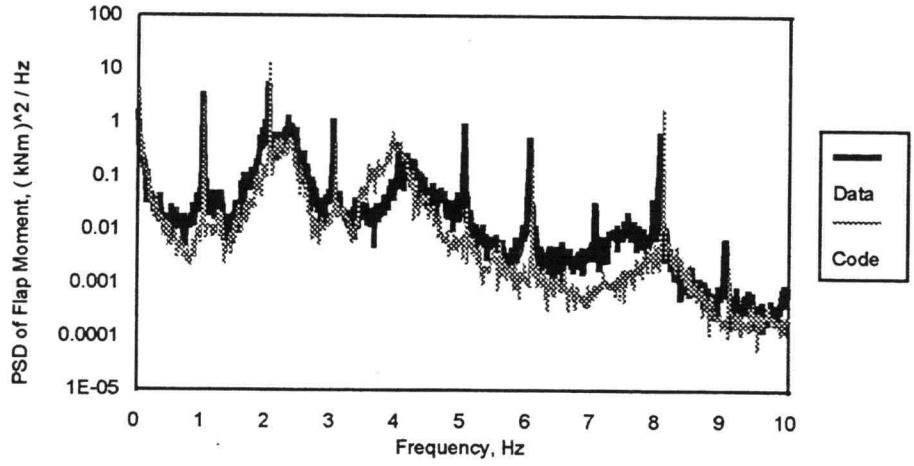


**Figure 3.1-8** Power Spectral Density of Blade Flap Moment at 60% Blade Station for ESI-80 Machine at 36 mph Wind Speed

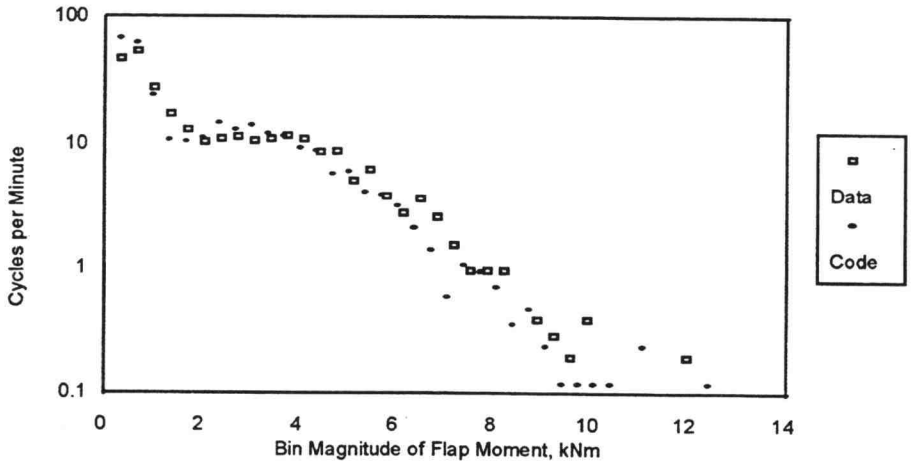


**Figure 3.1-9** Rainflow Cycle Count of Blade Flap Moment at 60% Blade Station for ESI-80 Machine at 36 mph Wind Speed

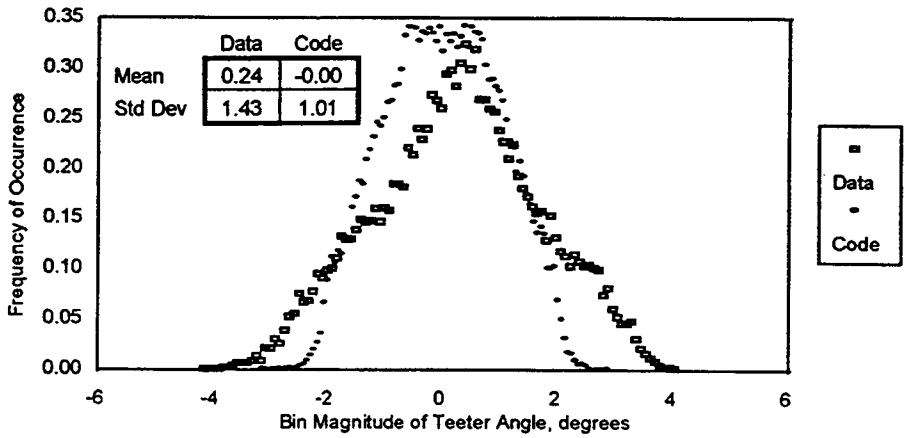


**Figure 3.1-10** Occurrence Histogram of Teeter Angle for ESI-80 Machine at 36 mph Wind Speed

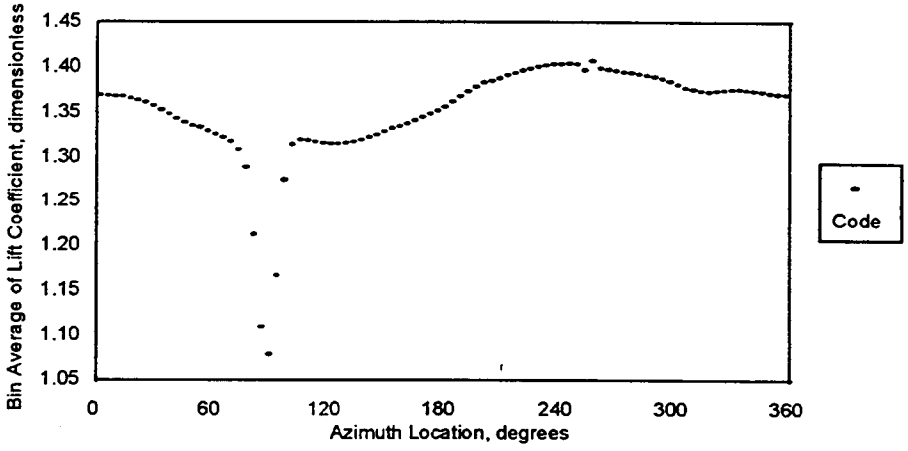


**Figure 3.1-11** Azimuth Binning of Lift Coefficient Near Tip for ESI-80 Machine at 36 mph Wind Speed

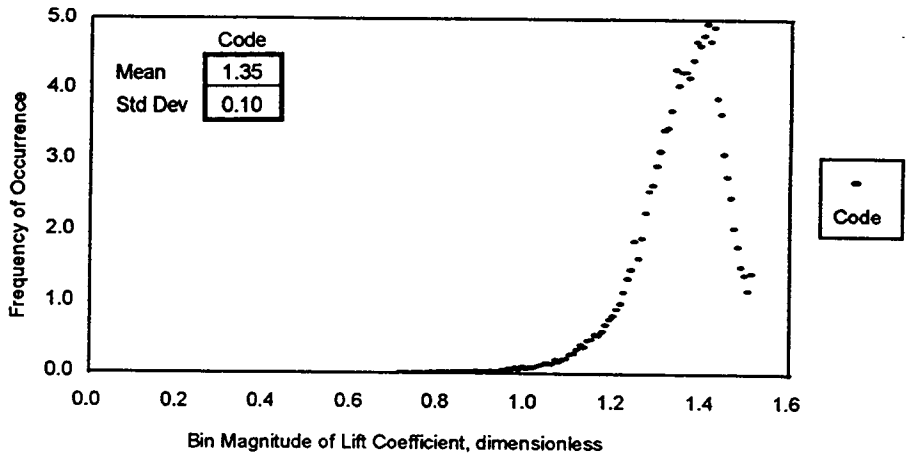


**Figure 3.1-12** Occurrence Histogram of Lift Coefficient Near Tip for ESI-80 Machine at 36 mph Wind Speed

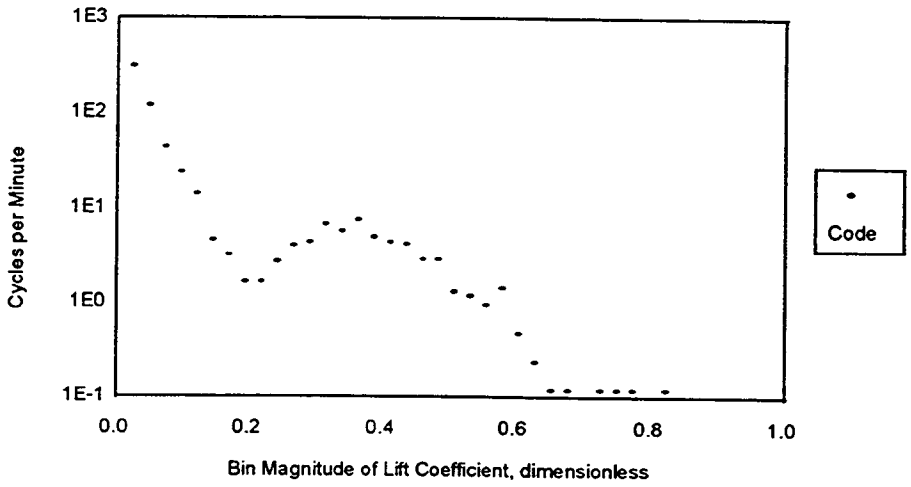


**Figure 3.1-13** Rainflow Cycle Count of Lift Coefficient Near Tip for ESI-80 Machine at 36 mph Wind Speed

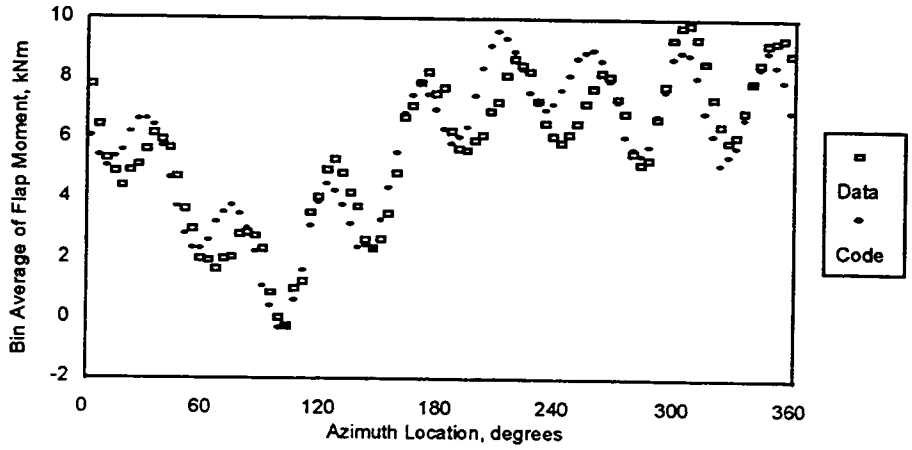


**Figure 3.1-14** Azimuth Binning of Blade Flap Moment at Root for ESI-80 Machine at 23 mph Wind Speed

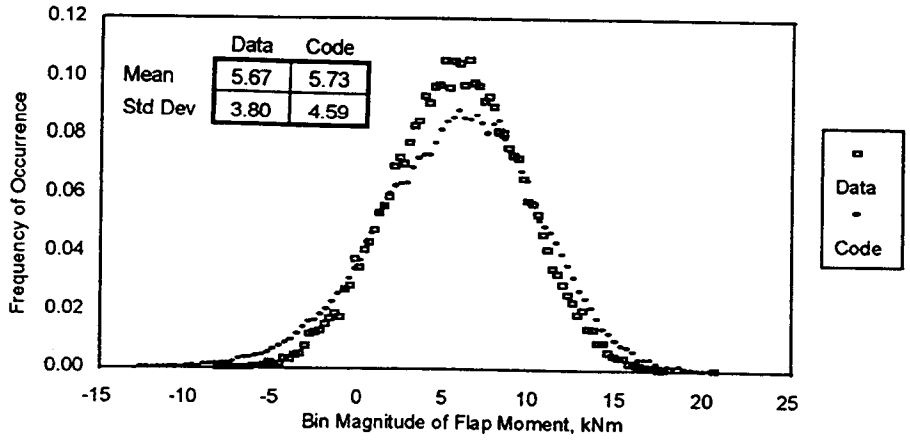


**Figure 3.1-15** Occurrence Histogram of Blade Flap Moment at Root for ESI-80 Machine at 23 mph Wind Speed

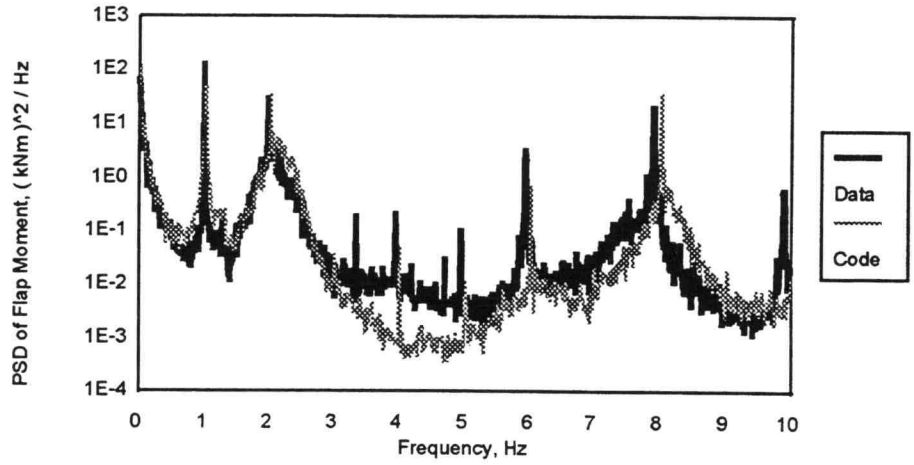


**Figure 3.1-16** Power Spectral Density of Blade Flap Moment at Root for ESI-80 Machine at 23 mph Wind Speed

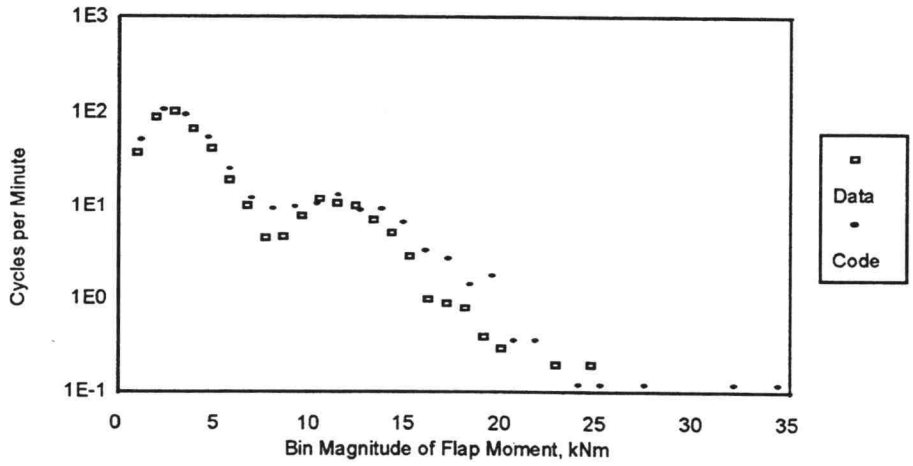


**Figure 3.1-17** Rainflow Cycle Count of Blade Flap Moment at Root for ESI-80 Machine at 23 mph Wind Speed

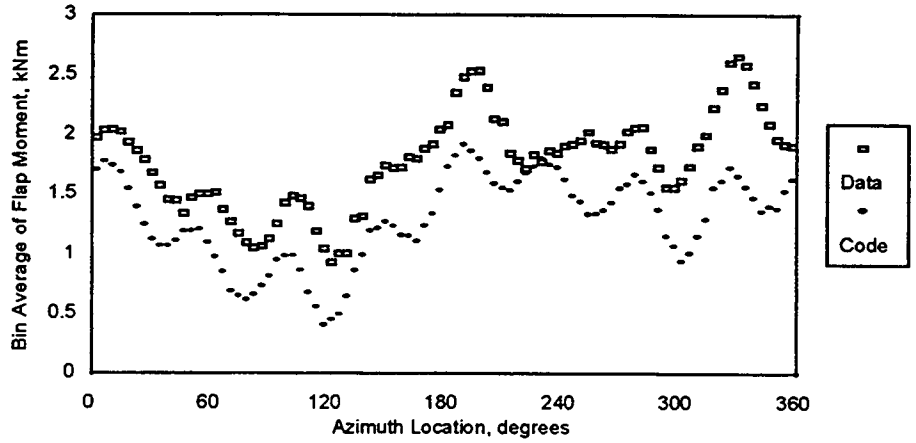


**Figure 3.1-18** Azimuth Binning of Blade Flap Moment at 60% Blade Station for ESI-80 Machine at 23 mph Wind Speed

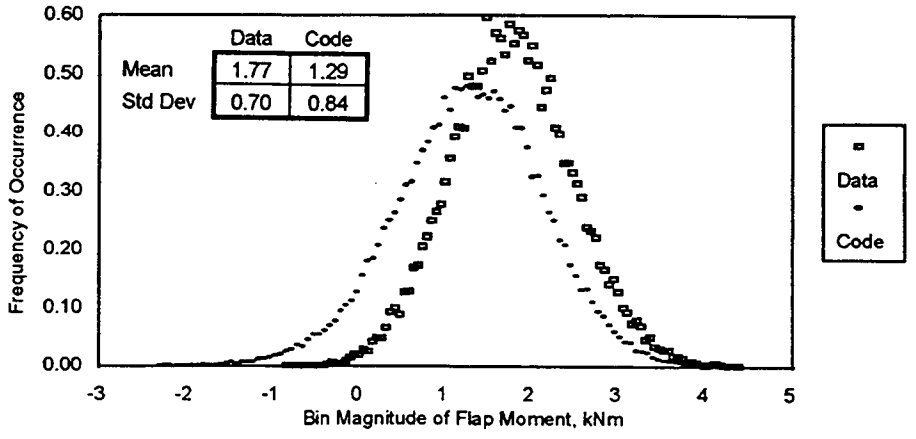


**Figure 3.1-19** Occurrence Histogram of Blade Flap Moment at 60% Blade Station for ESI-80 Machine at 23 mph Wind Speed

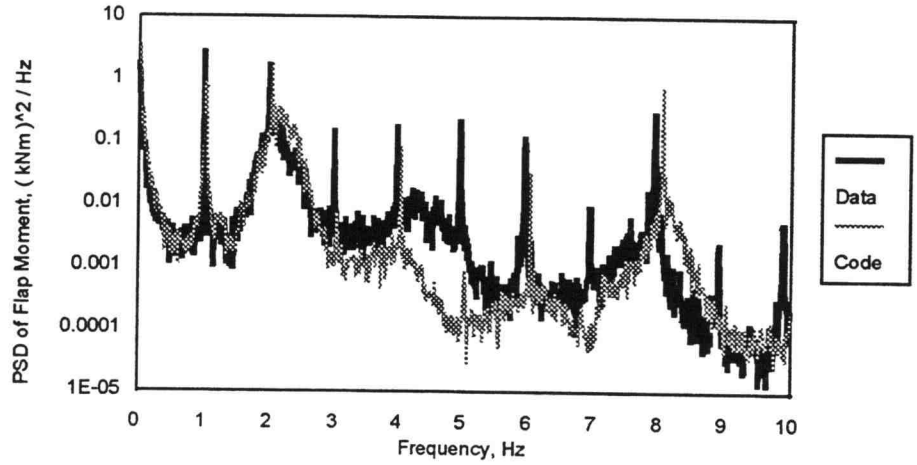


**Figure 3.1-20** Power Spectral Density of Blade Flap Moment at 60% Blade Station for ESI-80 Machine at 23 mph Wind Speed

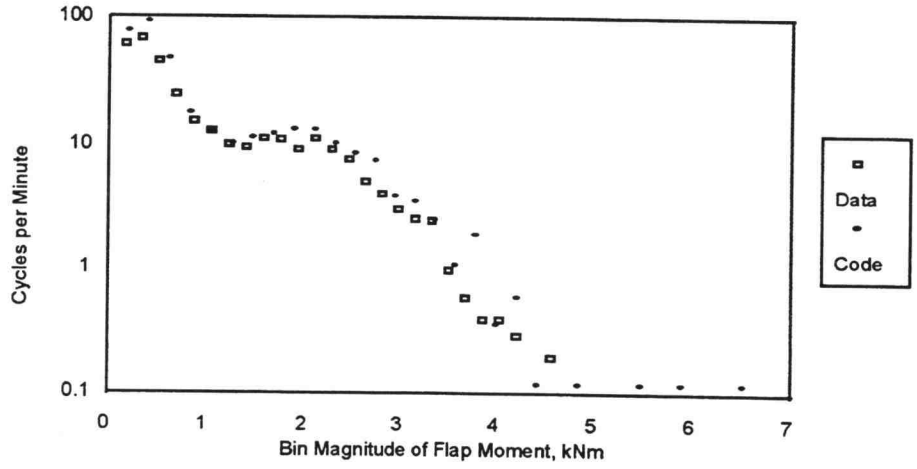


**Figure 3.1-21** Rainflow Cycle Count of Blade Flap Moment at 60% Blade Station for ESI-80 Machine at 23 mph Wind Speed

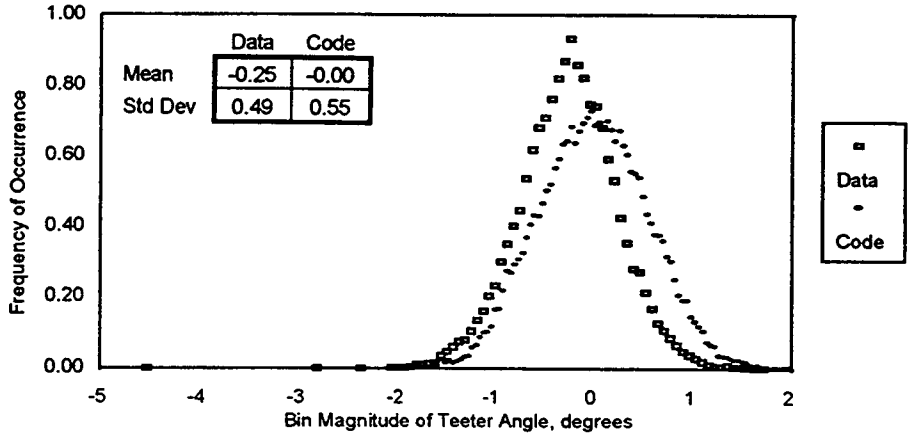


**Figure 3.1-22** Occurrence Histogram of Teeter Angle for ESI-80 Machine at 23 mph Wind Speed

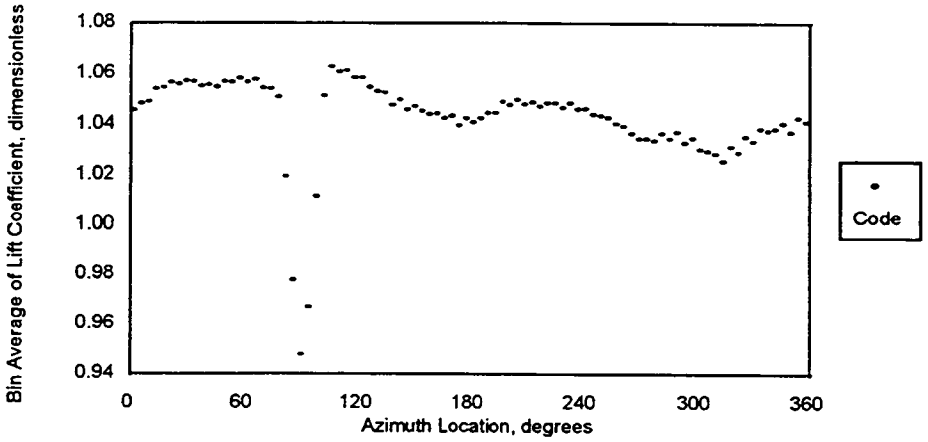


**Figure 3.1-23** Azimuth Binning of Lift Coefficient Near Tip for ESI-80 Machine at 23 mph Wind Speed

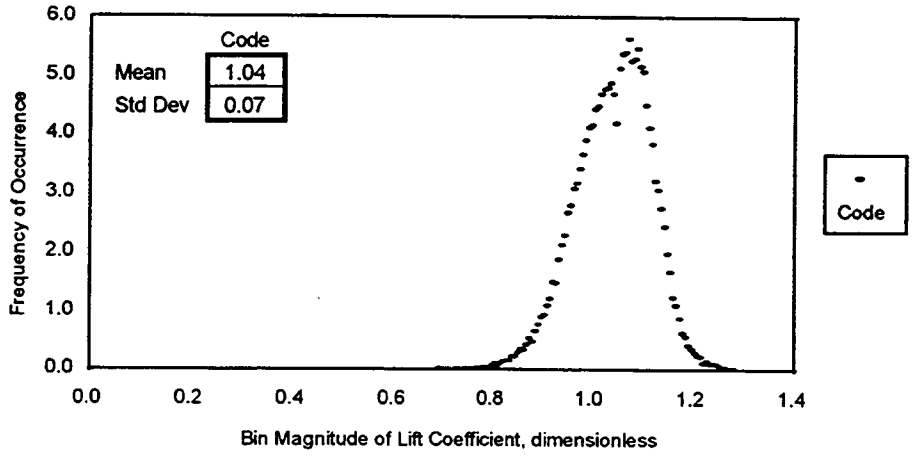


**Figure 3.1-24** Occurrence Histogram of Lift Coefficient Near Tip for ESI-80 Machine at 23 mph Wind Speed

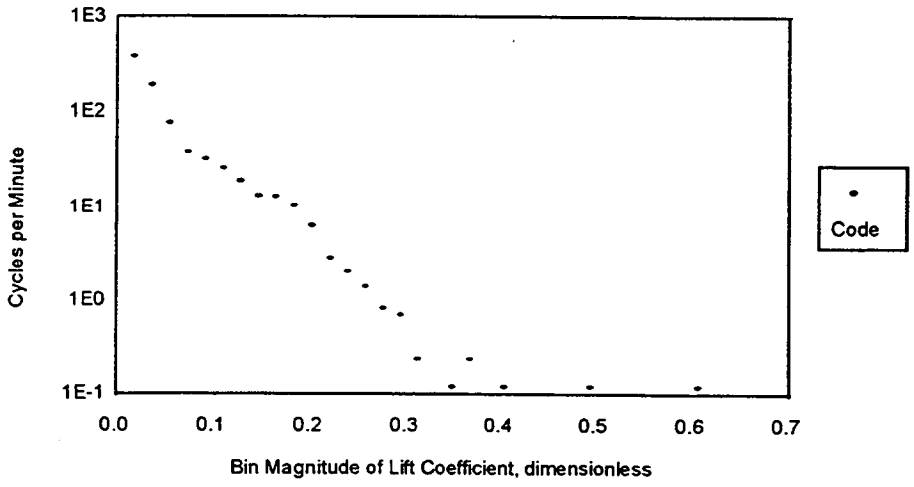


**Figure 3.1-25** Rainflow Cycle Count of Lift Coefficient Near Tip for ESI-80 Machine at 23 mph Wind Speed

## 3.2 The AWT-26-P1 Wind Turbine

The AWT-26-P1 is a stall-controlled, free yaw, downwind, teetering rotor with two fixed pitch blades coned at 7°. Close in appearance to the ESI-80, the AWT-26 P1 wind turbine operates at 57 RPM, is rated at 275 kW, and has a 26.2 m rotor diameter. The blade airfoils are from the NREL thick airfoil series employing near linear taper and a nonlinear twist distribution. The major turbine specifications are shown in Table 3-3.

**Table 3-3** AWT-26 Turbine Specifications

| | |
|---|---|
| **Physical characteristics** | |
| Rotor diameter | 26.2 meters(86 ft) |
| Rotor orientation | downwind, free yaw |
| Rotor type | stalled regulated, teetered |
| Rotor airfoil | NREL thick |
| Pitch | fixed |
| Gearbox | planetary, 31.5:1 |
| Hub height | 25 meters(82 ft) |
| Towers | up to 47.3 meters(155 ft) |
| **Operational characteristics** | |
| Rated Power | 275 kW |
| Cut-in wind speed | 5.4 m/s (12 mph) |
| Cut-out wind speed | up to 24.6 m/s (55 mph) |
| Survival wind speed | 59 m/s (133 mph) |
| Rotor rpm | 57.5 rpm |
| Generator type | induction |
| Coning | 7 degrees |
| Brakes | fail-safe, redundant |
| **Rotating natural frequencies** | |
| Teeter | 0.96 Hz |
| Tower | 1.12 Hz |
| First flapwise mode | 1.3 Hz |
| Second flapwise mode | 7.0 Hz |
| First edgewise mode | 8.7 Hz |

### 3.2.1 Field Measurements

The wind turbine was tested in Tehachappi Pass, California, at a test site at the 4500 foot level. Test data taken on the AWT-26-P1 wind turbine on July 22, 1993, was obtained from NREL. Note that data for this machine includes the edgewise blade bending moment, so the prediction accuracy of this load can now be examined.

Turbulence induced loads on the AWT-P1 were recorded at 50 Hz giving 10 minute data records of wind conditions and loads measurements. Table 3-4 shows the data that was recorded during the test. The mean wind speed for this test was 12.76 m/s (28.5 mph) and the turbulence intensity was 12%.

**Table 3-4** Data Recorded for the AWT-26 Turbine

| Channel | Description |
|---|---|
| 1 | Wind direction @ 40 ft |
| 2 | Wind speed @ 115 ft |
| 3 | Wind speed @ 80 ft |
| 4 | Wind speed @ 40 ft |
| 5 | North hinged tower leg load |
| 6 | East hinged tower leg load |
| 7 | West hinged tower leg load |
| 8 | Nacelle vertical pitching acceleration |
| 9 | Power |
| 10 | Rotor azimuth position |
| 11 | Blade1 root flapwise bending moment |
| 12 | Blade1 root edgewise bending moment |
| 13 | Shaft torque |
| 14 | Blade2 root flapwise bending moment |
| 15 | Blade2 root edgewise bending moment |
| 16 | Teeter angle position |

### 3.2.2 Wind Turbine Model

In order to facilitate the calculation of blade loads, the FAST code was run in a similar manner for this machine, with a total of ten degrees of freedom. Although the appendices indicate the quantities necessary to

model a machine, these values are not given for the AWT 26-P1. This is a prototype machine whose specific parameters are proprietary.

### 3.2.3 Comparison at 28.5 mph (12.8 m/s) Wind Speed

#### 3.2.3.1 Blade Flap Moment at Root

Figure 3.2-1 shows the azimuth binning of the flap moment for the AWT 26-P1. As the blade moves around the rotor plane, similar oscillations are seen in both the test data and code predictions.

A histogram comparing results of the blade loads is shown in Figure 3.2-2. Although the code predicts a skewed curve while the data is nearly symmetric, the agreement between the two is good. The code has a slightly higher mean than the data, but their standard deviations are similar.

The PSD shown in Figure 3.2-3 compares the harmonics excited in the blade. The broad peak near 2 Hertz is caused by the first natural frequency of the rotating blade. The two broad peaks above 7 Hertz are caused by the second natural frequency of the blade in the flapwise direction, and the first edgewise natural frequency. There is good agreement over most of the frequency range. The broad peak caused by edgewise excitation shows up near 6.5 Hertz in the data, and near 9 Hertz in the prediction.

The rainflow cycle count in Figure 3.2-4 shows good agreement between the test data and code. For each size of flap moment cycle along the horizontal axis, the frequency of occurrence of the cycles was about the same. The data indicates more cycles in the 20-30 kNm range, but the agreement for the larger amplitude cycles is very good.

### 3.2.3.2 Blade Edgewise Moment at Root

The azimuth bending plot, Figure 3.2-5, shows good agreement in the amplitudes of the higher frequency cycles. There is also the same general once per revolution rise and fall in the curves. However, the data indicates 7 cycles over one revolution, while the code predicts 10 cycles in the same period. This difference agrees with the PSD of the flap moment (Figure 3.2-3), which shows very different frequencies of response for the edgewise vibration.

The occurrence histogram is shown in Figure 3.2-6. There is good agreement between data and code over the entire range of loads. The test data mean loads is 15.5 kNm, while the code mean is 1.4 kNm higher. The standard deviation of the code is slightly lower than that for the data.

The PSD's of data and code are compared in Figure 3.2-7. The code predicts the frequency response at the lower frequencies fairly well, but there is a clear difference in the edgewise response at higher frequencies. The data shows broad responses near 4.5 Hertz and 6.5 Hertz, while the code shows these peaks near 7.5 Hertz and 9.5 Hertz. This shows the same discrepancy that appeared in the azimuth binning plot of the same data and prediction.

Figure 3.2-8 shows the rainflow cycle count of the blade edgewise flap moment. There is excellent agreement between test data and code prediction not only with the lower amplitude cycles, but more importantly, with the higher amplitude cycles.

### 3.2.3.3 Teeter History

The occurrence histogram for the teeter angle is shown in Figure 3.2-9. The code prediction shows good agreement with the test data in this case. The means and the standard deviations also agree.

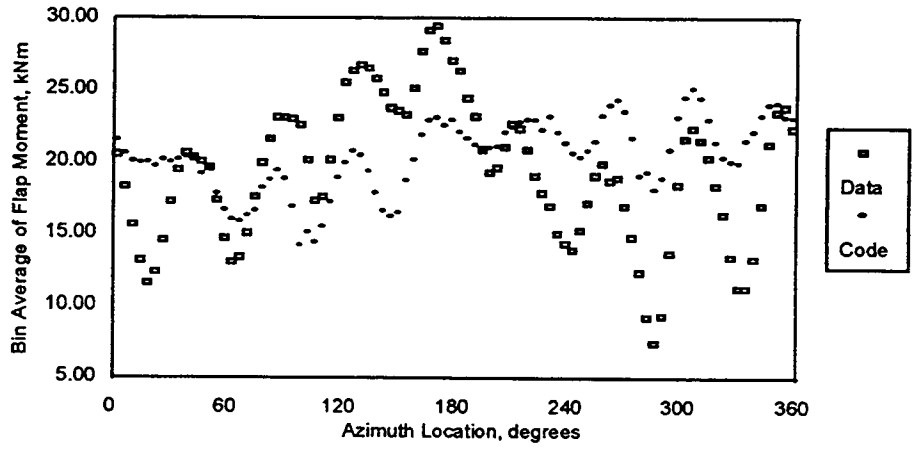


**Figure 3.2-1** Azimuth Binning of Blade Flap Moment at Root for AWT 26-P1 Machine at 29 mph Wind Speed

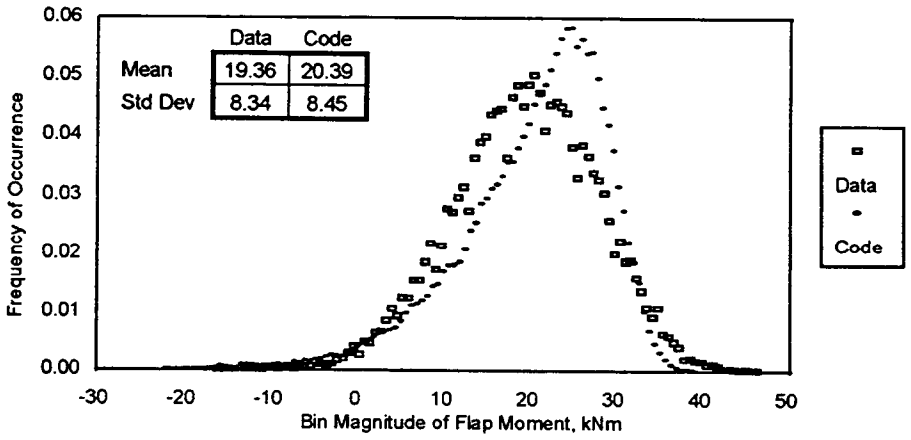


**Figure 3.2-2** Occurrence Histogram of Blade Flap Moment at Root for AWT 26-P1 Machine at 29 mph Wind Speed

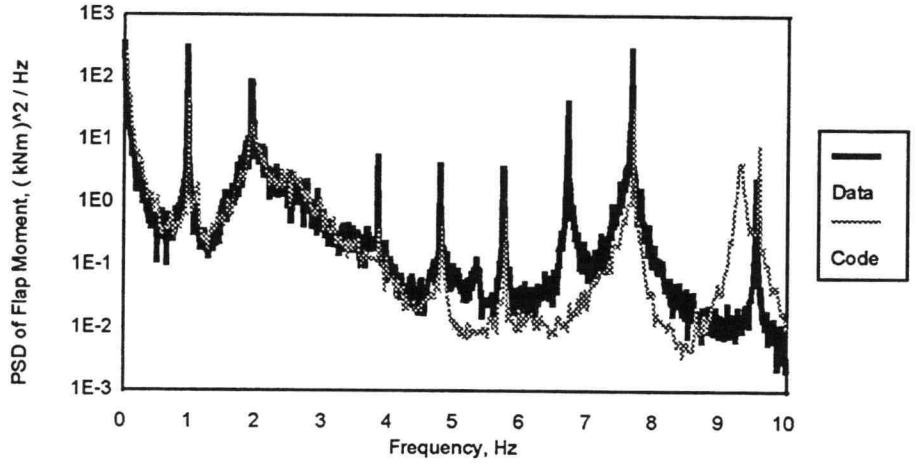


**Figure 3.2-3** Power Spectral Density of Blade Flap Moment at Root for AWT 26-P1 Machine at 29 mph Wind Speed

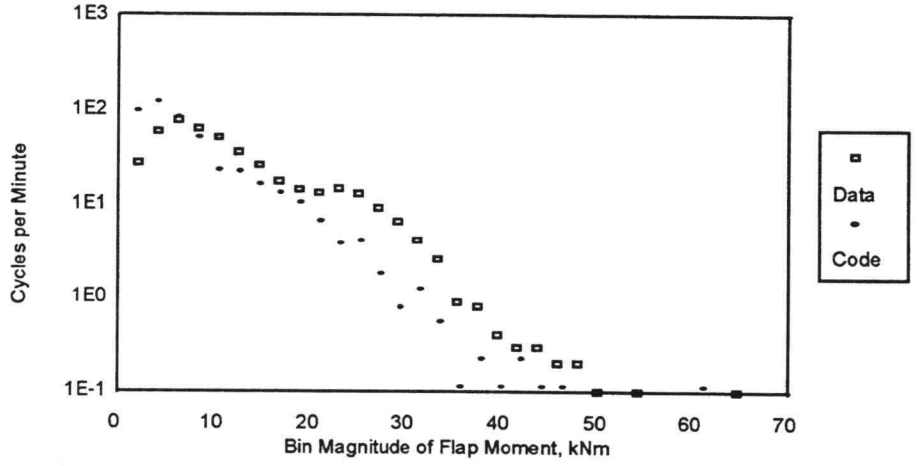


**Figure 3.2-4** Rainflow Cycle Count of Blade Flap Moment at Root for AWT 26-P1 Machine at 29 mph Wind Speed

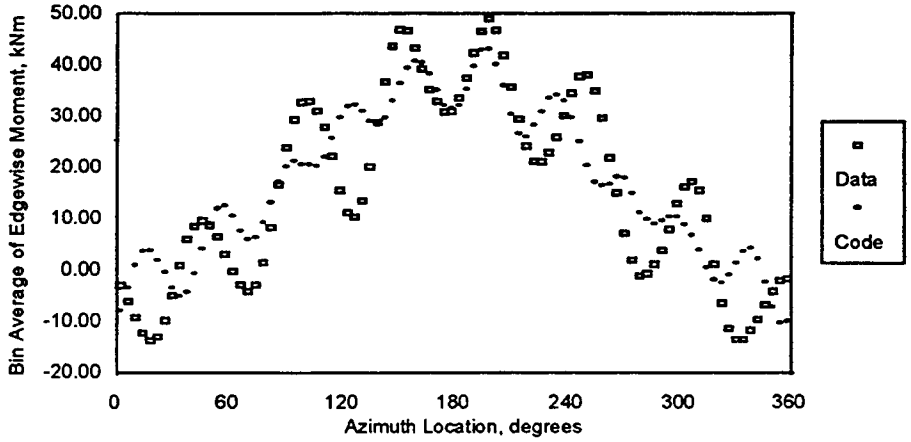


**Figure 3.2-5** Azimuth Binning of Blade Edgewise Moment at Root for AWT 26-P1 Machine at 29 mph Wind Speed

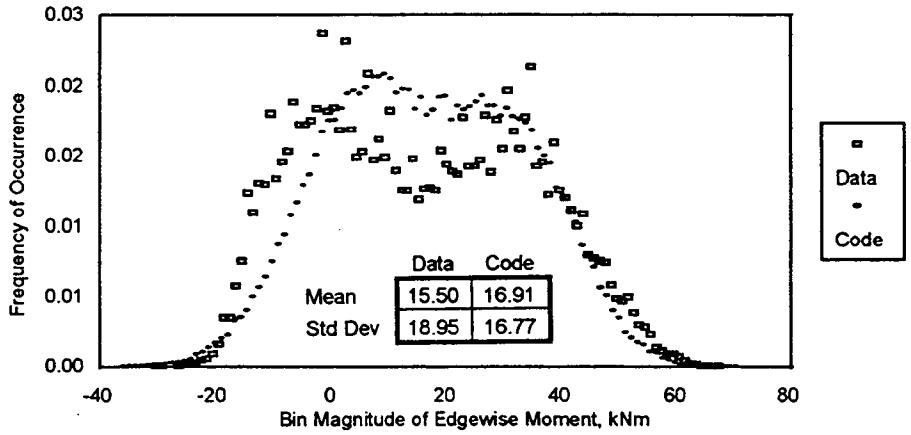


**Figure 3.2-6** Occurrence Histogram of Blade Edgewise Moment at Root for AWT 26-P1 Machine at 29 mph Wind Speed

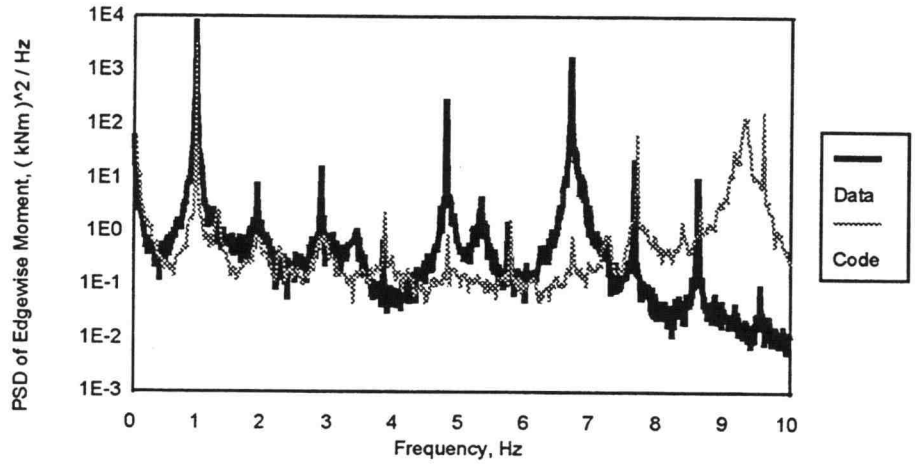


**Figure 3.2-7** Power Spectral Density of Blade Edgewise Moment at Root for AWT 26-P1 Machine at 29 mph Wind Speed

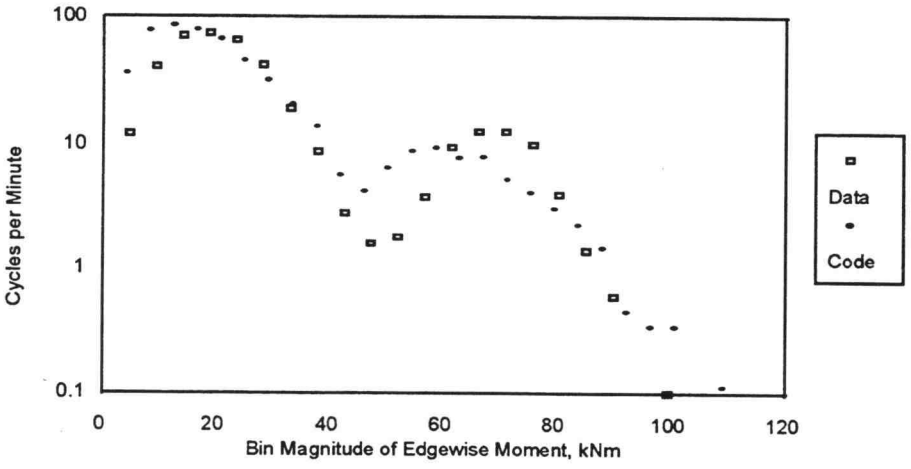


**Figure 3.2-8** Rainflow Cycle Count of Blade Edgewise Moment at Root for AWT 26-P1 Machine at 29 mph Wind Speed

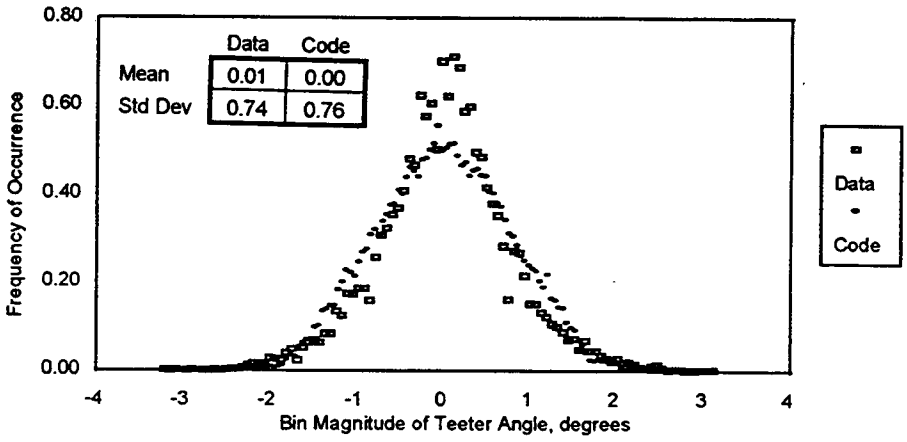


**Figure 3.2-9** Occurrence Histogram of Teeter Angle for AWT 26-P1 Machine at 29 mph Wind Speed

## 3.3 Modeling

Developing a model is an iterative process. Some of the input parameters are very well known in the beginning of the process. For example, rotor diameter, tower height, and shaft length are easily measured. Other quantities, such as those used to describe the tower shadow characteristics, are not so well known. Additionally, the results can be very sensitive to some parameters, while nearly insensitive to others. By systematically adjusting a single parameter at a time, the sensitivity of the results to that value can be evaluated. A fairly complete sensitivity analysis was performed by Wilson et al. (1994) using the FAST code. Several examples of the modeling process that occurred during this research are given below.

### 3.3.1 Tower Drag Coefficient

In modeling the ESI-80, the higher wind speed case was the initial focus. Once the code predicted the data reasonably well for this case, the comparison with the lower wind speed case was performed. It was noted that the average teeter amplitude was much lower than predicted. This indicated that a once per revolution input to the rotor, such as the tower shadow, might be too large. The properties of the tower wake were estimated based on the size of the three legs of the truss tower, and on the mean wind speed. Although the tower geometry is the same for the two cases, the Reynolds number of the flow over the tower legs is different. Originally it was assumed that this was a small effect, but studying the regime more carefully, it was discovered that in certain cases, the reduction of the Reynolds number could cut the drag in half. The lower drag coefficient produces a wake with a lower

velocity deficit. For the lower wind speed case, the smaller tower shadow produced much better predictions. Since there were no measurement taken specifically to estimate the behavior or size of the tower wake, it had to be approximated based on the information available. This included tower geometry, mean wind speed, and resulting machine loads and motion.

### 3.3.2 Teeter Springs and Dampers

Initially, the ESI-80 machine was modeled with no teeter dampers or springs, and only crude stops were used to limit the range of teeter motion. This assumption was based on the information available in the testing report for the machine (see Musial et al.). The teeter response modeled did not agree well with the data. Upon further investigation, it was discovered that the machine did indeed have dampers and springs that acted to restrict teeter motion. Data from these was obtained, and a model of their response to various teeter angles and rates was developed. Once these were added to the code, agreement between test data and prediction was greatly improved.

### 3.3.3 Blade Structural Damping

Originally, only a single blade degree of freedom, the first flap mode, was used to model the flexible blades. The broad peaks that occur at higher frequencies, seen in Figure 3.1-4, indicated that higher blade vibration modes were important. A second flapwise vibration mode and an edgewise degree of freedom were added to the model. Although the aerodynamics

provide damping in the flapwise direction, the edgewise degree of freedom tended to ring at its natural frequency and was never damped. In order to improve the model, blade structural damping was added. The model chosen to represent the damping is a commonly used formulation which damps out the higher frequencies of vibration first. This structural damping along with the added modes of vibration for the blade greatly improved the code predictions.

### 3.3.4 Blade Frequencies

The frequencies of the various blade modes are very important in the model. Several sources for information exist, including the manufacturer of the blades, who might supply the non-rotating blade frequencies. Using the blade distributed mass and stiffness, and the rotation rate and frequency, the rotating blade frequencies can be estimated. However, a PSD analysis of the code results will clearly show the frequencies which the blades exhibit in the model, as seen in Figure 3.1-4. Usually, the blade stiffness, can be adjusted slightly to force the blades to respond at the same frequencies as they do in the data. This method has worked well for the ESI-80, where the PSD's show good agreement near the broad peaks created by the blade resonance. The AWT 26-P1 shows good agreement for the first flap mode, but the higher modes may need further tuning (see Figure 3.2-3).

### 3.3.5 Lift and Drag Coefficients

One of the most important and least well known inputs is the aerodynamic characteristics. The lift and drag coefficients usually are measured in a wind tunnel, where the flow is less turbulent than it is near a wind turbine rotor. This means that the lift and drag data used by the model can be very different from the lift and drag experienced by the airfoil sections.

# 4. Discussion of Results

An important step in the design or analysis of a horizontal axis wind turbine is determining stochastic loads that occur on the structure. The objective of this work was to develop a method for estimating these loads. The structural dynamics model FAST simulates the behavior of the machine under cyclic loads, both deterministic and stochastic.

## 4.1 Conclusions

The FAST code is a useful modeling tool. It can account for a wide range of wind turbine design parameters, including teetered rotors with delta-3 angle, coned blades, and a tilted shaft; and can model up to 14 degrees of freedom. The computation time is relatively short for a workstation or pentium PC (2.5 hours for a 75 megaHertz pentium with 16 megabytes of RAM). A simulation of 10 minutes of operation takes only a few hours of computation time. The input files are easy to read, and include a brief description of each variable. The output files can be tailored to print only the information of interest. Finally, there is a post-processor which can analyze the data in the output files and produce rainflow cycle counts, PSD's, histograms, azimuth binnings, or statistics.

The code successfully predicts the response frequencies of the structure, and the cyclic loads the blades will undergo. By modeling both the ESI-80 and the AWT-P1, the code was validated for two different machines over a range of wind speeds from 23 to 36 mph. Good agreement was achieved between data and model results for each of the methods of

analyzing the time series, demonstrating that the model will make reasonable predictions for the frequency response, cyclic loading, and average loads for these machines.

## 4.2 Future Work

Of interest is the comparison of other methods of representing turbulence, including three dimensional turbulence. The code is capable of accepting full field, three dimensional turbulence as a grid of points and interpolating to find the turbulence at each blade position. While this method of representing atmospheric turbulence is more detailed, it has not been determined to affect significantly the final predictions.

Further validation of the code could also be performed. Comparison of code predictions to test data for machines that are not similar to the ESI-80 or the AWT 26-P1 might further indicate the model's usefulness. Modeling a single machine at a number of different wind speeds would also indicate how well the model predicts over a wide range of conditions.

Investigation of variable rotor speed options should be performed. The transient loads produced during start-up and shut-down are of particular interest. The interaction between variable rotor speed and the edgewise degree of freedom may be important.

The FAST code can also be used for parametric studies on a particular machine. This not only could indicate ways to make the code even faster, but also could identify the model's sensitivity to certain parameters which might be useful for designing future wind turbine tests. More information about certain aspects of the machine might prove important in the evaluation of the loads, and perhaps improve the accuracy of machine life predictions.

Improved modeling might also be achieved through different mode shapes. The mode shapes used here were always polynomials, but other functions might better represent the blade and tower deflection shapes.

Further validation of modeling techniques could be performed by comparing the predictions of FAST to those of other codes. This process could suggest strengths of the FAST code, such as its simplicity or short run time.

Finally, the FAST code could be used in the design and design analysis of wind turbines. Based on the failure modes of current machines, design improvements could be made and tested before they are ever implemented. The performance of an existing wind turbine design at various sites could also be evaluated to determine under which terrain conditions the turbine is most efficient.

# References

Anderson, M. B., 1982, "The Interaction of Turbulence with a HAWT," Proc. of the Fourth British Wind Energy Association (BWEA) Wind Energy Conference, Cavendish Laboratory, University of Cambridge, pp. 104-118.

Bywaters, G., Personal Communication, October 1992.

Connell, J. R., 1981, "The Spectrum of Wind Speed Fluctuations Encountered by a Rotating Blade of a WECS," PNL 4083, Pacific Northwest Laboratories, Richland, WA.

Connell, J. R., 1982, "The Spectrum of Wind Speed Fluctuations Encountered by a Rotating Blade of a WECS," Solar Energy, Vol. 29.

Cook, R. D., Malkus, D. S., and Plesha, M. E., 19xx, Concepts and Applications of Finite Element Analysis, John Wiley and Sons, New York, pp. 376-377.

de Vries, O., 1985, "Comment on the Yaw Stability of a Horizontal-Axis Wind Turbine at Small Angles of Yaw," Wind Energy, Vol. 9, No. 1, pp. 42-49.

Garrad, A. D. and Hassan, U., 1986, "The Dynamic Response of Wind Turbines for Fatigue Life and Extreme Load Prediction," European Wind Energy Conference (EWEC).

Holley, W. E., 1985, "An Atmospheric Turbulence Model for Wind Turbine Dynamic Simulation: Its Verification and Implementation into the FLAP Code," Oregon State University, unpublished OSU report.

Holley, W. E., Thresher, R. W., and Jafarey, N., 1981, "Wind Response Characteristics of HAWTs," Proc. of the Wind Turbine Dynamics Workshop, Cleveland, OH, Oregon State University.

Homicz, G. F., 1987, "VAWT Aerodynamic Modeling with Stochastic Winds," 7th Annual VAWT Aerodynamics Seminar, Bushland, TX, Sandia National Laboratory.

Homicz, G. F., 1988, "VAWT Stochastic Loads Using a Full 3-D Simulation," 8th Annual VAWT Aerodynamics Seminar, Bushland, TX.

Kane, T. R. and Levinson, D. A., 1985, Dynamics, Theory and Applications, McGraw-Hill Book Co., New York.

Kelley, N. D., 1993, "Full Vector (3-D) Inflow Simulation in Natural and Wind Farm Environments Using an Expanded Version of the SNLWIND (VEERS) Turbulence Code," Wind Energy - 1993, edited by S. M. Hock, ASME SED-Vol. 14.

Kristensen, L. and Frandsen, S., 1982, "Model for Power Spectra of the Blade of a Wind Turbine Measured from the Moving Frame of Reference," J. of Wind Engr. and Ind. Aero., Vol. 10.

Lindenburg, C. and Snel, H., 1993, "PHATAS-11 Program for Horizontal Axis Wind Turbine Analysis and Simulation Version 11," Wind Energy - 1993, edited by S. M. Hock, ASME SED-Vol. 14.

Madsen, P. H., 1986, "DAP-1, A Data Analysis Package for Spectral Analysis, Version 1.2," Solar Energy Research Institute, Golden, CO, SERI internal unpublished report.

Malcolm, D. J., 1987, "Modal Loading and Response of Darrieus Rotors in Turbulent Flow," 7th Annual VAWT Aerodynamics Seminar, Bushland, TX.

Malcolm, D. J. and Wright, A. D., 1994, "The Use of ADAMS to Model the AWT-26 Prototype," Wind Energy - 1994, edited by W. D. Musial, ASME SED-Vol. 15.

Musial, W. D., Butterfield, C. P., and Handman, D., 1985, "ESI-80/EPRI Test Program," EPRI Research Project RP1996-A, Final Draft Report.

Powles, S. J. R. and Anderson, M. B., 1984, The Effect of Stochastic and Deterministic Loading on Fatigue Damage in a Large HAWT, Sir Robert McAlpine & Sons Ltd., London, U.K.

Putnam, P. C., 1948, Final Report on the Smith-Putnam Wind Turbine, Engineering Research Division, New York University, War Production Board.

Rosenbrock, H. H., 1955, Vibration and Stability Problems in Large Wind Turbines Having Hinged Blades, Electrical Research Association Report, C/T 113, London, U.K.

Sundar, R. M. and Sullivan, J. P., 1981, "Performance of Wind Turbines in a Turbulent Atmosphere," Proc. of Wind Turbine Dynamics, NASA CP 2185, Purdue University.

Sutherland, H. J., 1993, "Effect of the Flap and Edgewise Bending Moment Phase Relationships on the Fatigue Loads of a Typical HAWT Blade," Wind Energy - 1993, edited by S. M. Hock, ASME SED-Vol. 14.

Thresher, R. W. and Hershberg, E. L., 1985, "Development of an Analytical Model and Code for the Flapping Response of a HAWT Rotor Blade," SERI/STR-217-2629, Oregon State University.

Thresher, R. W., Holley, W. E., and Lin, S. R., 1981, "The Response Sensitivity of Wind Turbines to Atmospheric Turbulence," Proc. of the Wind Turbine Dynamics Workshop, Cleveland, OH, Oregon State University.

Veers, P. S., 1984, "Modeling Stochastic Wind Loads on Vertical Axis Wind Turbines," SAND83-1909, Sandia National Laboratory.

Veers, P. S., 1988, "Three-Dimensional Wind Simulation," SAND88-0152, Sandia National Laboratory.

Weber, T. L., 1991, "Turbulence Induced Loads on a Teetered Rotor," Ph.D. Thesis, Oregon State University.

Wilson, R. E. and Walker, S. N., 1984, "Performance Analysis of HAWTs," Oregon State University, Corvallis, OR.

Wilson, R. E., Walker, S. N., Smith, C. E., and Freeman, L. N., 1993, "Advanced Dynamics Code," Wind Energy - 1993, edited by S. M. Hock, ASME SED-Vol. 14.

Wilson, R. E., Freeman, L. N., and Walker, S. N., 1994, "Parametric Analysis of a Teetered Rotor Model," Wind Energy 1994, edited by W. D. Musial, ASME SED-Vol. 15.

Winkelaar, D., 1991, "Fast Three-Dimensional Wind Simulation and the Prediction of Stochastic Blade Loads," Tenth ASME Wind Energy Symposium, Houston, TX.

Wright, A. D. and Butterfield, C. P., 1992, "The NREL Teetering Hub Rotor Code: Final Test Results and Conclusion," Eleventh ASME Wind Energy Symposium Proceedings, edited by Veers and Hack, ASME, New York.

# Appendices

# Appendix A
# Program Input Files

The code uses a main input file to describe the wind turbine's operating parameters and basic geometry. Depending on the options chosen in the main input file, additional input data files may be necessary. This appendix covers the main input files used to model a wind turbine. Descriptions of the turbulence inputs are provided in Appendix B, while Appendix C discusses the determination of the blade and tower mode shapes.

The main input file has a simple text format that can be read by most editors and imported into many word processing applications. Each line in the input file is divided into three sections: number, variable, and description. The number section contains the value assigned to the variable. Numbers of up to seven significant digits can be input, and must be separated from other sections by a space, tab, or comma. The variable section contains the name of the variable assigned to the numerical value which is used by the program. The description section of the line contains a brief description of the numerical value as a reminder to the user of its purpose. This section also contains the physical units of the numerical value, where appropriate. A sample line from the input file divided into its sections is shown below.

```
1000.   PRESS   - BAROMETRIC PRESSURE OF SITE - (MB)
```

Number  Variable  Description

Only the number is read by the computer and the rest of the line is only a comment.

Near the end of the input file, there are tables that describe the blade characteristics. Six columns of data are required in this section, each of which

must be separated from the other by a space, tab, or comma. There is also a table for the tower characteristics which requires four columns of data.

There are no blank lines in the input file. The program reads each line of the input file in sequential order, and if any lines are inserted or deleted, data will be read incorrectly. This should never be done unless the code is changed to accept such a format. Lines containing section or file titles may be altered to suite the user since these lines are read as text but not used by the program.

## A.1 Explanation of Input Parameters

The definitions and physical locations of some of the inputs to the main input file are not as obvious as others, so a brief description of each is given below. For inputs that require only a one or zero, a value of one indicates the desire to have that option and a value of zero indicates the opposite (i.e., 1 = yes or 0 = no). Units and reference to descriptive figures are also given where applicable.

### General Inputs

NRSTRT (dimensionless) - Number of revolutions before turbulence and recording. This tells the program how many revolutions to wait before outputting data to files. It also causes a delay in including the effects of turbulence. A delay of at least three revolutions is advisable to allow the initial transient effects to decay.

NREVMX (dimensionless) - Maximum number of revolutions for the turbine. The program stops running when NREVMX has been exceeded. If turbulence effects are included, the program will terminate at the end of the turbulence file if there are less lines of data in it than the maximum number of revolutions is not reached.

DT (seconds) - Step for numerical integration. Care should be taken in choosing a small enough value for DT, as the numerical solution will become unstable and cause an overflow error if DT is too large. Typical

values of DT are less than 0.01 seconds when blades are flexible. If two dimensional turbulence effects are included, DT should agree with the time incrementation in the turbulence file. Since the turbulence is generated using an FFT, the number of increments per revolution must be a power of 2. The time step is related by DT = period of revolution / $2^N$.

NTSKIP (dimensionless) - Allows user to pre-filter the data and save only a portion of the output. Useful if a very small time step is required.

V (m/s) - Mean wind velocity upstream of the rotor at the height of the hub.

ETA (dimensionless) - Wind shear power law exponent used to describe the roughness of the surrounding terrain at the wind turbine site. Typical values range from 0.1 to 0.2 with the higher value indicating rougher terrain. ETA is used in calculating the increase in wind speed with height due to the planetary boundary layer.

TEMP (K) /PRESS (mbar) - The ambient temperature and pressure of the wind turbine site. These are in turn used to calculate the ambient air density.

**Degree of Freedom Switches**

IZ(1) (yes or no) - Switch for including the first flapwise blade bending mode.

IZ(11) (yes or no) - Switch for including the second flapwise blade bending mode. Including this gives more accurate predictions of the blade vibration. This should not be used without the first flap mode.

IZ(13) (yes or no) - Switch for first edgewise bending mode.

IZ(3) (yes or no) - Switch to include rotor teetering. If this option is off, teeter can be set to a non-zero, fixed angle.

IZD(4) (yes or no) - Switch to include the effects of a variable rotor rotational speed. 0 = constant RPM, 1 = induction generator, 2 = start-up, 3 = shut-down. Note that the two-dimensional turbulence option and the variable speed option can't be used together.

IZD(5) (yes or no) - Switch to include flexibility of the drive train. This models the drive train between the generator and rotor as a lumped torsion spring.

IZ (6) (yes or no) - Switch for yaw degree of freedom. If this option is off, yaw can be set to a non-zero, fixed angle.

IZ (7) (yes or no) - Switch for first tower bending mode mode, which allows tower to bend in two directions. All mode shapes are in Appendix E.

IZ (9) (yes or no) - Switch for second tower bending mode. This should not be used without IZ(7), and used only when added accuracy is required for tower motion.

ISHAD (yes or no) - Switch for tower shadow. This models the loss in wind speed at the rotor due to tower interference. Note that tower shadow is applicable only to turbines whose blades are downwind of the tower.

ISHR (yes or no) - Switch for wind shear. This models the effects of the planetary boundary layer on the mean wind.

ITRB2D (yes or no) - Switch to include the effects of two dimensional turbulence. This models the effects of turbulence on the local wind and requires a turbulence data file generated by the Veers' Turbulence Code [3]. The time increment of the data file should be the same as DT. Note that this turbulence option and the variable speed option can not be used together.

ITRB3D (yes or no) - Switch to include three dimensional turbulence field. A binary turbulence data file is required for each velocity component.

IDYNST (yes or no) - Switch for dynamic stall. This models dynamic stall with the Gormont Model. This option can not be used with the airfoil data file.

IWNDIR (yes or no) - Switch for varying wind direction. This option requires an input data file and can only be used with ITRB2D = 1. A sample data file is shown in Appendix A.4.

**Initial Conditions**

Z(1) (m) - Initial flapwise blade tip displacement (see Figure 2.3-1). Note that by specifying values for initial conditions close to the steady state conditions, the numerical solution technique will converge faster and shorten computational time. This is especially useful when making repetitive runs.

Z(13) (m) - Initial edgewise blade tip displacement (see Figure 2.3-1).

Z(3) (deg) - Initial or fixed teeter angle (see Figure 2.3-1).

Z(4) (deg) - Initial azimuth angle for blade 1 (see Figure 2.3-1).

ZD(4) (RPM) - Steady state angular velocity (see Figure 2.3-1).

Z(6) (deg) - Initial or fixed yaw angle (see Figure 2.3-1).

Z(7) (m) - Initial longitudinal tower displacement (see Figure 2.3-1).

Z(8) (m) - Initial lateral tower displacement (see Figure 2.3-1).

**Machine Parameters**

RT (m) - Blade tip radius (see Figure 2.3-1).

RH (m) - Blade hub radius (see Figure 2.3-1).

THETA (deg) - Blade collective pitch for partial-span aileron control devices (see Figure 2.3-1).

RRGAP (dimensionless) - Location of end of gap between blade and partial-span aileron control devices (see Figure 2.3-1).

RLU (m) - Underslung length (see Figure 2.3-1), measured from the teeter pin. Positive is in the downwind direction.

RLUM (m) - Distance to hub mass center from teeter pin (see Figure 2.3-1). Positive is in the downwind direction.

DN (m) - Distance from yaw axis to rotor/teeter pin (see Figure 2.3-1). Positive is in the downwind direction.

DNM (m) - Distance to nacelle mass center from yaw axis (see Figure 2.3-1). Positive is in the downwind direction.

HH (m) - Hub height above ground level (see Figure 2.3-1).

HS (m) - Tower rigid base height (see Figure 2.3-1).

CHI (deg) - Fixed drive shaft tilt angle (see Figure 2.3-1).

DELTA3 (deg) - Teeter pin orientation angle (see Figure 2.3-1).

BETA(1) (deg) - Blade one coning angle (see Figure 2.3-1).

BETA(2) (deg) - Blade two coning angle (see Figure 2.3-1).

**Mass and Inertia**

XMNAC (kg) - Nacelle mass.

XMHUB (kg) - Hub mass.

TIPM(1) (kg) - Blade one aerodynamic tip brake mass (see Figure 2.3-1).

TIPM(2) (kg) - Blade two aerodynamic tip brake mass (see Figure 2.3-1).

HSINER (kg - $m^2$) - Generator moment of inertia.

HYINER (kg - $m^2$) - Nacelle moment of inertia about yaw axis.

HINER (kg - $m^2$) - Hub moment of inertia about teeter axis.

**Drive Train Parameters**

ETAGB (dimensionless) - Gearbox efficiency.

ETAGEN (dimensionless) - Peak generator efficiency.

OMEGR (RPM) - Rated speed for induction generator (see Figure 2.8-1).

OMEG0 (RPM) - Initial induction generator speed for producing electricity (see Figure 2.8-1).

CINGEN ((N-m)/(r/s)) - Induction generator slope constant for generator side of turbine (see Figure 2.8-1).

YN (dimensionless) - Gearbox ratio.

QFL (N-m) - Fixed loss constant.

QVL (N-m) - Variable loss constant.

QBRAKE (N/m) - Mechanical brake torque value.

QMOTOR (N-m) - Motor start-up torque for generator side of turbine (see Figure 2.8-1).

ZKDRV ((N-m)/rad) - Drive train torsional spring constant.

CDRV ((N-m)/s) - Drive train torsional damper constant.

**Tower Parameters**

CTWR (%) - Tower structural damping in percent of critical.

EL (dimensionless) - Tower shadow width/rotor radius. Tower shadow width is L in Figure 2.9-1.

EPP (dimensionless) - Tower shadow velocity deficit. This varies from 0 to 1 and is shown as in Figure 2.9-1.

NXTWR (dimensionless) - Number of tower increments.

N2 (dimensionless) - Number of input stations to specify tower geometry.

AMSTWR (dimensionless) - Factor to adjust tower mass.

STFLNG (dimensionless) - Factor to adjust longitudinal stiffness.

STFLAT (dimensionless) - Factor to adjust lateral stiffness.

**Tower Distributed Parameters**

RAD (dimensionless) - Fractional height along tower of the following parameters:

MASS (kg/m) - Mass per unit length of tower section.

LONG STIF ($Nm^2$) - Longitudinal tower stiffness.

LAT STIF ($Nm^2$) - Lateral tower stiffness.

**Yaw and Teeter Parameters**

ZKYAW ((N-m)/rad) - Yaw spring constant.

COULMB (Nm) - Coulomb friction moment at teeter hinge.

ITSPDM (dimensionless) - Teeter damper type. Choices are: 0 = no teeter damper, 1 = linear damper, 3 = user's function. Option 3 requires modification of the source code.

CTEET ((N-m)/(rad/s)) - Teeter damper constant.

ZKTEET(1) (N-m) - First teeter spring coefficient for cubic curve fit.

ZKTEET(2) ((N-m)/rad) - Second teeter spring coefficient for cubic curve fit.

ZKTEET(3) ((N-m)/rad$^2$) - Third teeter spring coefficient for cubic curve fit.

QCTEET (deg) - Angle where teeter damper begins (see Figure 2.3-1).

QKTEET (deg) - Angle where teeter spring begins (see Figure 2.3-1).

TSTOP (deg) - Teeter stop angle (see Figure 2.3-1).

**Blade Parameters**

CBLD (percent) - Blade structural damping in percent of critical.

CDA (ft$^2$) - Flat plate drag area for establishing drag coefficient on tip brake.

IAIRFO (0, 1, 2, or 3) - Blade airfoil choice. Choices are as follows: 0 = Table look up, 1 = NASA LS-1, 2 = NACA 23000, 3 = NACA xxxxx experimental. Option 0 requires a airfoil data file. An example of this file is provided in Appendix A.5.

NR (dimensionless) - Number of increments along blade for integration of forces. The more increments, the more accurate the integral, but longer the computational time. A good compromise for NR is 20.

N1 (dimensionless) - Number of rows of data in blade sectional data per blade.

STFFAC(1), (2) - Factor to adjust blade flapwise stiffness in blade sectional data.

STEFAC(1), (2) - Factor to adjust blade edgewise stiffness in blade sectional data.

AMSFAC(1), (2) - Factor to adjust blade mass per unit length in blade sectional data.

CHDFAC(1), (2) - Factor to adjust blade chord in blade sectional data.

TWIFAC(1), (2) - Factor to adjust blade aerodynamic twist angle in blade sectional data.

TWSFAC(1), (2) - Factor to adjust blade structural twist angle in blade sectional data.

**Blade Sectional Data**

RAD (dimensionless) - Fractional location along turbine blade of following parameters:

CHORD (m) - Length of airfoil section from the leading edge to trailing edge.

THICK (dimensionless) - Maximum thickness of the airfoil/chord length.

AERO TWIST (deg) - Blade aerodynamic twist angle.

MASS (kg/m) - Mass per unit length of blade section.

FLAP STIFF ($Nm^2$) - Blade flapwise stiffness.

STRUC TWIST (deg) - Blade structural twist angle.

EDGEW STIFF ($Nm^2$) - Blade edgewise stiffness.

**Mode Shapes**

PC(1,1-6) (dimensionless) - Coefficients of polynomial equation used to model first flapwise mode shape of blade.

PC(2,1-6) (dimensionless) - Coefficients of polynomial equation used to model second flapwise mode shape of blade.

PC(3,1-6) (dimensionless) - Coefficients of polynomial equation used to model first edgewise mode shape of blade.

PC(4,1-6) (dimensionless) - Coefficients of polynomial equation used to model first mode shape of tower.

PC(5,1-6) (dimensionless) - Coefficients of polynomial equation used to model second mode shape of tower.

**Format of Output File**

NC(1-30) (dimensionless) - Choice of variables to output to files. There are 30 available spaces for output data, ten in each of three files. The list of data available for output follows this section.

NCMAX (dimensionless) - Maximum number of variables to output. Not all of the spaces available in output files must be used. If less than 30 columns of output is desired, NCMAX may be set to less than 30. It should not be set to more than 30. If this number is less than 10, only one output file will be created. If this number is less than 20, only two output files will be created.

By varying the values in the array NC( ), the form of the output files can be changed. For example, if the only output desired is time, azimuth angle of the rotor, and teeter angle, then the first three elements of NC would be 0, 13, 9, and NCMAX would be set to 3. Only one output file will be created, and it will have only three columns of data.

## A.2 ESI-80 Machine Input File

The ESI-80 has two blades, a teetered hub, and other specifications given in Table 3.1-1. This run includes the effects of two-dimensional turbulence, which means that an additional input data file developed with the Veers' Turbulence Code is required. A discription of the turbulence modeling is contained in Appendix B.

This run did not use a variable speed drive train or variable wind direction. If these options were desired, the appropriate "switches" in the input file should be turned on. In the case of a variable speed drive train, the user would have to change the variable IZD in the main input file (induction generator, start up, shut down, or variable speed generator). In the case of a variable wind direction, the interactive selection for wind direction should be responded to with a one and a

data file name given. The following is a listing of the input file used to describe the ESI-80 horizontal axis wind turbine.

```
---------------------- SAMPLE TWO BLADED TEETERING ROTOR WITH SECOND MODE ---------------
---------------------- MODIFIED FEBRUARY 1, 1996 ----------------------------------------
       3       NRSTRT          - NUMBER OF REVOLUTIONS BEFORE TURBULENCE, RECORDING
       135     NREVMX          - MAXIMUM NUMBER OF REVOLUTIONS
       .00773  DT              - TIME INCREMENT (s)
       0       NTSKIP          - NUMBER OF TIME STEPS TO SKIP FOR OUTPUT (0 = NONE)
---------------------- ATMOSPHERIC CONDITIONS -------------------------------------------
       16.38   V               - MEAN WIND VELOCITY UPSTREAM AT HUB HEIGHT (m/s)
       .19     ETA             - WIND SHEAR POWER LAW EXPONENT (dim.less)
       1000.   PRESS           - BAROMETRIC PRESSURE OF SITE - (MBAR)
       289.    TEMP            - TEMPERATURE AT HUB (degrees Kelvin)
---------------------- DEGREE OF FREEDOM SWITCHES ---------------------------------------
       1       IZ(1)           - FIRST FLAPWISE BLADE MODE (YES=1)
       1       IZ(11)          - SECOND FLAPWISE BLADE MODE (YES=1)
       1       IZ(13)          - FIRST EDGEWISE BLADE MODE (YES=1)
       1       IZ(3)           - TEETERED (YES=1)
       0       IZD(4)          - (0) CONSTANT SPEED (1) IND. GEN. (2) START UP (3) SHUTDOWN
       0       IZD(5)          - DRIVETRAIN FLEXIBILITY (YES=1)
       1       IZ(6)           - YAW DEGREE OF FREEDOM (YES=1)
       1       IZ(7)           - FIRST TOWER MODES (YES=1)
       0       IZ(9)           - SECOND TOWER MODES (YES=1)
       1       ISHAD           - TOWER SHADOW INCLUDED (YES=1)
       1       ISHR            - WIND SHEAR INCLUDED (YES=1)
       1       ITRB2D          - 2D TURBULENCE INPUT (YES=1)
       0       ITRB3D          - 3D TURBULENCE FIELD (YES=1)
       0       IDYNST          - DYNAMIC STALL INCLUDED (YES=1)
       0       IWNDIR          - VARYING WIND DIRECTION FOR 2D TURBULENCE (YES=1)
---------------------- INITIAL CONDITIONS -----------------------------------------------
       0.01    Z(1)            - BLADE TIP INITIAL FLAPWISE DISPLACEMENT, (meters)
       0.      Z(13)           - BLADE TIP INITIAL EDGEWISE DISPLACEMENT, (meters)
       0.      Z(3)            - INITIAL OR FIXED TEETER ANGLE (degrees)
       0.      Z(4)            - INITIAL AZIMUTH ANGLE FOR BLADE 1 (degrees)
       60.66   ZD(4)           - STEADY STATE ANGULAR VELOCITY OF BLADES (RPM)
       0.      Z(6)            - FIXED OR INITIAL YAW ANGLE (degrees)
       0.005   Z(7)            - INITIAL LONGITUDINAL TOWER DISPL. (m)
       0.001   Z(8)            - INITIAL LATERAL TOWER DISPL. (meters)
---------------------- MACHINE PARAMETERS -----------------------------------------------
       12.19   RT              - BLADE TIP RADIUS (meters)
       .92     RH              - BLADE HUB RADIUS (meters)
       0.      THETA           - BLADE COLLECTIVE PITCH (degrees)
       0.      RRGAP           - LOCATION OF GAP END IN FRACTION OF TIP RADIUS
       .59     RLU             - UNDERSLING LENGTH (meters)
       .42     RLUM            - DISTANCE FROM HUB MASS TO TEETER PIN (meters)
       2.17    DN              - DISTANCE FROM YAW AXIS TO ROTOR / TEETER PIN (meters)
       -.30    DNM             - DISTANCE TO NACELLE MASS FROM YAW AXIS (meters)
       24.1    HH              - HUB HEIGHT ABOVE GROUND LEVEL (meters)
       0.      HS              - TOWER RIGID BASE HEIGHT (meters)
       0.      CHI             - FIXED GENERATOR TILT ANGLE (degrees)
       0.      DELTA3          - DELTA3 ANGLE (degrees)
       7.      BETA(1)         - BLADE 1 CONING ANGLE (degrees)
       7.      BETA(2)         - BLADE 2 CONING ANGLE (degrees)
---------------------- MASS AND INERTIA -------------------------------------------------
       3860.   XMNAC           - NACELLE LUMPED MASS (kg)
       650.    XMHUB           - MASS OF HUB (kg)
       20.2    TIPM(1)         - MASS OF TIP BRAKE, BLADE 1 (kg)
       20.2    TIPM(2)         - MASS OF TIP BRAKE, BLADE 2 (kg)
       5.      HSINER          - INERTIA OF GENERATOR (kg m^2)
       2600.   HYINER          - INERTIA OF NACELLE  ABOUT YAW AXIS (kg m^2)
       220.    HINER           - INERTIA OF HUB ABOUT TEETER AXIS (kg m^2)
---------------------- DRIVETRAIN PARAMETERS --------------------------------------------
       .985    ETAGB           - GEARBOX EFFICIENCY (dim.less)
       .94     ETAGEN          - GENERATOR EFFICIENCY (dim.less)
       60.9    OMEGR           - RATED SPEED FOR INDUCTION GENERATOR (RPM)
       60.     OMEGO           - INITIAL INDUCTION GENERATOR SPEED (RPM)
       590.    CINGEN          - INDUCTION GENERATOR CONSTANT ((N m)/(r/s))
       30.     YN              - GEARBOX RATIO (dim.less)
       17.7    QFL             - FIXED LOSS CONSTANT (N m)
       17.7    QVL             - VARIABLE LOSS CONSTANT (N m)
       250000. QBRAKE          - MECHANICAL BRAKE TORQUE VALUE (N/m)
       550.    QMOTOR  - MOTOR START-UP TORQUE (GENERATOR SIDE) (N m)
       3135000.        ZKDRV           - DRIVETRAIN TORSIONAL SPRING (N m)/rad
       8855.   CDRV            - DRIVETRAIN TORSIONAL DAMPER (N m)/sec
---------------------- TOWER PARAMETERS -------------------------------------------------
       3.      CTWR            - TOWER STRUCTURAL DAMPING IN PERCENT OF CRITICAL (%)
       .45     EL              - TOWER SHADOW WIDTH / ROTOR RADIUS  (dim.less)
```

```
       .3      EPP             - TOWER SHADOW VELOCITY DEFICIT (dim.less)
       20      NXTWR           - NUMBER OF TOWER INCREMENTS (dim.less)
       3       N2              - NUMBER OF INPUT STATIONS TO SPECIFY TOWER GEOMETRY
       1.      AMSTWR          - FACTOR TO ADJUST TOWER MASS (dim.less)
       1.      STFLNG          - FACTOR TO ADJUST LONGITUDINAL STIFFNESS (dim.less)
       1.      STFLAT          - FACTOR TO ADJUST LATERAL STIFFNESS (dim.less)
--------RAD----------MASS------------LONG STIF ------------ LAT STIF --------------------
         %            kg/m              Nm^2                    Nm^2
---------------------- TOWER-------------------------------------------------------------
       .0,           1520,           664000000.,           664000000.
       .5,           1520,           664000000.,           664000000.
       1.0,          1520,           664000000.,           664000000.
---------------------- YAW AND TEETER PARAMETERS ----------------------------------------
       0.      ZKYAW           - YAW SPRING (N m)/rad
       0.      COULMB          - COULOMB DAMPING MOMENT, Nm
       1       ITSPDM          - DAMPER SWITCH:  0 = NONE, 1 = LINEAR, 3 = USER
       14000.  CTEET           - TEETER DAMPER (N m)/(rad/s)
       13700.  ZKTEET(1)       - TEETER SPRING COEFFICIENTS Nm, Nm/rad, Nm/rad^2
       206000.         ZKTEET(2)       - teeter moment = ZKT(1) + ZKT(2) * (NET Q3)
       9.76E6  ZKTEET(3) -                     + ZKT(3) * (NET Q3)^2
       2.      QCTEET          - ANGLE WHERE TEETER DAMPER BEGINS (degrees)
       2.      QKTEET          - ANGLE WHERE TEETER SPRING BEGINS (degrees)
       10.     TSTOP           - TEETER STOP ANGLE (degrees)
---------------------- BLADE PARAMETERS -------------------------------------------------
       .5      CBLD            - BLADE STRUCTURAL DAMPING IN PERCENT OF CRITICAL (%)
       .00372  CDA             - TIP BRAKE FLAT PLATE AREA (FT^2)
       1       IAIRFO          - (0) TABLE (1) NASA LS1  (2) NACA 23000 (3) NACAXXXX
       20      NR              - NUMBER OF BLADE INCREMENTS          (dim.less)
       12      N1              - NUMBER OF INPUT STATIONS TO SPECIFY BLADE GEOMETRY
       1.      STFFAC(1)       - FACTOR TO ADJUST BLADE 1 STIFFNESS  (dim.less)
       1.      STFFAC(2)             (FLAP)      BLADE 2           (dim.less)
       1.      STEFAC(1)       - FACTOR TO ADJUST BLADE 1 STIFFNESS  (dim.less)
       1.      STEFAC(2)             (EDGE)      BLADE 2           (dim.less)
       1.      AMSFAC(1)       - FACTOR TO ADJUST BLADE 1 MASS               (dim.less)
       1.      AMSFAC(2)                         BLADE 2           (dim.less)
       1.      CHDFAC(1)       - FACTOR TO ADJUST BLADE 1 CHORD      (dim.less)
       1.      CHDFAC(2)                         BLADE 2           (dim.less)
       1.      TWIFAC(1)       - FACTOR TO ADJUST BLADE 1 TWIST              (dim.less)
       1.      TWIFAC(2)             (AERO)      BLADE 2           (dim.less)
       1.      TWSFAC(1)       - FACTOR TO ADJUST BLADE 1 TWIST              (dim.less)
       1.      TWSFAC(2)             (STRUCTURAL)    BLADE 2               (dim.less)
--- RAD -- CHORD - THICK - AERO -- MASS ---- FLAP------STRUC--EDGEW.-STIFF-
     %       m       t/c     TWIST     kg/m      STIFF       TWIST       Nm^2
---------------------- BLADE 1 ----------------------------------------------------------
   0.075    .6350,    .54,     2.02,    79.01,    15100000     2.02    172500000
   0.15,    .7102,    .45,     1.84,    55.05,     9120000     1.84     62000000
   0.25,    .8466,    .34,     1.66,    49.10,     4830000     1.66     67200000
   0.30,    .8888,    .32,     1.56,    43.89,     3100000     1.56     64300000
   0.35,    .8778,    .30,     1.47,    40.17,     2470000     1.47     57300000
   0.45,    .8047,    .29,     1.20,    32.73,     1770000     1.20     37300000
   0.55,    .7330,    .28,     0.83,    25.29,     1190000     0.83     19900000
   0.65,    .6604,    .26,     0.49,    17.59,      694000     0.49      9570000
   0.75,    .5877,    .25,     0.00,    12.35,      452000     0.00      5390000
   0.85,    .5154,    .22,    -0.62,    10.71,      307000    -0.62      4060000
   0.95,    .4427,    .19,    -1.45,     9.02,      197000    -1.45      2820000
   1.00,    .4063,    .17,    -1.99,     8.20,      145000    -1.99      2150000
---------------------- BLADE 2 ----------------------------------------------------------
   0.075    .6350,    .54,     2.02,    79.01,    15100000     2.02    172500000
   0.15,    .7102,    .45,     1.84,    55.05,     9120000     1.84     62000000
   0.25,    .8466,    .34,     1.66,    49.10,     4830000     1.66     67200000
   0.30,    .8888,    .32,     1.56,    43.89,     3100000     1.56     64300000
   0.35,    .8778,    .30,     1.47,    40.17,     2470000     1.47     57300000
   0.45,    .8047,    .29,     1.20,    32.73,     1770000     1.20     37300000
   0.55,    .7330,    .28,     0.83,    25.29,     1190000     0.83     19900000
   0.65,    .6604,    .26,     0.49,    17.59,      694000     0.49      9570000
   0.75,    .5877,    .25,     0.00,    12.35,      452000     0.00      5390000
   0.85,    .5154,    .22,    -0.62,    10.71,      307000    -0.62      4060000
   0.95,    .4427,    .19,    -1.45,     9.02,      197000    -1.45      2820000
   1.00,    .4063,    .17,    -1.99,     8.20,      145000    -1.99      2150000
---------------------- MODE SHAPES------------------------------------------------------
       0.              PC(1,1)         - BLADE MODE 1 , COEFF OF X^1
       0.              PC(1,2)                        , COEFF OF X^2
       0.              PC(1,3)                        , COEFF OF X^3
       5.35912         PC(1,4)                        , COEFF OF X^4
      -6.93726         PC(1,5)                        , COEFF OF X^5
```

```
        2.57815         PC(1,6)                         , COEFF OF X^6
        0.              PC(2,1)         - BLADE MODE 2
        0.              PC(2,2)
        0.              PC(2,3)
        -45.69367       PC(2,4)
        87.33445        PC(2,5)
        -40.65079       PC(2,6)
        0.              PC(3,1)         - EDGEWISE MODE 1
        0.              PC(3,2)
        2.49702         PC(3,3)
        -2.47299        PC(3,4)
        0.97597         PC(3,5)
        0.              PC(3,6)
        0.              PC(4,1)         - TOWER MODE 1
        0.              PC(4,2)
        4.09673         PC(4,3)
        -4.78786        PC(4,4)
        1.69133         PC(4,5)
        0.              PC(4,6)
        0.              PC(5,1)         - TOWER MODE 2
        0.              PC(5,2)
        -132.816        PC(5,3)
        243.102         PC(5,4)
        -109.286        PC(5,5)
        0.              PC(5,6)
---------------------- FORMAT OF OUTPUT FILES - EACH HAS 10 COLUMNS --------------------
        0       NC(1) = 0       FILE 1 BEGINS HERE
        21      NC(2)
        22      NC(3)
        29      NC(4)
        30      NC(5)
        31      NC(6)
        33      NC(7)
        34      NC(8)
        35      NC(9)
        13      NC(10)
        0       NC(11)          FILE 2 BEGINS HERE
        10      NC(12)
        11      NC(13)
        12      NC(14)
        1       NC(15)
        2       NC(16)
        3       NC(17)
        4       NC(18)
        9       NC(19)
        13      NC(20)
        0       NC(21)          FILE 3 BEGINS HERE
        13      NC(22)
        14      NC(23)
        15      NC(24)
        16      NC(25)
        39      NC(26)
        36      NC(27)
        37      NC(28)
        32      NC(29)
        13      NC(30)
        10      NCMAX = 30      MAX # COLUMNS TO PRINT
-------------------------------------------------------------------------------------
```

The previous input file was for the 36 mph (13.7 m/s) case. Table A-1 lists the input parameters that are different for the 23 mph (10.1 m/s) case.

**Table A-1** Input Parameters for Two ESI-80 Cases

| | Case 1 | Case 2 |
|---|---|---|
| Wind Speed, mph | 36.1 | 22.6 |
| Wind Speed, m/s | 13.68 | 10.09 |
| Turb. Intensity, % | 11.6 | 8.3 |
| Wind Shear Exponent | 0.19 | 0.08 |
| Tower Shadow Deficit | 0.3 | 0.15 |
| Blade Damping, % | 0.5 | 0.1 |
| Rotor Speed, rpm | 60.7 | 60.2 |

# Appendix B
# 2D Turbulence Input

Turbulence is included as part of the wind input and created from a separate program. A rotationally sampled two dimensional turbulence record is created by the Sandia Wind Simulation, as discussed in section 2.9.3. This code creates a full three-dimensional turbulence field, and samples it at one or several points on the blade given the constant rotor rotation speed and the rotor diameter. An example of the turbulence file and the specific files used for the ESI-80 simulation are discussed below.

## B.1 Turbulence Input Data File

The following is a partial listing of the two-dimensional turbulence input data file. This file was generated by Veers' Turbulence Code, a separate program widely used in generating turbulence data for wind turbines. The first column is time (in seconds) and the other two are changes in local wind speed (in m/s) at 80% of the total blade radius for each blade. Note that the time incrementation must be the same as DT in the main input file.

```
0.008   1.1313  -2.0381
0.015   0.6474  -2.3888
0.023   0.4296  -2.1087
0.031   0.3852  -2.0901
0.039   0.2810  -1.5972
0.046   0.6279  -1.2952
0.054   0.5156  -1.5683
0.062   0.3805  -0.7162
0.070   0.2408  -0.2483
0.077   0.0506  -0.4010
0.085   -0.0500 -0.2885
0.093   0.2492  -0.4293
0.100   0.1226  -0.8623
0.108   0.3650  -1.0109
0.116   0.5668  -1.0396
0.124   0.7678  -1.4122
0.131   1.0201  -0.7217
```

```
0.139   1.2262  -0.4884
0.147   1.2878  -0.4424
0.155   1.1814  -0.1629

9.953   -1.7212 -0.7388
9.961   -1.9242 -0.7797
9.968   -2.4258 0.0809
9.976   -2.7682 -0.2888
9.984   -3.2124 0.4651
9.992   -3.4016 0.8541
9.999   -3.4071 1.6542
10.007  -2.7631 1.5058
10.015  -2.5940 1.1607
10.023  -2.5897 0.7330
10.030  -2.6049 0.8823
10.038  -2.8925 0.4002
10.046  -2.8301 0.2034
10.053  -3.2622 0.3824
10.061  -3.4199 0.3251
10.069  -3.6561 -0.0470
10.077  -4.0499 0.3926
10.084  -3.0990 0.2088
10.092  -2.6836 0.4964
10.100  -3.1562 0.5929
10.108  -2.5330 0.8538
10.115  -2.3791 0.3618
10.123  -2.1627 -0.0755
10.131  -1.8783 -0.0360
10.138  -1.5554 0.3699
```

A sample input file for the turbulence code is shown below.

```
      2  | NUMBER OF BLADES
    256  | NUMBER OF POINTS PER REVOLUTION
 131072  | LENGTH OF ROTATIONALLY SAMPLED TIME SERIES (# OF SAMPLES)
      8  | NUMBER OF POINTS TO BE FREQUENCY AVERAGED
      6  | NUMBER OF BLOCKS TO BE SIMULATED (AND ENSEMBLE AVERAGED)
  1.011  | ROTATIONAL FREQUENCY (HZ)
   24.1  | HUB HEIGHT (M)
      1  | NUMBER OF RADIAL POSITIONS
 9.7535  | RADIAL POSITIONS (M)
 16.3778 | MEAN WIND SPEED AT 10 METERS (M/S)
   .007  | SURFACE ROUGHNESS COEFFICIENT, Z0
   0.00  | WIND SHEAR EXPONENT, SHEEXP
    20.  | COHERENCE DECREMENT, COHDEC
   0.25  | COHERENCE EXPONENT, 0 - EXPONENTIAL, .25 - SOLARI, <0 - DEFAULT
197569085| RANDOM SEED, ISEED (BETWEEN 0 AND 2147483647)
 'Z5.DAT' | THE ENTIRE NAME OF THE H MATRIX FILE TO BE READ OR DEFINED
   'NO'   | options: 1. USE A PREVIOUSLY DEFINED H MATRIX? YES-NO
   'YES'  | 2. CREATE TIME SERIES FILES? YES-NO
  'RSTS'  |  ROTATIONALLY SAMPLED TIME SERIES FILE NAME (IGNORED IF OPT 2='NO')
   'NO'   | 3. ESTIMATE THE ROTATIONALLY SAMPLED PSD? YES-NO
 'RSPSD'  |  ROTATIONALLY SAMPLED PSD FILE NAME (IGNORED IF OPT 3 = 'NO')
   'NO'   | 4. CALCULATE THE PER REV VARIANCE OF THE ROT. SAM. PSD ? YES-NO
   'NO'   | 5. INCLUDE MEAN WIND PROFILE (WIND SHEAR)? YES-NO
'SOLARI'  | 6. TURBULENCE PSD TYPE: SOLARI, KAIMAL AND FROST ARE THE CHOICES
   'YES'  | 7. DO YOU WANT TO SIMULATE THE WIND AT THE HUB? YES-NO
   'YES'  | 8. DO YOU WANT TO SPECIFY THE TURBULENCE INTENSITY? YES-NO
    .1    |  SPECIFIED TURBULENCE INTENSITY (IGNORED IF OPTION 8 = 'NO'):
```

The turbulence code generates a time series of turbulent wind, then rotationally samples this array of values based on the rotor rpm and the blade segment location.

## B.2 ESI-80 Machine

The mean wind speed and turbulence intensity were calculated from the wind speed data, and the mean rotor speed was found from the loading data. For the first data set, the turbulensity was 13.6%, with a wind speed of 36 mph and a mean rotor rotational speed of 60.7 rpm. The resulting turbulence at the hub has a PSD that has the expected -5/3 slope, as shown in Figure B-1. The data drops off more rapidly above 1 Hertz, which is presumed to be caused by the relatively slow response time of the wind measurement device. The mean and standard deviation of the hub turbulence agree with the specified mean and turbulence intensity.

For the second data set for the ESI-80 machine, the turbulence intensity was 11.2%, with a mean wind speed of 23 mph, and rotor rotational speed of 60.2 rpm. The resulting turbulence at the hub has a PSD that also has the expected -5/3 slope, as shown in Figure B-2. The mean and standard deviation of the hub turbulence agree with the specified mean and turbulence intensity.

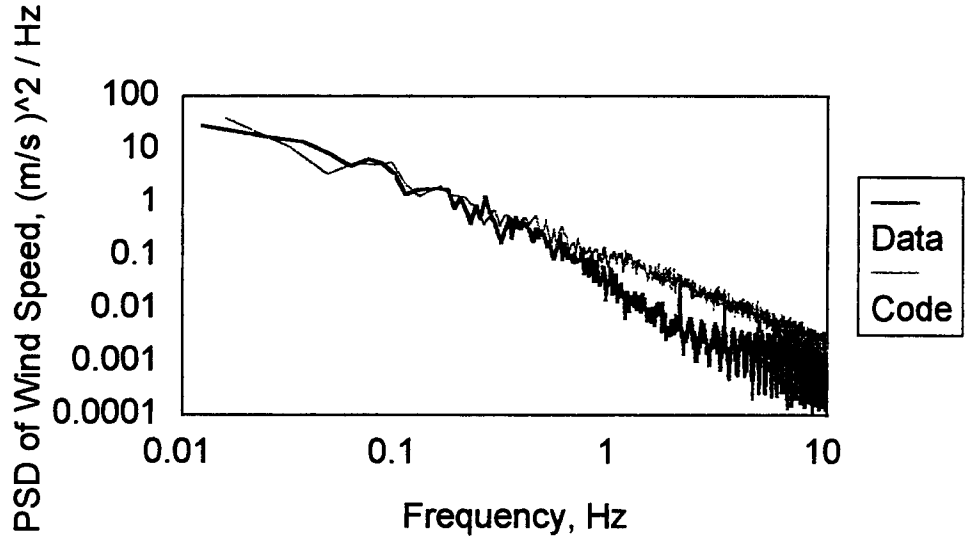


**Figure B-1** Comparison of Wind Data and Code Input Turbulence for the ESI-80 with a Mean Wind Speed of 36 mph

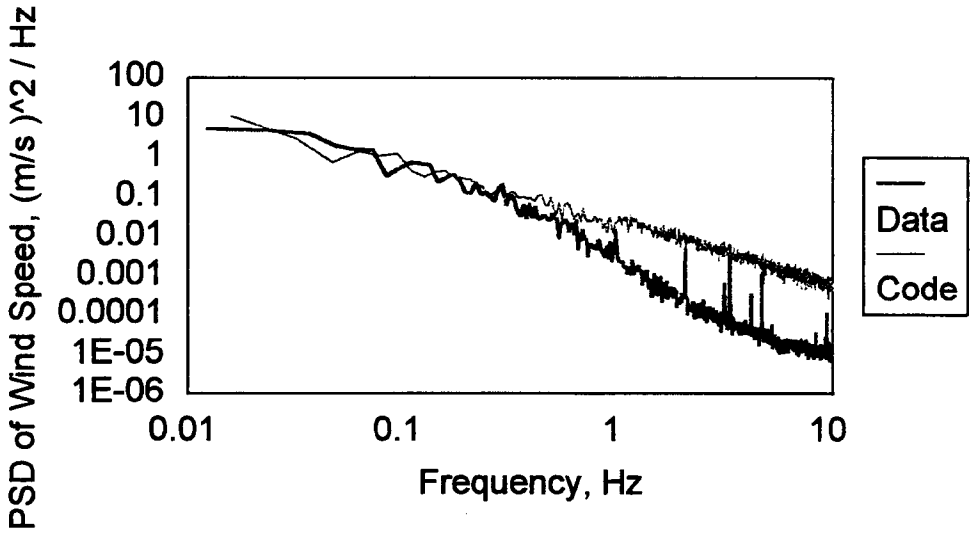


**Figure B-2** Comparison of Wind Data and Code Input Turbulence for the ESI-80 with a Mean Wind Speed of 23 mph

# Appendix C
## Aerodynamics of Blade Sections

The blades are made up of airfoil segments. Lift and drag characteristics of these airfoils can either be read into the code from a file of tabulated data, or it can be calculated in a routine as some built in airfoils are. A sample airfoil data file is given below.

The ESI-80 blade aerodynamics are calculated from a set of curve fits hard-wired into the code. The lift and drag coefficients for various thicknesses are plotted against angle of attack in figures C-1 and C-2.

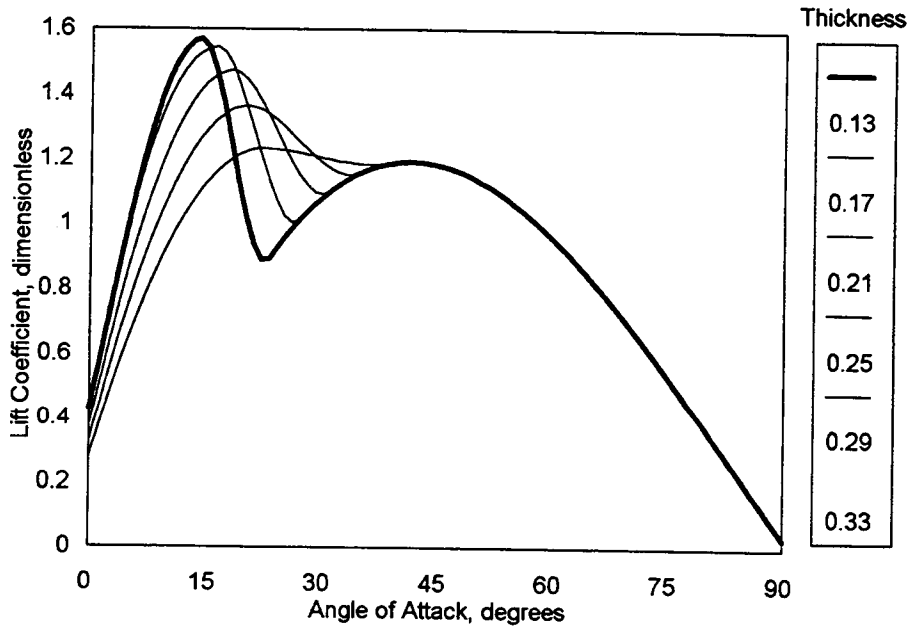


**Figure C-3** Lift Coefficient for NASA LS Airfoil Series

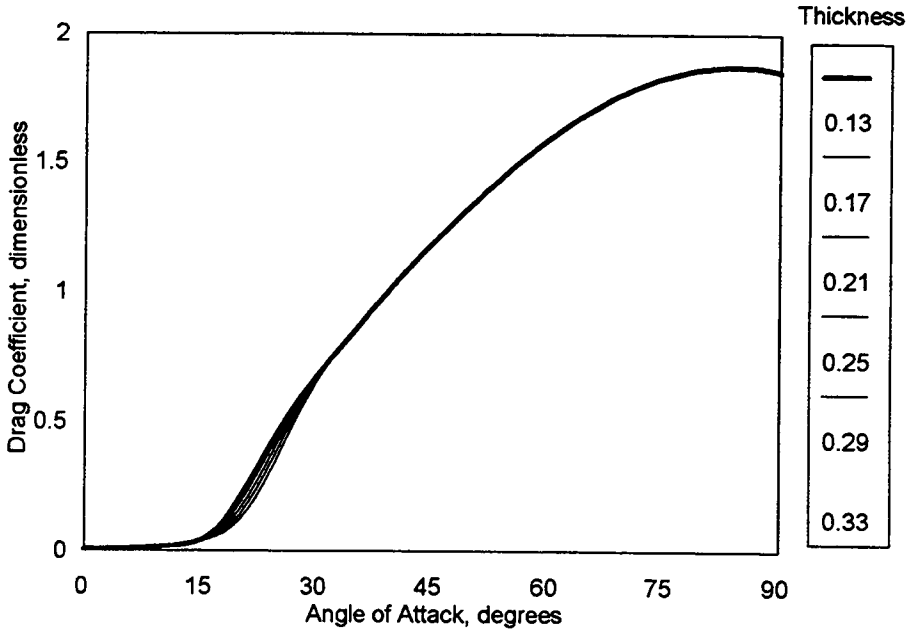


**Figure C-4** Drag Coefficient for NASA LS Airfoil Series

# Appendix D

# Planform Data

The distributed parameters shown in Table D-1 of the blades are read in as part of the input file in appendix A. Blade stiffness, mass, and geometry can vary along each blade. These values contained in the input file are interpolated to fit the specified number of blade segments.

Blade characteristics for the ESI-80 are shown in Figures D-1 through D-4, with the input values shown as points.

**Table D-1** ESI-80 Blade Parameters

| % Radius | Chord | Thick/ Chord | Aero. Twist (deg) | Mass (kg/m) | Flapwise Stiffness ($N\text{-}m^2$) | Struct. Twist (deg) | Edgewise Stiffness ($N\text{-}m^2$) |
|---|---|---|---|---|---|---|---|
| 0.075 | 0.6350 | 0.54 | 2.02 | 79.01 | 15100000 | 2.02 | 172500000 |
| 0.15 | 0.7102 | 0.45 | 1.84 | 55.05 | 9120000 | 1.84 | 62000000 |
| 0.25 | 0.8466 | 0.34 | 1.66 | 49.10 | 4830000 | 1.66 | 67200000 |
| 0.30 | 0.8888 | 0.32 | 1.56 | 43.89 | 3100000 | 1.56 | 64300000 |
| 0.35 | 0.8778 | 0.30 | 1.47 | 40.17 | 2470000 | 1.47 | 57300000 |
| 0.45 | 0.8047 | 0.29 | 1.20 | 32.73 | 1770000 | 1.20 | 37300000 |
| 0.55 | 0.7330 | 0.28 | 0.83 | 25.29 | 1190000 | 0.83 | 19900000 |
| 0.65 | 0.6604 | 0.26 | 0.49 | 17.59 | 694000 | 0.49 | 9570000 |
| 0.75 | 0.5877 | 0.25 | 0.00 | 12.35 | 452000 | 0.00 | 5390000 |
| 0.85 | 0.5154 | 0.22 | -0.62 | 10.71 | 307000 | -0.62 | 4060000 |
| 0.95 | 0.4427 | 0.19 | -1.45 | 9.02 | 197000 | -1.45 | 2820000 |
| 1.00 | 0.4063 | 0.17 | -1.99 | 8.20 | 145000 | -1.99 | 2150000 |

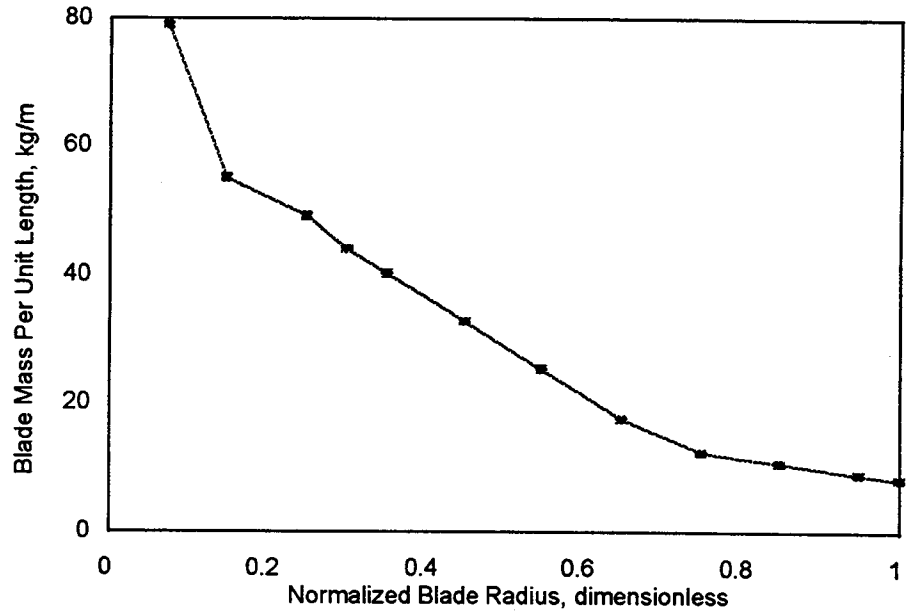


**Figure D-1** Distribution of Mass on ESI-80 Blade

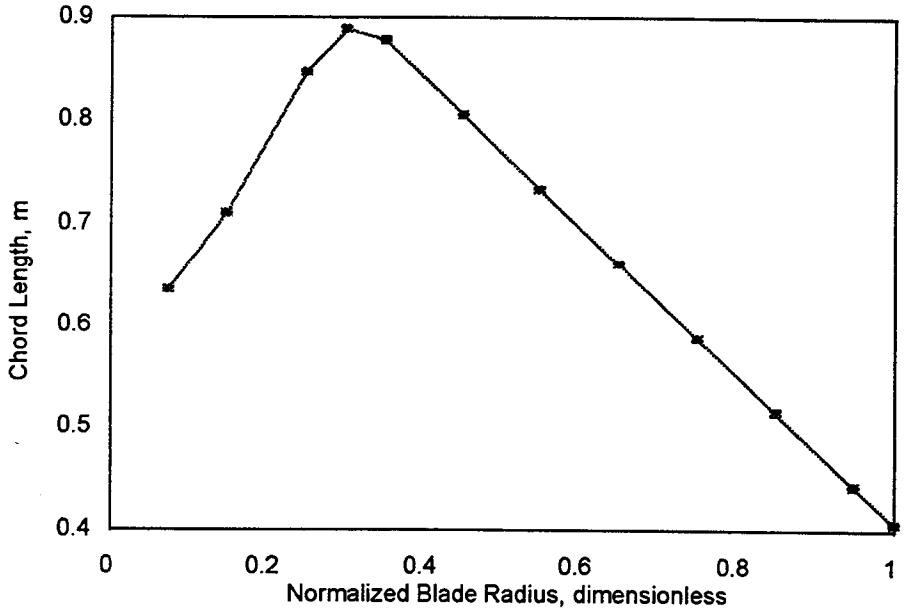


**Figure D-2** Distribution of Chord Length Along ESI-80 Blade

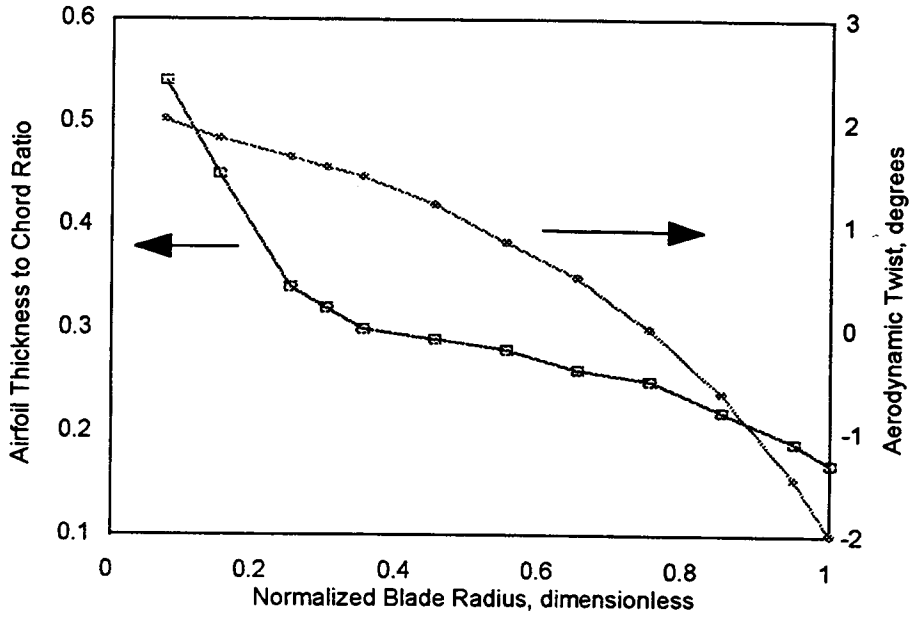


**Figure D-3** Distribution of Thickness and Twist Along ESI-80 Blade

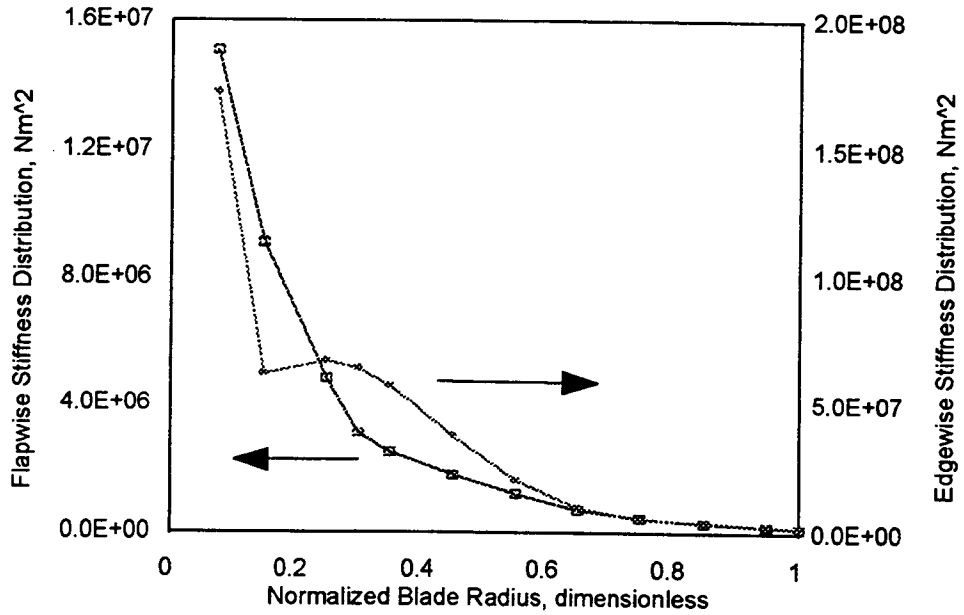


**Figure D-4** Distribution of Stiffness Along ESI-80 Blade

# Appendix E
# Mode Shapes

This appendix contains instructions for determining the mode shapes for blades and tower. These shape equations are read in as coefficients of a polynomial of the form:

$$\phi(\eta) = C_1\eta + C_2\eta^2 + C_3\eta^3 + C_4\eta^4 + C_5\eta^5 + C_6\eta^6$$

where $\phi$ is the shape function, $\eta$ is the dimensionless distance along the flexible beam, and $C_1$ through $C_6$ are coefficients specified in the input file. Note that at the fixed end, $\eta = 0$ and $\phi = 0$; and at the free end, $\eta = 1$ and $\phi = 1$. These mode shapes are not arbitrary, but depend on the distribution of mass and stiffness of the flexible body and on its motion.

A separate program, MODES, included with FAST, allows computation of these mode shape coefficients. The program requires one input file, summarized in Table E-1. Note that the form is similar to the input file for the FAST code.

The first two parameters indicate what type of polynomial will be produced. The first parameter, N, indicates how many mode shapes to compute and, more importantly, how many coefficients will be used. The second parameter, P, indicates the order of the first coefficient. For example, the combination of N = 2 and P = 4 produces a coefficient for the polynomial $\phi(\eta) = C_4\eta^4 + C_5\eta^5$. The remaining coefficients are forced to be zero. Note that N must match the parameter NN in the code, and to change it from a hardwired value of NN = 3 the code must be recompiled.

**Table E-1** Input File MODES.INP

```
3          N              - NUMBER OF MODES OR COEFFICIENTS (MUST MATCH NN)
3          P              - ORDER OF FIRST COEFFICIENT
60.66      ZD(4)          - STEADY STATE ANGULAR VELOCITY OF ROTOR (RPM)
1          IBODY          - SWITCH:  1=BLADE, 2=TOWER
12.19      RT             - BLADE TIP RADIUS OR TOWER HEIGHT (M)
0.92       RH             - BLADE HUB RADIUS OR TOWER RIGID BASE (M)
20.2       TIPM           - BLADE TIP MASS OR MASS ATOP TOWER (KG)
12         N1             - NUMBER OF INPUT STATIONS FOR DISTRIBUTED PARAMETERS
1.         STFFAC         - FACTOR TO ADJUST STIFFNESS
1.         AMSFAC         - FACTOR TO ADJUST MASS
.075,              79.01,                12553000.
.15,               55.05,                7604000.
.25,               49.10,                4021000.
.30,               43.89,                2581000.
.35,               40.17,                2062000.
.45,               32.73,                1475000.
.55,               25.29,                992000.
.65,               17.59,                578000.
.75,               12.35,                377000.
.85,               10.71,                256000.
.95,               9.02,                 164000.
1.00,              8.20,                 121000.
```

The mode shapes for the blades are affected by the centrifugal stiffening as the rotor turns, so the code also reads in ZD(4), the rotational speed of the rotor in RPM. The switch IBODY indicates whether a blade (1) or the tower (2) is to be considered. The next two parameters give the length of the flexible part of the body. For a blade, RT is the tip radius and RH is the hub radius. For the tower, RT will be the hub height (HH in FAST) and RH will be the base height (HS in FAST). The parameter TIPM should be the mass of the blade's tip brake or the total mass on top of the tower, including nacelle and rotor. The parameter N1 indicates how many lines of data for the distributed parameters should be read in. The stiffness and mass can be adjusted using the factors STFFAC and AMSFAC. The final portion of the table is a list of the characteristics distributed along the flexible body. The first column is the normalized location, the second column is lineal density, and the final column is stiffness. The same values as those read in the FAST code are used.

The code produces one output file which lists the frequencies and mode shapes computed for the data given, shown in Table E-2. These frequencies

are estimates and may not agree exactly with the frequencies estimated or demonstrated by the FAST code.

The code uses a method which assumes the shape functions are made up of the individual terms of the polynomial specified. For example, if P = 4 and N = 2, the shape functions are a combination of the functions $\varphi_1 = \eta^4$ and $\varphi_2 = \eta^5$. These are used to form the following matrices:

$$M_{ij} = \int_0^R \mu\, \varphi_i\, \varphi_j\, dr + M_{Tip}$$

$$K_{ij} = \int_0^R EI\, \varphi_i''\, \varphi_j''\, dr$$

$$C_{ij} = \int_0^R \{ M_{Tip}\, R + \int_r^R \mu\, s\, ds \}\, \varphi_i'\, \varphi_j'\, dr \qquad i,j = 1 \ldots N$$

where $\varphi_i'$ is the derivative with respect to the distance along the blade,

**Table E-2** Output File MODES

| | | | |
|---|---|---|---|
| 3 | Number of Modes | | |
| 3 | Order of First Coefficient | | |
| 60.66 | Rotor RPM | | |
| 12.19 | Blade Radius | | |
| 1.00 | Stiffness Multiplier | | |
| 1.00 | Mass Multiplier | | |
| 20.2 | Tip Mass | | |
| Mode Number: | 1 | 2 | 3 |
| Frequencies: | 2.32 | 7.28 | 20.99 |
| Mode Shapes: | | | |
| 1 | .000 | .000 | .000 |
| 2 | .000 | .000 | .000 |
| 3 | 1.827 | -21.647 | 49.595 |
| 4 | -.885 | 38.542 | -133.017 |
| 5 | .058 | -15.895 | 84.421 |
| 6 | .000 | .000 | .000 |

$\mu$ is the lineal density, EI is the stiffness, $M_{Tip}$ is the mass at the free end, and r is the position along the flexible body from the fixed end at 0 to the free end at R.

For the blades which have centrifugal stiffening, these matrices are combined to give the matrix

$$[ K + \Omega_0^2 C ]^{-1} [M]$$

which has eigenvalues (frequencies) and eigenvectors (mode shapes). The final coefficients are normalized so that $\phi |_{Tip} = 1$.

For the tower, the M and K matrices are similar and C becomes

$$C_{ij} = \int_0^H \{ M_{Top} + \int_x^H \mu \, ds \} \varphi_i' \varphi_j' \, dx \qquad i,j = 1 \ldots N$$

where $M_{Top}$ is the mass atop the tower. These matrices are used to form:

$$[ K + g C ]^{-1} [M]$$

which has eigenvalues (frequencies) and eigenvectors (mode shapes).

The specific mode shapes calculated for the ESI-80 machine can be seen in Figures E-1 through E-3.

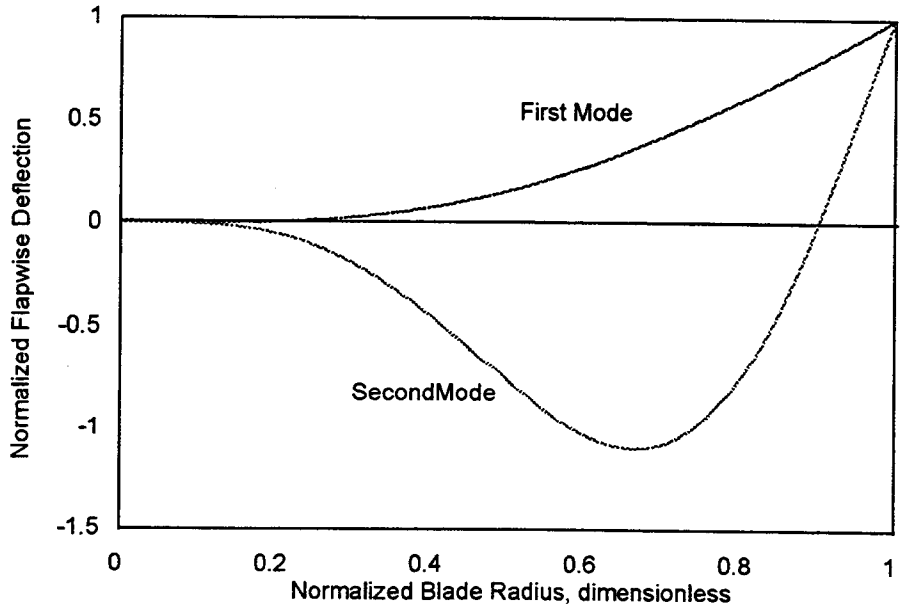


**Figure E-1** Normalized Blade Flap Mode Shapes for the ESI-80

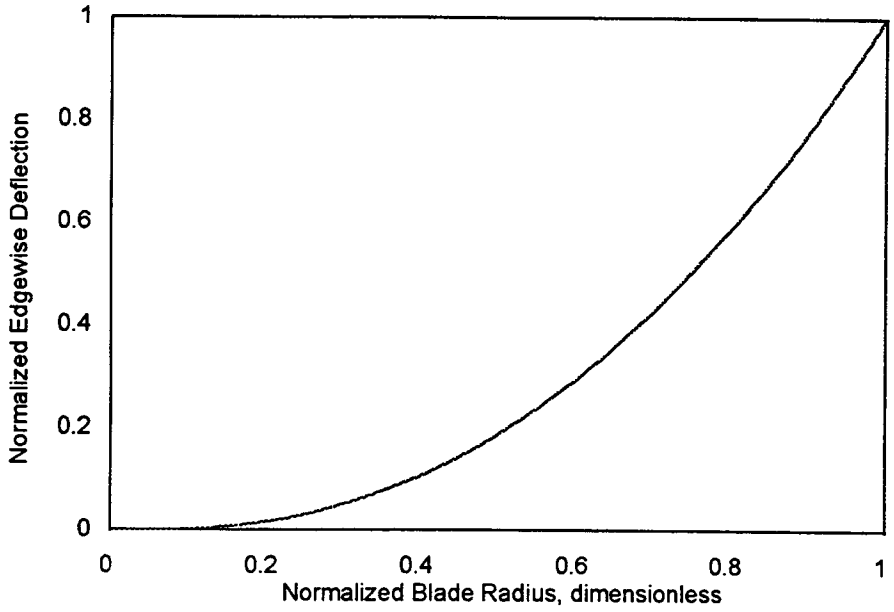


**Figure E-2** Normalized Blade Edgewise Mode Shape for the ESI-80

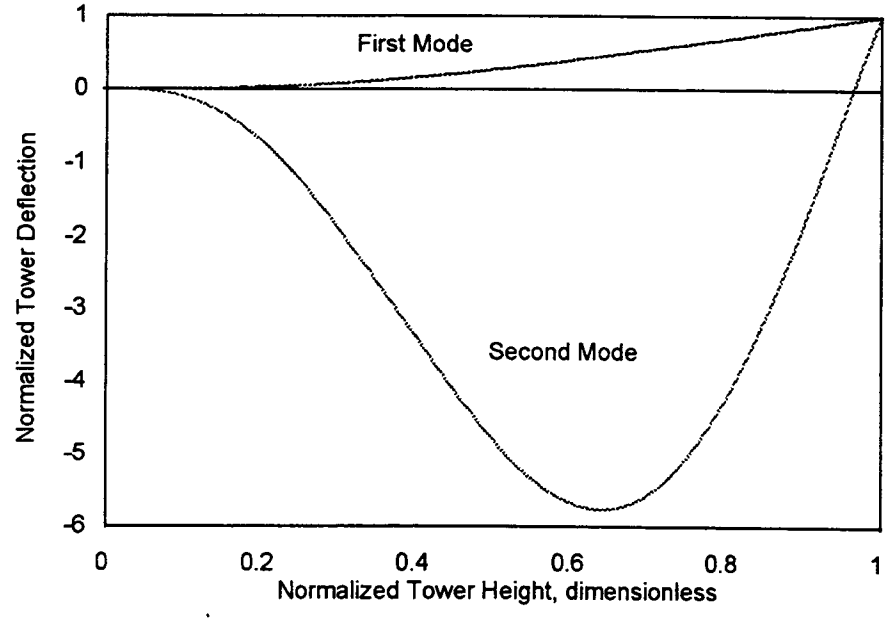


**Figure E-3** Normalized Tower Mode Shapes for the ESI-80

# Appendix F
## Teeter Springs and Dampers

Teeter motion is restricted by teeter springs, teeter dampers, teeter stops, and coulomb friction. If the teeter angle exceeds the specified maximum and is still increasing, a large counteracting moment is supplied, simulating rigid teeter stops. Coulomb friction in the teeter hinge is supplied as a constant moment resisting teeter motion.

Finally, springs or dampers which also restrict teeter motion may exist on the actual machine. In modelling these, springs are considered to store and return the energy when compressed, while dampers will dissipate engery, supplying less or no force as the teetering rotor returns to a centered position. Since these springs and dampers are different for every machine, a few simple equations to describe their action are built into the code, as is a space to provide equations specific to a new machine. Note that the linear effects of springs and dampers on the teeter angle must be converted to an angular effect since the geometric location of actual springs or dampers has not been included.

The ESI-80 machine has linear teeter dampers that act only in one direction, and it has teeter springs that can be described as a quadratic function of their amount of compression. These springs and dampers come into effect when the teeter angle exceeds 2 degrees. Figure F-1 shows a plot of the moment supplied at a certain teeter angle, both for increasing and decreasing angle.

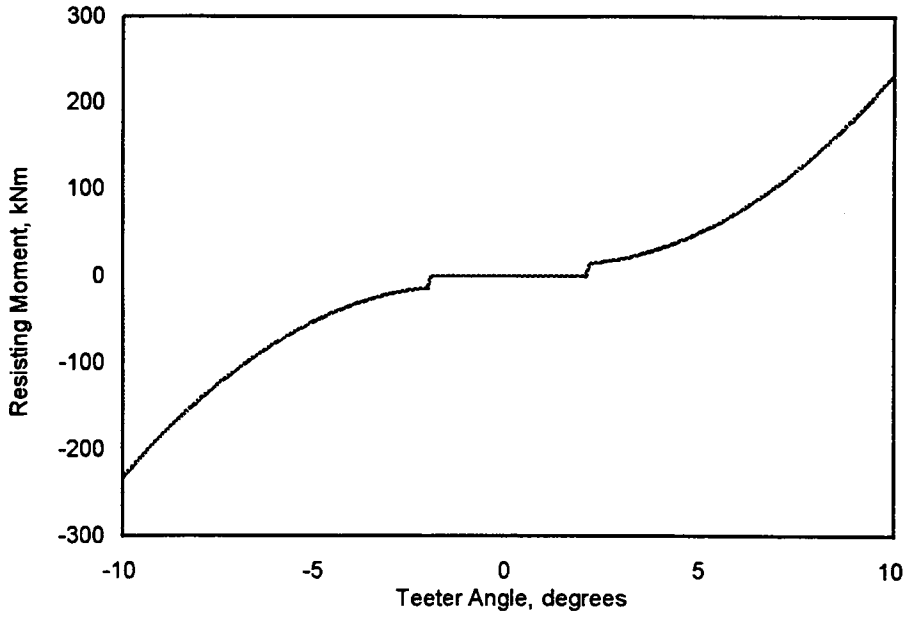


**Figure F-1** Effect of ESI-80 Teeter Springs and Dampers